INTERNATIONAL ATOMIC ENERGY AGENCY
UNITED NATIONS EDUCATIONAL, SCIENTIFIC AND CULTURAL ORGANIZATION
INTERNATIONAL CENTRE FOR THEORETICAL PHYSICS
I.C.T.P., P.O. BOX 586, 34100 TRIESTE, ITALY. CABLE CENTRATOM TRIESTE

H4.SMR/845-10

Second Winter College on Optics

20 February - 10 March 1995

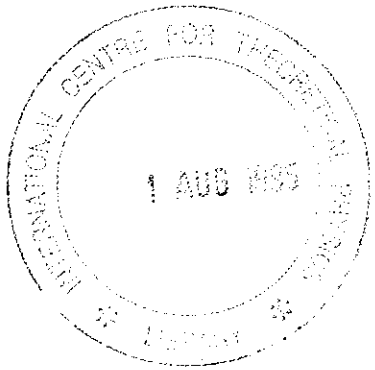

Near-Field Optics

A. Lewis

Hebrew University of Jerusalem
Division of Applied Physics
Jerusalem, Israel

Beyond the Diffraction Limit:
Instrumentation for Near-field Subwavelength Optical Characterization and Fabrication

KLONY LIEBERMAN AND AARON LEWIS
DIVISION OF APPLIED PHYSICS
THE HEBREW UNIVERSITY OF JERUSALEM
JERUSALEM, ISRAEL

This article describes a new breed of instruments that use the advantages of imaging with electromagnetic radiation but are not limited by the resolution criteria that restrict all lens based optical instruments presently in use today. Boldly stated the ultimate goal is the development of an area of optics that would have the potential for spectrally imaging and manipulating single molecules with light.

I. INTRODUCTION

This emerging field of near-field optics, unlike its far-field cousin (which governs the behavior of all presently available lens-based optical instruments), is based in its simplest form on transmitting light through a subwavelength hole (see Figure 1) which is scanned above a surface at a distance of a few hundred Angstroms. This distance corresponds to what is known as the optical near-field in which the light emitted by the aperture does not have a chance to spread out to its far-field diffracted dimensions. The present review highlights both the advantages and the drawbacks of near-field optics. It reviews the exciting results that have already been obtained in this important and exponentially growing field of research. It indicates the variety of applications that could result from these novel advances in optics and it points to future directions in this innovative field of optical physics and engineering.

Since the discovery of the lens all optical instruments used for imaging have had stringent resolution criteria that are fundamentally tied to the wavelength of the electromagnetic radiation employed in the imaging. This resolution limitation is ultimately defined by several factors. One of these is the finite dimension of lenses results in a physical aperture that rejects rays of light from the object and causes a loss of information. In essence, the physical aperture restricts the acceptance angle of light rays from the object. This acceptance angle of the lens together with the index of refraction of the medium in which the lens is operating defines the numerical aperture (N.A.) of the lens in question. With such a definition of N.A. the minimum separation between two points in the object that can be resolved was given by Lord Raleigh as

$$r_{min} = \lambda / 2.44\ (N.A.) \qquad (1)$$

Thus, for green light, which has a wavelength $\lambda = 0.5\mu$, $r_{min} = 0.146\mu$ for an oil immersion objective with the best N.A. of 1.4 that is readily available today. In the visible region of the spectrum this is close to the 0.2μ resolution being achieved by the best lens based optical techniques and instrumentation in use today.

A standard method to achieve higher resolution within this fundamental limitation of wavelength has been to preserve the lens and to use shorter and shorter wavelengths of radiation. In principle as the wavelength decreases the resolution increases provided that the quality of the lenses used remain constant. Unfortunately, as the wavelength decreases the optical quality of the lenses significantly deteriorates and this approach has generally had limited applicability in achieving super-resolution.

As noted above, near-field optics in its simplest form breaks this wavelength dependent resolution barrier imposed by geometrical optics by replacing the lens in either the illumination or the collection path by a subwavelength hole in the near-field. Such a replacement is not instituted without considerable thought. Lenses are optical elements that work in parallel. In other words all the points in the object plane are transferred to the image plane in parallel. To replace a lens with a wavelength independent optical element generally means to give up the luxury of parallel imaging and to develop an image serially by scanning either the sample or the optical element.

With a lensless optical approach optics has the potential to regain some of the ground lost in recent years to imaging techniques not based on visible light. In essence when magnifications >1000 times are required electron microscopes have been the instrument of choice. Now with the advent of near-field optics all the interactions between light and matter, which have been so exhaustively studied for over the past centuries remain applicable in a resolution regime that has up until now been the exclusive domain of destructive beams of electrons which can image only in vacuum environments.

The concept of near-field optics has been reinvented at least five times in the past 65 years without the inventors knowing about the previous work in this field. The first known efforts in this field were uncovered recently in a delightful historical review of the field by McMullen [1]. In this article we learn that Edward Synge had a lively correspondence with Einstein on the subject and even published a paper in 1928 in this field which we

now call near-field optics. The next known effort was by an astrophysicist John O'keefe who was in the Goddard Space Center [2]. He, without knowledge of Synge, published a short note in 1956, which is the most succinct description of the essential basis of near-field optical imaging. His efforts were unknown to any of us in this area until 1987 when O'Keefe read a short account of the work of Lewis and wrote him a letter (see Figure 2) in which he described his work in the field.

The ideas of near-field optics were then once more forgotten until in 1972 Ash and Nichols [3] published an experiment on near-field imaging with microwave radiation. These workers were able to achieve with such radiation $\mu/60$ resolution by passing 3 cm waves through a 0.5mm hole and scanning the hole over a surface to achieve 0.5 mm resolution. Efforts in near-field microscopy in the optical regime began in the early 1980s with the independent efforts of D. W. Pohl at the IBM Research Laboratories in Zurich [4] and by Aaron Lewis at Cornell University [5,6]. This was the beginning of experimental near-field scanning optical microscopy (NSOM).

Since the initial papers of the Lewis and Pohl groups about a decade ago there has been a growing interest in this exciting new field of optics which defies a dogma that was accepted for at least 100 years. Today there are dozens of groups working actively in the field and daily new groups are entering the area. There is a rush of theoretical and experimental work and this portends important fundamental and applied developments that depend on this new field. In essence from biology to microelectronics a wall of resolution is being approached when conventional optical imaging is applied and near-field optics gives significant hope that this barrier of resolution is overcomable. This is seen in Figure 3 which places near-field optics and its resolving power within the constellation of microscopic techniques that are available today. The resolution of near-field optics clearly bridges the gap between classical lens-based optical methods and the super-reolution capabilities of electron optics and lensless scanned probe techniques.

Besides the present review there have been at least three previous reviews on the subject[7,8,9]. In this paper we attempt to give as thorough and as up to date an account on near-field optics and its applications as is possible in this rapidly expanding field. We hope that we have accurately represented all the contributors to the field and we apologize if some workers have not been appropriately cited. It should be noted that throughout this review the acronym NSOM is used but the acronym SNOM (scanning near-field optical microscopy) has also been used for aperture based imaging. The acronyms emphasize different aspects of the technique with NSOM that was devised in our laboratory emphasizing the importance of the near-field while SNOM emphasizes the similarity to the other scanned probe techniques that based upon scanning a probe and started with the invention of scanning tunneling microscopy (STM). For the apertureless based near-field optical techniques based on frustrated internal reflection that will be described below PSTM (photon scanning tunneling microscopy) is the most commonly used term.

II. THE OPTICAL NEAR-FIELD - THEORY

A. APERTURE BASED NEAR-FIELD IMAGING

What is of practical interest in defining the constraints of near-field optics is to understand the distribution and intensity of the radiation within the near-field region of a subwavelength light probe e.g. an aperture. Unfortunately, a rigorous mathematical description of optical near-field radiation patterns has not been achieved. What is known is that the radiation emitted from such a probe consists of both propagating terms which extend into the far-field and non-propagating, evanescent terms which combine to determine the structure of the distribution of radiation in the near-field. These terms are a direct result of Maxwell's equations for a propagating electromagnetic field when the boundary conditions for an appropriate discontinuity in the permitivity are inserted into the equations. For example in the case of an aperture the derivative of the permitivity, which is the second term in the expanded version of the Maxwell equation:

$$\Delta(\varepsilon E) = \Delta E + \Delta\varepsilon = 0 \tag{2}$$

is non-zero in the plane of the aperture which gives rise to the non-propagating near-field terms. In addition, the shape of the probe, the optical properties of the intervening media and the nature of the sample with which the radiation is interacting can also strongly influence the structure of the radiation in the near-field.

1. Propagation Through A Subwavelength Aperture In An Infinitely Conducting Screen

In order to deal with the problem of the near-field one first has to consider the type of probe that is to be used to investigate the subwavelength optical properties of a surface. As noted above, in its simplest implementation a tiny aperture is used to create a spot of light that is less than the dimensions of optical wavelengths. Several workers have considered the functional dependence of the radiating field emanating from such a subwavelength aperture in a conducting medium. The first to consider these questions was by Bethe in1944[10] whose concern was mainly in the microwave regime in which the surrounding metal screen acts as an infinitely conducting medium. Bethe found that the power transmitted through a subwavelength hole in such a *thin screen* decreases as a^6/λ^4 where a is the aperture radius and λ is the wavelength of the radiation being used. These calculations set the stage for many other studies that have been completed in the past few years. The most prominent features of the calculations of Bouwkamp (1950) [11] and more recently Leviatan (1986) [12] and others [13,14] is that there are no propagating electromagnetic modes within the confines of a subwavelength aperture in a conducting screen of finite thickness. These non-propagating, evanescent modes have a field density which decays exponentially in the axial direction as they penetrate such an aperture. This can be understood by considering the electromagnetic wave vector as it enters such a subwavelength region. The solutions to the wave equation are plane waves of the form:

$$E = \Phi e^{i(k_x x + k_y y + k_z z)} \qquad k_x^2 + k_y^2 + k_z^2 = \frac{\omega^2}{c^2}$$

If the aperture dimension is less than $\lambda/2$ ($\lambda=2\pi c/\omega$), then the transverse width of the field is less than $\lambda/2$ at that point, requiring that: $k_z^2=\omega^2/c^2-k_x^2-k_y^2<0$ Hence k_z is an imaginary number and the field component vanishes exponentially as it propagates in the z direction. The energy is either absorbed and/or reflected by the screen and this introduces a cardinal problem in near-field imaging which is the significant decrease in the intensity of an electromagnetic wave as it passes through a subwavelength hole.

The coupling between the two sides of a circular hole in a thick, perfectly conducting screen was investigated by Mcdonald [15] with the microwave regime in mind. The least attenuated mode was found to be the TE_{11} for which the energy decays at a rate of:

$$E = E_0 e^{d/a}$$

where d is the screen thickness and a is the aperture radius. It is possible that as the TE_{11} mode decays additional higher order modes are generated which also decay exponentially but this has not been fully investigated theoretically. It should be noted that the finite conductivity of metallic screens at optical frequencies results in weaker attenuation of all the modes. In essence when radiation is propagating in such a cylindrical waveguide and reaches a region of the waveguide which is less than the dimension of the wavelength of the light there is an exponential decrease in the intensity of the light as described above. Such a phenomenon is well-known in optical fibers and is referred to as the cutoff frequency below which the radiation is not confined in the fiber.

2. Theoretical Factors Limiting Aperture Size in NSOM

The evanescence of the fields below cutoff, as calculated by McDonald [15] sets a lower limit on the useful aperture size in a metal screen [16]. This arises from the finite conductivity of the screen in the optical regime that has been noted above and thus some of the energy will penetrate into the metal itself at a rate given by $E = E_0 e^{-d/\delta}$ where δ is the extinction length of the metal. When the attenuation due to the waveguide effect of the aperture exceeds the attenuation into the metal itself the contrast between the aperture and the surrounding media is lost. Any further reduction in aperture size will simply result in a decreased throughput without improvement in the effective spot size. The metal with the shortest skin depth in the visible regime is aluminum with δ=65A which results in a minimum effective aperture size of 50nm. These initial calculations took into account the finite conductivity of the metallic screen in terms of the penetration of the optical wave but treated the evanescence of the field as if the metallic waveguide was infinitely conducting. Recent suggestions by Betzig et al. [17] taking into account this effect of the finite conductivity on the attenuation through the hole (eq. 1) indicates that minimum spot sizes of approximately half this value may be attainable.

3. Functional Dependence Of The Radiation Field As It Expands Through The Near-field

The first numerical calculations of the near-field behavior of radiation emanating from a region of subwavelength confinement was completed by Betzig et al. [16]. These workers considered a plane wave passing through a subwavelength infinite slit in a screen of finite thickness and were able to obtain the functional dependence of the radiation as it expanded from such a slit. The calculations demonstrated that the radiation remained confined to the dimension of the slit for a region from the screen approximately equal to the slit width, and that the narrower the slit width, the more rapid the subsequent divergence. Such a configuration is not directly applicable to NSOM since there is always at least one propagating mode regardless of the slit width. Nonetheless these calculations provided the first indication that the field does remain collimated to a subwavelength dimension for a finite distance from the screen containing the subwavelength slit.

The radiation field that is emitted by a subwavelength circular aperture was first calculated by Leviatan [12] and is seen in Figure 4. These calculations which were carried out for a thin screen show the normalized Poynting's vector in a region immediately below the aperture. The result in this case, similar to the slit examined by Betzig, shows that the field also remains collimated up to a distance approximately equal to the aperture diameter. This field can be broken up into three distinct zones. First there is a very near-field region, which has been called by Pohl and coworkers the proximity zone [8]. This region extends to a dimension r from the aperture which is $<<\lambda$ where dipole approximations are totally inadequate since the magnetic components are unchanging because of quadrupole contributions. Second, there is an intermediate regime where the fields could be approximated by the near-field zone of a dipole which is the useful region for near-field optics. The emission of a point dipole antenna was a problem that was first considered by Sommerfield in 1926 [18]. Such calculations of a radiating dipole show that the intensity of the field decreases exponentially. Finally, a far-field regime is reached which exhibits the classical 1/r dependence.

Although the calculations of Leviatan are more realistic for near-field imaging they give no indication of the coupling losses that are incurred when a light wave is transmitted through an aperture in a screen of finite thickness. These losses are included in the calculations of Roberts [13,14] who considered both the problems of a thick screen and a circular geometry. The approach of Roberts used a modal analysis in which an infinite

superposition of modes was considered. These calculations were completed both for a circular aperture in a thick screen and for a conically shaped aperture which is the most realistic geometry that has been theoretically investigated. The results that Roberts obtained for the region beyond the screen are very similar to those obtained by Leviatan. This is understandable since the functional dependence of the region beyond the screen would not be expected to be affected by the thickness of the screen. What would be affected by a thick screen would be the power transmitted and this was calculated by Roberts for particular geometries as a function of final aperture radius and cone angle. The calculations verify what is observed experimentally that larger cone angles increase throughput.

4. Alterations In The Near-Field Intensity Distribution Resulting From Sample Interactions

Recent calculations by Novotny et. al. [19] have used a Multiple Multipole (MMP) analysis to model a two dimensional tapered slit aperture. These workers modeled the fields in and around a metal coated glass wedge both in free space and when perturbed by a small particle. Figure 5 shows the energy coupled out of the probe into a second dielectric medium for s and p polarizations. Since in the slit geometry that was investigated the p polarization has a propagating mode large intensities couple into the medium for this polarization. More interesting are the calculations shown in Figure 6 which show the near field energy distribution around a small, perfectly conducting cylinder that is placed on the surface of the second medium. For the s polarization the s polarization is pushed away since the boundary conditions require that the electric field vanish at the object surface. For p polarization the near-field is less disturbed and is actually attracted by the object.

The effects of varying the dielectric constant of the cylinder on the intensity of the radiation in the near-field is seen in Figure 7. In this figure one sees that as the dielectric constant is altered a point is reached at which a large enhancement of the field occurs when a plasmon resonance is reached. Since the real and the imaginary components of the dielectric constant affect the intensity and distribution of the field the near-field can be sensitive both to phase and amplitude modulations. Thus both absorption and refractive index changes in the sample contribute to the contrast that is observed and this is different to conventional microscopy.

These investigators also calculated the far-field distribution of the transmitted radiation from the slit when perturbed by the cylinder. An interesting feature of these calculations is that, for p polarization, a significant portion of the energy is scattered at relatively large angles from the axis of the aperture (see Figure 8). More importantly, calculations of the far field patterns for scattering objects of various dielectric constants show that significant changes in the radiated intensity occur only at these large angles. This would indicate that better contrast should be obtained if the far field light is only collected over these solid angles. We have actually observed similar effects experimentally, whereby changing the numerical aperture of the collection optics results in not only a change in the signal intensity but also a change in the image contrast. Again, one must be careful in extracting too much information from the various slit geometries that have been studied since these models are fundamentally different from the circular geometry that is actually employed in NSOM in that there is always a propagating mode regardless of the slit width.

5. Ramifications For Experimental Near-Field Imaging

Several important conclusions can be drawn from these attempts to theoretically model subwavelength apertures and the near-field intensity distribution that emanates from these apertures.

- There is an exponential decrease in the radiation as it passes through a subwavelength aperture.
- From the aperture surface there is a region called the near-field which typically extends a few tens of nanometers.
- Within the near-field zone the energy density decreases exponentially.

- Any surface brought within this zone will be illuminated by a subwavelength spot of light whose size depends on the distance from the aperture.
- The dimensionality and the dielectric constant of the illuminated sample has strong and complex influence on the structure of the field.

Two problems that result from these conclusions have to be addressed. The first problem is the considerable reduction in the intensity of light as it passes through such an aperture and the second is the accuracy of placement of the aperture relative to the surface which the exponentially decreasing nature of the near-field zone demands. In terms of numerical simulations of this near-field zone it would appear that the aperture has to be placed relative to the surface with an accuracy of better than 3nm in order to maintain a constant spot size and intensity. This has been one of the experimental challenges of near-field optics especially when one considers real surfaces which in general have considerable surface roughness. As will be seen below both these experimental problems that arise from the theoretical basis of near-field optics have indeed been solved.

B. NON-APERTURE BASED NEAR-FIELD IMAGING

Alternate approaches to near-field optics, that do not use a subwavelength aperture, involve the use of dielectric and metallic tips that probe the near-field optical characteristics of a surface. In these approaches instead of generating the near-field from the probe one uses the probe interaction with the surface to sense the variations of the surface near-field. These variations arise from local evanescent fields, surface plasmons or other phenomena connected with the microscopic surface structure interacting with the probing tip. These interactions have been treated in great detail theoretically by several workers including Girard, Courjon and coworkers [20, 21, 22, 23], Reddick et al [24], Wessel [25] and Specht and coworkers [26].

1. Extended Evanescent Surface Waves

This approach involves the launching of an evanescent field on a surface and probing alterations in this field by inserting an uncoated dielectric probe such as a tapered glass rod or fiber into the evanescent electromagnetic field. For these measurements the probe is etched or pulled to a subwavelength point. In essence the surface of the dielectric probe samples the evanescent field on the surface and changes in this field due to the surface topography are monitored. An evanescent field is produced when light passes from an optically dense medium to one which is less dense at an angle which is greater than the critical angle, θ_c. This can be accomplished with an arrangement as shown in Figure 9. In this figure light that enters the prism is totally reflected by the interface on which the sample is placed. The extent of the propagation of the evanescent field as given in Equation 5 is determined by the wavelength, the angle of incidence and the difference in the dielectric constant (which is related to the index of refraction, n) between the prism and the air [27].

$$I \sim \exp\{-2kz\,[\sin^2\theta_i - (n_t/n_i)^2]^{1/2}\} \qquad (5)$$

The extent of the evanescent field typically ranges from one tenth of a wavelength for grazing incidence to several wavelengths for angles close to θ_c [28]. Placing a dielectric probe into this region frustrates the internal reflection and allows some light, in proportion to the strength of the field at the location of the probe, to propagate from the surface. This technique, is referred to by several names such as photon scanning tunneling microscopy (PSTM), scanning tunneling optical microscopy (STOM) and Evanescent scanning optical microscopy (ESOM). These names have generally been chosen for the functional analogy of this technique to electron tunneling.

There have been several attempts to characterize theoretically these evanescent fields which closely follow small (subwavelength) variations in the surface height and the sensitivity of the measurement to changes in dielectric constant and topography. These variations, which are too small to produce propagating fields, change the structure of the evanescent field in a very complex fashion. The phenomena that affect this field requires a detailed understanding of the local interactions of the microscopic variations with the polarization of the light.

The theoretical approach of Girard, Courjon and coworkers [20,20,21,22,23] is based on a microscopic approach in which one considers multipolar interactions between each atom of the tip and the object studied. This technique is in contrast to solving the macroscopic Maxwell equations with the appropriate boundary conditions. In essence, in this microscopic treatment a coupling matrix between the tip and the surface is introduced and this matrix includes all correlations between each volume element in the tip and the surface. An advantage of this approach is the ability to simulate tips of arbitrary geometry without introducing boundary conditions at the surface of the probe. These calculations have been used to simulate various PSTM images by considering the interaction of objects with a variety of polarizations. For example, as is seen in Figure 10, the PSTM images under different polarizations vary significantly. This is an indication of the complexity of image interpretation in PSTM.

2. Localized Plasmon Interactions

An electromagnetic field can be locally enhanced by several orders of magnitude by the introduction into the field of a metallic particle in which the propagation of free electron waves in the metallic surface can be induced by light. The energy of these free electron states are determined by the size of the metallic particle with maximum enhancement determined by a balance between radiative damping in larger particles and the electron mean free path for the smaller particles. Such plasmons can be excited either in the tip of a probe or on a surface. These free electron waves can be modulated by the presence of a tip in proximity to a surface or of a surface in proximity to a tip and this results in a change in an optical signal that is present when the tip and the surface are in the vicinity of one another.

Plasmons at the tip of the probe

The first investigator to consider this approach was John Wessel [25]. He was concerned with the problem of plasmons located in a metallic tip sitting on a probe. He based his calculations on those that were previously completed to understand a phenomenon known as surface enhanced Raman scattering (SERS) in which a molecule is placed on a roughened silver surface. The intensity of the Raman scattering observed can be enhanced from 5 to 7 orders of magnitude depending on a variety of conditions including the size of the metallic particles on the roughened silver surface [29]. Since it is expected that non-linear optical phenomena, which depend on higher powers of the electromagnetic field, would be enhanced to a greater degree than a spectral phenomenon such as incoherent Raman scattering, which has a linear dependence on the electric field, Wessel focused on such non-linear optical phenomena and considered both the enhancement and the particle size that would maximize such an interaction.

The work of Denk and Pohl [30] extended the results of Wessel. They obtained an exact solution of Laplace's equations which basically calculates the potential and field energy distributions for various tip/sample interfaces. These workers have calculated the relative ability of various materials to affect field enhancements within the small volume at the tip of the probe. For suitable interfaces (e.g. silver tip/silver sample) field enhancements of approximately three orders of magnitude are predicted (seeFigure 11). A table of different material combinations is also provided by these authors to guide future experimental work.

Plasmons on the surface

The optical interaction between a metallic tip and a propagating surface plasmon has been examined in a paper by Hansch and coworkers [26]. These investigators considered theoretically and demonstrated experimentally that if a surface plasmon is launched using an evanescent field then the presence of a metallic tip could damp the propagation of the surface plasmon. This damping can be appropriately monitored as described below. These workers consider the metal tip as a classical oscillating dipole, the oscillating field of the surface plasmon and the non-radiative coupling of the two in the near-field. The two main effects that are seen in this case, both theoretically and experimentally, are the alterations in the plasmon field due to scattering of the surface plasmons by the presence of the metallic tip and damping by radiationless energy transfer to the tip. The scattering term is found to have an exponential distance dependence with significant effects extending out to approximately 200 nm. At distances below 10 nm non-radiative energy transfer between the tip and surface becomes dominant and

dampens the surface plasmons. This strong distance dependence provides a very high lateral resolution as will be described in the experimental section below.

Plasmon resonances can also be excited in small metallic particles by near-field illumination through an aperture. The calculations of Novotny et. al. [19] indicate that almost no energy is radiated in the forward direction when the conditions for a plasmon resonance exist. This effect can manifest itself as very large apparent contrast variations when imaging a sample containing metallic surface features on the order of several tens of nanometers.

3. Surface Induced Luminescence

Besides the use of freely propagating and evanescent photons to induce surface luminescence there have been two distinct alternate suggestions for inducing localized surface luminescence.

Tip/surface excitons

An approach that has been suggested that is quite similar to the technique described by Hansch and coworkers is the proposal by Lieberman et al [31]. These workers describe an approach in which a tip containing a molecular crystal in which excitons are produced is brought into close proximity to a surface. At an appropriate distance between the tip and the surface molecular energy transfer occurs and this leads to damping of the exciton by either quenching or non-radiative energy transfer to an appropriate molecular acceptor in the surface.

When excitons transfer from one molecule to another they do so via a direct energy transfer process rather than a photon emission-reabsorption process. This is a dipole-dipole interaction between the donor and the acceptor molecules and at sufficiently small distances is highly efficient. According to the theory developed by Fyrster [32] the rate of energy transfer k_t and the efficiency E are given by:

$$k_t = r^{-6} J K^2 n^{-4} k_f \times 8.71 \times 10^{23} \sec^{-1} \quad , \quad E = \frac{r^{-6}}{r^{-6} + r_0^{-6}}$$

where r_0, the distance at which the energy transfer is 50%, is:

$$r_0 = (J K^2 Q_0 n^{-4})^{\frac{1}{6}} \times 9.7 \times 10^3 \ \text{Å}$$

The geometric variables are r, the distance between the center of the chromophores; and K^2, the orientation factor for the dipole-dipole interaction. The spectral variables are J, the spectral overlap integral; n, the refractive index of the medium between the donor and acceptor; k_f, the rate constant for fluorescent emission by the donor; and Q_0 the quantum yield of the fluorescence of the energy donor in the absence of an acceptor. For a singlet exciton the distance r_0 (known as the Fyrster Radius) typically extends on the order of 5-8 nm, with measurable effects extending beyond 10 nm [33,34]. Triplet excitons, on the other hand, have a smaller radius of interaction typically on the order of 1nm.

This efficient energy transfer has significant ramifications for highly sensitive excitation and detection [31]. In order to optically excite with certainty a single fluorophore, a minimum flux on the order of 10^9 photons per second must pass within half a wavelength of the molecule. This is because the optical absorption cross section depends on both the fluorophore concentration and the optical pathlength. Thus, for a single molecule, even for a highly efficient absorber such as rhodamine which has a quantum efficiency near unity, the probability of excitation per photon is very low. A single exciton, however, brought to within the Fyrster radius will have a 50% probability of transferring to the acceptor fluorophore and exciting it. Thus, a few excitons can have the same effect as 10^9 photons. The question remains, however, how many photons does it take to create the required few excitons? Theoretically [35] it will take only 10^4 to 10^5 photons with a single crystal. Furthermore, if the crystal surface is covered with appropriate *exciton traps* that can act as donors for the fluorophore, the host crystal will serve as an antenna. This effective antenna could easily consist of 10^6 to 10^7 molecules. Thus, only about 10^3 photons would be required in this case. This results in a five to six orders of magnitude increase in sensitivity over

ordinary optical excitation. Such a reduced photon flux will also significantly reduce linear and non-linear effects on the sample and will reduce local heating, chemical decomposition and Raman scattering. Furthermore, not only will the fluorophore be located non-destructively, its position will be established to within the Förster radius.

Tunneling induced luminescence

An alternate approach to eliciting luminescence from a surface is based on the injection of electrons by the tip of a scanning tunneling microscope into the surface [36]. The recombination of these electrons in semiconductors produces a near-field emission whose characteristics is determined by the local structure of the sample. The scanning tunneling microscope has also been applied to induce luminescence in molecules on a metal surface [37]. One suggestion for these emissions is that the tip and the metal surface form a cavity and this cavity dramatically affects the molecular photon emission.

III. SUBWAVELENGTH OPTICAL ELEMENTS

The theory section above describes a variety of approaches that have evolved to obtain optical information of surfaces with nanometer resolution. In each case the geometry of the experiment involves a tip interacting with a surface and this interaction is the origin of the highly localized, near-field optical signal that is being monitored. In this section we consider the type of near field optical elements that have emerged as suitable probes for nanometer dimension optical resolution.

A. SUBWAVELENGTH APERTURES

The first demonstration that light could be transmitted effectively through well-defined holes that were significantly smaller than the wavelength was presented by Lewis et al. [5,6]. These workers produced well-characterized (15 nm - 240 nm) holes using electron beam lithography on a silicon chip, imaged the holes with electron microscopy and then detected visible light even through 30nm apertures. A subsequent investigation [38] also was able to produce subwavelength apertures in a flat metal plate using a considerably simpler technique. In this method a solution of latex spheres was dispersed, dried on a glass slide and subsequently coated with metal. The resulting combination was sonicated in metal chloride to remove some of the balls and using this method apertures between 90 nm to 1000 nm could be produced. In spite of these advances such apertures in flat plates were not effective subwavelength optical elements because of the difficulty of bringing a hole in a flat plate within the near-field of a surface that was rough.

A solution to this problem was actually suggested by Synge in the first known paper on near-field optics in 1928 [39]. In this paper Synge proposed that a subwavelength aperture could be produced at the tip of quartz rod. As he wrote in 1928 "A better method would be if one could construct a little cone or pyramid of quartz glass having its point brought to a sharpness of the order of 10^{-6} cm. One could then coat the sides and point with suitable metal (e.g. in a vacuum tube) and then remove the metal from the point until it was just exposed. I do not think that such a thing would be beyond the capabilities of a clever experimentalist." In fact this is exactly what Dieter Pohl and coworkers accomplished in their first paper on the subject [4]. The idea of producing such a subwavelength tip was independently arrived at by Pohl since no one was aware of the suggestions of Synge until a historical perspective written by Dennis McMullan in 1990 [1]. In this implementation, a quartz rod was etched to a point with hydrogen fluoride (HF). The rod was subsequently, coated with metal and then crushed at the tip to form a small aperture. Such a method produced apertures whose subwavelength nature could only be inferred.

1. Micropipette Apertures

The first well-defined apertures at a point were produced by Harootunian et. al. [40]. These workers introduced techniques that were standard in electrophysiology to pull glass capillaries to tips that were in the range of 0.1μ. These microtipped capillaries were then coated with metal along the wall and at the tip to make them opaque to light thus producing a highly reproducible subwavelength optical aperture at the tip of a tapered glass structure. The aperture at the tip was illuminated with a optical fiber that was introduced into the back of the pipette as close to the subwavelength aperture as possible (see Figure 12). Within the last two years the capillary pulling technology, that was introduced to near-field optics in our laboratory, has been extended to quartz capillaries by the use of a carbon dioxide laser rather than a resistance wire as a heating element. This procedure is capable of producing capillaries with apertures at the tip of <10nm [41]. An example of such a capillary tip is shown in Figure 13A. It is known that an aperture exists at the tip of such a pipette since water introduced at the large end eventually exits the nanometer hole in the tapered end of the capillary. If larger structures are any indication the hole is <5 nm in diameter in such quartz capillaries. Such tips are not only smaller than anything that has been obtained with borosilicate or aluminum silicate capillaries but also are achieved with a tapering that rapidly approaches these small dimensions from the 0.5 mm starting diameter of the capillaries. In addition these microtips are much more resistant to breakage.

A recent discovery (see section IV A 2 below) that is particularly relevant to the use of these tapered glass structures in NSOM is the observation that such near-field optical elements are sensitive force sensors as will be discussed in the section on mechanisms that allow tracking the tip in close proximity to the surface.

2. Optical Fiber Apertures

More recently, with the availability of CO_2 laser pullers the technology we introduced for pulling pipette apertures has been extended to pulling single mode optical fibers [42]. These probes overcome the problem of bringing the illuminating fiber as close to the subwavelength aperture as possible and eliminate the coupling loss when the illuminating fiber is surrounded by air. Such probes have higher throughput since they efficiently couple all the inputted light directly into the region where the evanescent losses occur. Therefore, they have recently come into wide spread use as an efficient subwavelength aperture for NSOM applications. Unlike pipettes, that are coated both on the sides walls and on the front surface, the fiber apertures are produced by coating only the sides of the evanescent region of the fiber tip leaving the front surface exposed (see Figure 13B).

It should be noted that alternate techniques had been previously developed to produce tapered fibers that were based on etching of fiber tips. Such probes were used for PSTM [43]. For this technique one requires a fiber with a point without the need for the defined aperture that was essential in the original approach of near-field imaging. The etching procedure is capable of producing a much more rapid taper than the fiber produced with the pipette puller and this decreases the evanescent portion of the tip. Nonetheless, it not appropriate for NSOM since etching unlike pulling does not produce the cleaved, flat surface needed for a well-defined aperture. Rather, it generates rounded tips that are suitable for PSTM.

In addition an interesting new approach is the use of selective etching of the core and cladding of an optical fiber [44,45] to produce the structure shown in Figure 13C. The tip of this structure has unique bending force constants that are very important for lateral force sensing.

3. Microfabricated Apertures

Subwavelength apertures may also be produced by the clever use of conventional microfabrication techniques. An example of this is the recent work of Tortenese et. al.[46,47]. These workers have shown that such a subwavelength, protruding, conical tip can be produced in a thin silicon nitride membrane (see Figure 13D). The membrane in which this conical tip sits flexes with interactions of the tip with the surface and this leads to a direct method of force feedback to be described below. Presently such interesting applications of microfabrication technology do not compete with dimensionalities and characteristics of pipette and fiber probes but they do offer the significant advantage of the possibility of mass production.

4. Coaxial Waveguides

A most interesting structure that should give significant transmission of light through a subwavelength aperture is the analogue of an electrical coax in the optical regime. Such a structure would require a metallic core surrounded by a dielectric medium which is coated with another metal layer. An optical coax of this type acts just like the infinite subwavelength slit which was studied theoretically by Betzig et. al. [16]. It, like the infinite subwavelength slit, always contains at least one propagating mode regardless of the diameter of the tip and this should vastly increase the transmission through a subwavelength aperture. Fischer [48] performed preliminary experiments to define the characteristics of such probes for visible light transmission. The use of such a technique has been demonstrated for far infrared light by Keilman et al [49,50].

In these experiments a conically tapered, machined metal waveguide with the structure of the tip of pipette was used as an aperture (see Figure 13E). Since this structure was for use in the far infrared regime the dimension of the tip was on the order of tens of microns. By inserting a thin metal wire inside the waveguide an increase in throughput of over three orders of magnitude was recorded (see Figure 14). This structure is very useful for the far infra-red and microwave regions of the electromagnetic spectrum where the almost perfect conductivity of most metals provides an essentially zero skin depth in the waveguide medium. In such a case the reflection of the propagating radiation inside the waveguide is basically negligible at any dimension. This should be compared to the severe, $radius^6/\lambda^4$, coupling loss for a simple apertured structure. Thus, these structures allow for significant

intensities to be transmitted through apertures that would not otherwise emit any radiation whatsoever. Whether this technique can produce a significant transmission gain in the optical regime, where the finite conductivity produces a skin depth on the order of the final aperture diameter, remains to be seen.

Recently we have been able to pull a thin platinum wire to the tip of the micropipette using a CO_2 based laser puller. The walls of the micropipette were coated with metal and the resulting structure is seen in the SEM photograph reproduced in Figure 13F. The experiments to define the transmission increase that this probe can give are presently underway.

B. SUBWAVELENGTH LIGHT SOURCES

The ultimate NSOM probe that should be able to carry near-field imaging to the single nanometer regime and beyond would be a point source of light of dimensions that could approach a single molecule or atom. The micropipette forms an ideal basis for achieving such nanometer dimension light sources. Such sources which confine the light beam can be several orders of magnitude smaller than semiconductor technologies can achieve and, with the appropriate materials deposited in the tip of a pipette, have the flexibility of producing wavelengths that can extend deep into the ultraviolet. Such wavelengths are only a dream for present day diode lasers. In addition what is particularly relevant to NSOM is the fact that the micropipette structure on which all of the sources below are based is also a very sensitive sensor of surface forces and this will be elaborated below.

1. Optical Excitation

Fluorescent probes

The approach of producing a point source of light at the tip of a pipette was first described by Lieberman et al [34]. These workers demonstrated this approach by growing a highly fluorescent microcrystal in the tip of a micropipette (see Figure 15 A). Once such a fluorescent material was placed in the tip of the metal coated micropipette, a light source could be produced by simply illuminating the tip with an external beam of light incident on the front surface of the pipette. As will be seen below such a geometry could be readily integrated into a scheme for near-field microscopy [51]. The exciting aspect of such microtips of light is that the intensity reduction as a function of tip size is not exponential as is the case with transmission of light through a subwavelength aperture but rather depends solely on the change in area. We have obtained intensities of 40 nanowatts in dimensionalities approaching 100 nm which is approximately an order of magnitude greater than the best aperture based techniques. In addition, these intensities can be obtained without regard to the shape of the tip which is critical in the use of such probes as apertures and without the intendent difficulties of heating of the tip of the probe which is a limiting problem in fiber based aperture probes.

One of the initial subwavelength light sources investigated was a microcrystal of anthracene which was highly sensitive to photooxidation and bleaching. To overcome this problem highly stable organic plastics have been produced in the pipette tip [52]. These microplastics are readily formed in the smallest pipettes by using polymethylmethacrylate (PMMA) dissolved in chloroform with the appropriate organic dye mixed in the solution. This mixture is then inserted into the large end of a pipette that contains an internal filament and this filament draws the liquid into the very tip. Capillary action prevents the solution from escaping and contaminating the surface of the tip. As the chloroform evaporates a tiny fluorescent plug is formed inside the tip of the micropipette (see Figure 15 B and C). We have found that the most stable dye that can be used for these nano sources of light is a form of pyrelene that can be commercially obtained from BASF (for example BASF #384). These dyes which were designed for solar collectors [53] have a very high quantum efficiency and are extremely stable especially in encapsulating plastics in which photochemical destruction is minimized. Thus these plastic tipped pipettes are ideal for application as the smallest probes in NSOM microscopy.

Alteration of photon wavelength

Materials at the tip of the pipette can add several advantages and allow unique approaches to increasing the intensity of a light beam transmitted through a subwavelength aperture. One such advantage is when the

material in the pipette tip has a high index of refraction. In the region of the pipette which has a dimension larger than the wavelength the high index material acts to effectively guide the light wave to the subwavelength tip. In addition when the light reaches the tip because the effective wavelength of the light is shortened due to the high refractive index of the material the evanescence in the transmission will be reduced. Working near the absorption edge of a dye molecule can give a refractive index increase of at least 30 times which should reduce the effective wavelength to one that is not evanescent even in the smallest tips. The gain that this provides should be significantly larger than any small losses that may result from the light being passed through a few microns of absorbing material. Furthermore, it should be noted that if it can be arranged so that the sample has an index of refraction that matches the probe then the subwavelength light wave emanating from the probe would maintain its dimensionality as it penetrates the sample. Under such specialized conditions the super-resolution characteristics of near-field microscopy which are limited to regions in close proximity of the aperture may be extended to regions below the surface. This is an interesting result of a technique that would generally allow increasing the light transmitted through subwavelength holes and tubes. To our knowledge no experiments along these lines have been as yet completed.

Exciton enhanced transmission

In addition to the index of refraction effects, a crystal such as anthracene that allows the effective propagation of excitons in a subwavelength tip has been shown to be useful in enhancing the optical throughput of such a subwavelength tip [31]. This is accomplished by having the crystal span the region in which freely propagating photons have difficulty existing. The exciton can be generated in a region of the pipette with a diameter larger than the photon wavelength and diffuse through the subwavelength regime where photons cannot propagate. This effect may also result in an extension of the exciton lifetime since in such a subwavelength region radiative transitions should be prohibited. The incorporation of excitonic materials in the tip o f micropipette can be used to enable the reduction of the dimensions of the light source down to the level where the surrounding metal film will result in a quenching of the exciton. Quenching only occurs with a fall-off of r^6 and therefore, this direct quenching of the metal should not be apparent until the dimension of the light source is reduced to about 5 nm (see discussion below of exciton microscopy). Presently, experiments are underway to test this hypothesis by examining the exciton lifetime as a function of the diameter of the pipette.

In experimental tests of this phenomenon Lieberman et al [31] studied throughput experiments with and without crystals of anthracene in the tip of the micropipette. The results showed gain in the throughput when the crystal had been grown in the pipette tip. Anthracene was chosen for these experiments because of the considerable information available on the properties of excitons in these crystals. However, anthracene was not an ideal choice for the experiments since this material bleaches upon light excitation. In fact, in these experiments there was a burst of photons upon initial excitation of the anthracene crystal with the laser and then a subsequent reduction in the intensity of the emitted light due to bleaching. Thus, the gain by a factor of three in the transmission with the crystal was certainly only a lower estimate. This whole problem has considerable fundamental interest since the crystal can act as a bridge between a region where the photon can propagate freely and the tip of the pipette.

In terms of the two effects discussed above both the wavelength modification and energy transfer capabilities of material tipped pipettes can work in unison to aid in increasing the throughput of light through subwavelength regimes.

Non-linear probes

The subwavelength tip of a micropipette can also be used as a vessel for containing non-linear optical materials. Such materials can introduce a new set of properties to the tip of the micropipette. Two general classes of non-linear optical materials have been investigated. The first class of these materials is based on the considerable data that has been accumulating on two photon dyes. A particular interesting material in this regard is the electroluminescent polymer p-phenylene vinylene (PPV) [54]. Studies have indicated that this polymer has a two photon emission [55]. In our laboratory, Nily Kuck Ben-Ami has formed these polymers in the tip of the micropipette and has investigated the two photon emission that emanates from these tips. Data indicate that under femptosecond illumination, a 1 micron resolution pixel excited with two photon excitation elicits enough two

photon fluorescence in a μsec from a 100 micro molar concentration of dye in the pixel to generate exceptional images with conventional two photon microscopy [56]. These intensities should be more than sufficient for fluorescence excitation in a sample by a two photon tipped micropipette. This should be important for certain illumination schemes that have been used in NSOM and will be discussed below.

A second material that has been introduced into the micropipette tip is the non-linear optical crystal beta barium borate (BBO). In Figure 15 D is an example of a second harmonic generation (SHG) micropipette tip filled with BBO. This SHG was excited with a mode-locked titanium-sapphire laser emitting 120 fsec pulses at 720nm. Such tips have the potential for being used as subwavelength cross correlators of femtosecond pulses in femptosecond spectroscopic applications [57].

2. Near-Field Fiber Laser Probe

An improvement in the signal detected from a near-field optical fiber probe has been demonstrated by Betzig et al [58] by converting the passive fiber into an active lasing media. This was accomplished by pulling an Nd^{3+} doped single mode optical fiber and coating the tip as in the standard near-field fiber probe. The reflection from the tapered region acts as a mirror at one end of the cavity while the cleaved back end of the fiber acts as the other. The fiber was then pumped at the cleaved end with 753 nm light from a Kr^+ laser resulting in a 1060nm laser emission from the fiber. When such a probe is brought into the near-field of a surface changes in the boundary conditions can change the effective reflectivity of the tip of the probe. Small changes in this reflectivity are amplified throughout the gain medium and can result in significant changes in the intensity emitted out the back end of the laser. This effect is amplified further by operating the laser near the lasing threshold.

While the total signal emitted from the tip of the probe remains the same as in the fiber probe discussed above such a system allows one to observe changes in the sample reflectivity on an optical signal 3 to 4 orders of magnitude greater than the typical NSOM signal. This reduces the detection requirements and can potentially increase the imaging bandwidth in situations where shot noise in the detected signal is the limiting factor.

3. Stand Alone Subwavelength Light Sources

Chemiluminescent sources

The ideal near-field probe would be a microlight source without the need for any exciting laser beam. We have demonstrated such a source using chemiluminescent materials. To obtain such a light source a Cynalun light stick was bought from an auto parts store. These light sticks made by the American Cyanamid Company are obtainable in many colors and are used as 12 hour flares. They consist of two liquids that are held in separate compartments in the light stick until the stick is required to be lit. These two liquids can be extracted individually and then inserted together into the pipette. The liquid is sucked to the tip of the pipette by capillary action and the combination glows for several hours. The number of photons emitted by a 0.5μ pipette is only ~2,000 photons/sec and the stability of the light source is less than desirable because of the limited material present in the confined space of the pipette [7]. Such sources thus do not appear at the present time to be useful as a near-field optical probe.

Electroluminescent sources

In view of the considerable interest in electroluminescence for display technology this seems like an ideal method for generating a subwavelength source of light. This is especially true when one considers the structure of the pipette which allows for a material to be encased in a dielectric with an electrode inserted into the pipette and in contact with the electroluminescent material deposited in the tip. The pipette can then be covered with a metal from the outside such that it makes contact at another point with the material in the tip. The application of an electric voltage across the electroluminescent material in either an AC or DC fashion is sufficient to generate electroluminescence. Such a subwavelength, ZnS:Mn based green light source is presently working in our laboratories in Jerusalem [59] (see Figure 15 E). The limiting factor in the size of our light source is due to the grain size of the Zn particles which was 0.3 microns.

In 1990 a group of researchers in Cambridge announced the discovery of electro-luminescence in conjugated semiconducting polymers [60]. The initial results with poly(*p*-phenylenevinylene (PPV) [61] produced internal efficiencies (photons emitted per electron injected) of 0.001%. Significant improvements in efficiency (in excess of 1%) have been realized recently. Thus, to overcome the problems of particle size of inorganic electroluminescent materials discussed above we initiated a collaborative effort of our group with the laboratories in Cambridge and have shown that the sulfonium precursor to the electroluminescent polymer poly(*p*-phenylenevinylene (PPV) and the solvent processible polymer MEH-PPV can be grown in the tip of a pipette. In the past one difficulty in using these interesting polymer systems has been the requirement for the introduction into the pipette of a low work function electrode to inject electrons into the polymer. This has recently been overcome by the development of polymer systems that can work with electrodes such as aluminum [62]. In view of this development and the increase in efficiencies in these polymers that have been realized, we are confident that with some additional developments bright, long-lived electroluminescent polymer light sources with efficiencies of >10 % and dimensions of a few nanometers will be achievable.

C. RELATIVE BRIGHTNESS OF APERTURES AND LIGHT SOURCES

The important question for the various applications of near-field techniques (which include both imaging and patterning operations) is the brightness of the subwavelength sources of light that can be produced by the diverse methods that have been devised. Such a crucial question will determine the speed and the contrast that an imaging or patterning operation will require for the highest resolution points of light. In terms of the simple question of how much light can be passed through a subwavelength aperture at the tip of a hollow pipette or a single mode fiber the answer is clear cut. Experiments have demonstrated that for equal tip diameters the single mode fiber transmits approximately three orders of magnitude more photons. Absolute powers of nanowatts have been extracted by Betzig et al [17] for an 80nm aperture using 15 mW input power. The losses observed in the pipette and the fiber can be analyzed in terms of evanescence, area and coupling losses and maximum practically allowable input powers. For the single mode fiber the total observed seven orders of magnitude attenuation can be divided into a 4 orders of magnitude area loss and 3 additional orders of magnitude that can be attributed to the evanescent loss. If one compares this result with a multimode 50 micron fiber inserted into a micropipette with a 5 micron single mode fiber there is immediately a difference of two orders of magnitude in area loss in favor of the single mode fiber. In addition we have found that in the pipette there is an additional two orders of magnitude coupling loss in the micropipette which is not found in the single mode fiber. Nevertheless, a pipette can have considerably more power inputted into it and this reduces the difference between the pipette and the fiber by more than one order of magnitude. Furthermore, if one adds a suitable index matching liquid into the pipette one should be able to minimize the coupling losses and bring the overall throughput of the pipette to within one order of magnitude of the fiber. This is important because we have found in our efforts that the ease of using micropipettes coupled with advantages that the hollow structure provides compensates for the somewhat lower throughput in the aperture mode of use.

The absolute limit in the intensity of such transmission apertures is limited by the absorption of the light by the aperture in the evanescent region. For example using input powers larger than 15 mW in the 80 nm aperture experiments described above, would burn off the metal coating required at the tip of the fiber. Even at lower powers there is significant heating of the tip and this may prove problematic in certain situations. Rapid tapering to reduce the extent of the evanescent region may allow somewhat higher throughput but even for such geometries, the large absorption in the evanescent region ultimately limits the throughput of transmission apertures.

An important resolution of this problem was the transformation of the pipette tip from an aperture into a vessel for the deposition of a whole variety of materials that can create, modify and modulate light at the tip of the pipette. A pipette light source with a dimension that is <100 nm can have an intensity of as much as 40 nanowatts. This intensity can be readily understood by considering the BASF dye embedded plastic mentioned above which has been used as a solid state dye laser medium and has a photodestruction threshold 4kW/cm^2 [53]. This allows a very high power level to be used to illuminate the fluorescent plastic pipette tip. This translates to an excitation of approximately 0.5 microwatts from a 0.1 micron light source. Given a quantum efficiency approaching unity, the

limited penetration depth into the pipette given evanescent losses and the known absorption cross section of the dye permits an emission of ~40 nanowatts for a 0.1 μ diameter tip. This is an order of magnitude larger than the best aperture methods and thus such light sources can be reduced considerably in dimension since the intensity scales linearly with the volume of the fluorescent element at the tip of the pipette. A limit of ~5 nm will be reached only when the metal coating begins to quench the metal emission. In this case the intensity that could be extracted from such a structure should be on the order of nanowatts. These tip dimensionalities are only obtainable with long drawn pipettes or fiber structures which would transmit no light whatsoever in the aperturing mode because of their extended region of evanescence. With non-evanescently excited pipette light sources this problem does not exist. Finally, for such intensities there is no need to dissipate large amounts of evanescently absorbed light which reduces the heating problems.

D. OTHER PROBES

In addition to the near-field optical apertures and light sources discussed above other potential elements for sensing the near-field optical characteristics of surfaces can be envisioned.

1. Metallic Probes

Sharp metal probes such as the tips commonly used for scanning tunneling microscopy can also be used to study a variety of near-field surface optical phenomenon. These probes, which have atomically sharp tips can be used to scatter surface plasmon fields [26,63] and locally quench surface fluorophores [64]. In addition these tips can be used to tunnel electrons into directly into excited surface states to produce highly localized luminescent emissions [65,37]. In addition to such effects of tunneling induced luminescence metal tips can be used as point scattering sources for near-field illumination with specialized detection schemes that will be described below. Furthermore, if appropriately sized metal particles are placed strategically at the tip of a pipette, fiber or other probe and these particles are chosen specifically for generating the plasmon resonances described above these particles can be used for enhancing locally non-linear optical phenomena.

2. Optically Trapped Particle Probes

An interesting near-field probe, based on an isolated dielectric particle suspended just above a surface, has been proposed by Malmquist and Hertz [66]. The electromagnetic field of an infrared beam focused to a diffraction limited spot holds the particle in place just below the focus by the well known technique of optical trapping [67, 68]. This particle, which can be a few tens of nanometers in dimension, can be used to probe a surface in a number of ways. One possibility is to use a second visible laser beam to interact with the particle in either a scattering or fluorescence modality. A second possibility, which has been investigated [69, 70], is to use a particle that has strong non-linear optical properties. In this case the infrared trapping beam doubles as a source to drive a second harmonic [69] or two photon emission [70] from the trapped particle. The visible light produced by such a point source could provide the necessary illumination for an appropriately positioned surface. These interesting suggestions could extend near-field optical imaging into the realm of three dimensions subwavelength fluorescence imaging.

One of the nice features of such a technique is that the particle probe isn't necessarily destroyed by crashing it into the sample. Excessive force applied to the probe by interacting with a surface simply pushes the particle out of the trap. If the work is done in a solution containing multiple particles one simply has to wait for a second particle to settle into the trap and work may continue. Similar techniques have also been applied to atomic force microscopy [71].

3. Subwavelength Detectors

In addition to the light sources discussed above another method that has potential of relieving the problem of light throughput through a subwavelength aperture is to use the probe as a detector. The pipette provides an ideal structure for such an endeavor. At the Hebrew University of Jerusalem we have succeeded in growing a CdSe crystal that is in contact to a thin carbon fiber that has been inserted into the pipette [72]. The surrounding glass

acts as a dielectric shield around this structure and from the outside the pipette is covered with a metal coating that acts as the second electrode in this scheme that uses the CdSe as a detector of light. In spite of the fact that this detector is several orders of magnitude less sensitive than currently available photomultipliers this is compensated by the possible circumvention with this method of the large losses in transmitting light through a region below cut-off where the light wave is evanescent. Nonetheless the current sensitivities that we obtained were insufficient for effective near-field imaging.

4. Subwavelength Optically Excited Chemical Sensors

Recently, Kopelman et al [73] have extended the use of tapered optical fibers to create a probe capable of optically measure the local concentration of protons in a medium. These workers used techniques of photopolymerizing a pH sensor at the tip of fibers [74] and extended this to the tapered structures that are used in NSOM. The tip was immersed in the dissolved monomer solution and the light that was transmitted through the fiber and exited from the tip polymerized the material onto the tip of the tapered fiber. The polymer that was formed replicated the mode structure of the light that was exiting the fiber tip. The sensing molecules changed both their fluorescence intensity and their emission spectrum in response to the pH of the surrounding medium. This elegant technique creates a sensing region which can be precisely the dimension of the near-field region of the probe depending on the polymerization conditions. The molecules on the surface of this structure are then excited by light that is transmitted though the fiber and both the intensity and the spectrum of the emission can be monitored to determine the concentration of protons.

Micropipettes are unique vesicles for such chemical sensors. We have shown that a sol gel glass can be inserted into the tip of the pipette with appropriately chosen dye molecules encapsulated into the gel which is porous and allows the diffusion of water [75]. Dye molecules that are sensitive to proton and calcium concentration can be embedded in these sol gels and these molecules have been shown to respond to ionic concentrations. Such structures allow both chemical sensing and conductivity measurement through the tip to be performed simultaneously. We have shown that it is possible to monitor the reduction in the flow of ions through such a sol gel filled micropipette tip as the tip approaches a surface [76]. An additional advantages of this technique of embedding sensor molecules in a sol gel media rather than photopolymerizing the material is the fact that the sensor molecule can be freely interchanged to create sensors for a wide variety of specific ions. Since the sensor molecules are encapsulated in the pores in the matrix and are not involved in the chemical formation of the sol gel, switching the sensor does not involve reworking the chemistry of the sol gel growth.

These structures are also compatible with the epi-illumination non-evanescent technology that we have established. There is no need to transmit light through a fiber or through a pipette. The resolution that is achieved by such ion sensors comes from the confinement in the pipette tip itself. Thus the large signal to noise that we get from dye tipped pipettes for imaging is also applicable to these ion sensors. The response time and the z resolution of these sensors is also enhanced by the near-field effects of epi-illumination. Since the excitation fields decay rapidly upon entering the micropipette only the volume of material at the very tip of the probe will be excited and its emission detected. Thus the sensing region is kept small despite the fact that the entire probe tip is filled with the fluorescent sensor molecules.

5. Non-Diffracting Sources Of Excitation

The approach we have developed over the past decade for the controlled pulling of glass to produce elements for near-field optics [40] can be directly applied to the production of singular x-ray concentrators and apertures. X-ray apertures are notoriously difficult to achieve since the production of small dimension apertures have to be impressed in very thick metal screens in order to provide sufficient contrast between the x-rays emitted by the aperture and the x-rays transmitted through the screen. Because of this it is difficult to produce small apertures with sufficiently smooth walls to obtain well-defined x-ray beams of submicron dimensions.

The tapered pipette structure also forms the basis of x-ray concentrators. This is a result of the fact that the hollow structure of a tapered pipette provides for a medium such as air with a complex index of refraction that is larger than glass. This allows for total external reflection to occur from the surface of the inner walls of the

tapered glass capillaries. This seems to be the most promising design available today which can in principle achieve sub-micron beam size, a broad energy bandpass, and enhanced brightness (defined as photon flux/area).

The basic idea of x-ray concentrators, based on the pipette structure, is that the demagnification of the beam size results from repeated total external reflection from the inner walls of a tapered glass capillary. This idea, that was first suggested and theoretically investigated by Stern et al. [77], uses the demagnification of the cross section of a divergent beam by consecutive total external reflections from the internal walls of a tapered capillary. A capillary having a linear taper of angle β is shown in Figure 16. Unlike the other areas in which such tapered glass structures have been used in our laboratory in which Maxwell's equations have to be solved with the appropriate boundary conditions, in the x-ray regime, all the considerations are geometric. This arises both from the short wavelength and the index of refraction characteristics presented by an air filled tapered glass pipette. Assuming that α is the angle of incidence of the extreme ray of the divergent beam and θ_c is the critical angle for total external reflection, it can be shown [77] that the maximum demagnification of the beam's cross section from that at the entrance is given by

$$m_m = (\alpha + \beta) / \theta_c$$

Assuming perfectly reflecting walls, this yields a theoretical maximal demagnification as β goes to 0 of: $m_{max} = \alpha / \theta_c$ and a consequent brightness increase of $M = m_{max}^2$. For example, for a typical undulator $\alpha = 5 \times 10^{-3}$ μrad and a beam diameter of 0.5mm at the experimental station built around a synchrotron source, we obtain with a lead glass capillary a critical angle of 5 mrad at a wavelength, $\lambda = 1.5$ Å, and a theoretical demagnification of the beam cross section of 1000, to 0.5 μ. Since the total number of photons in the beam is conserved, the resultant brightness increases by 10^6. A smaller entrance capillary of say, 50 μ with the same taper will yield a beam size of 500 Å at the exit. In practice several mechanisms operate to reduce this theoretical gain and demagnification, among which the most important are shape imperfections and surface roughness. Theoretical studies [77] show that by using piece-wise linear, and non-linear tapers much higher demagnification and brightness enhancement are possible. The optimal shape, an elliptical taper, or a piecewise linear approximation thereto, could achieve spot sizes of 100 Å in diameter with intensity enhancement factors of order 10^8.

These results are of great importance since previous methodologies to generate submicron x-ray beams with sufficient intensities for practical applications have relied on complicated wavelength dependent solutions. Unlike visible light no focusing elements like lenses and wide-angular range mirrors exist for x-rays. Hence, a source of small size is often generated by illuminating a pinhole by a larger diameter beam . This in turn results in a great loss of intensity, as the size reduction is not accompanied by an increase in the brightness. More sophisticated devices, which in principle allow beam focusing, and hence an increase in brightness, suffer in practice from several shortcomings. Zone plates, for example, can only be used with monochromatic radiation, and, due to the short wavelength and large absorption length require thin zone widths and a large plate thickness. The resultant large aspect ratio, 100 or more, render such plates extremely difficult to construct. Furthermore, aberrations due to structural imperfections limit the focal spot size to >6-7 μ in the best plates available today Saitoh [78]. Aberrations also limit the focal spot size to similar dimensions in grazing-incidence x-ray mirrors as well [79]. Multiple-asymmetric-reflection perfect crystal monochromators are, again, narrow energy-bandpass devices, allowing, in practice, spot sizes no smaller than mirrors [80].

On the other hand, tapered glass capillaries provide a method of x-ray concentration which is wavelength independent and generates a beam of x-rays that can be highly directed over many hundreds of aperture diameters under the appropriate conditions. Thus, they can be used for nanometer dimension, three dimensional tomographic analysis. This is unlike the near-field optical probes discussed above which have a very small depth of field corresponding to less than one aperture diameter, and therefore can only be applied to detect surface optical phenomena. So far structures have been produced with spot sizes as small as 0.1 μ [81] and brightness enhancement of 960 at 6 keV have been obtained [82]. Theoretical considerations indicate that spot sizes as small as 100 Å are feasible with gains as large as 10^8. Furthermore, these capillaries are particularly well suited to low emittance third generation synchrotron sources and insertion devices. The current status of the results

demonstrating the potential of such glass structures as intense microfocus sources can be found in a number of papers in the literature in addition to those mentioned above [83,84,85,86,87,88].

6. Solid Immersion Lens

Mansfield and Kino [89] have investigated the use of a lens formed of a high index of refraction material to increase the numerical aperture obtainable and decrease the focal spot obtainable with ordinary lenses by a factor that is directly proportional to the change in the refractive index. This was accomplished by forming a hemisphere of a high index of refraction material which is placed beneath a conventional objective. This is an important extension of the standard oil immersion methodology of allowing for the use of objectives with numerical aperture larger than 1 by the introduction of a high index of refraction liquid that fills the region between the lens and the sample. This improvement in resolution is only capable of being used for imaging an object if the base of the lens is close enough to the object for evanescent coupling to occur.

IV. NEAR-FIELD INSTRUMENTATION DESIGN

A near-field optical system has to incorporate microstability and micromovement capabilities as in all scanned probe microscopes. In addition, near-field microscopes have to transparently incorporate a good far-field optical microscope for collection of light and overlapping field of view. Such integration has not been readily available in scanned probe microscope designs. With regard to the stability and micromovement requirements the resolution of the system is defined by the nature of the near-field collimation. The experimental information presently available on this collimation is at present minimal. Nonetheless there is total agreement that the near-field distance is some fraction of the aperture or light source diameter.

In view of these critical factors in NSOM this section focuses on two main topics. First, technologies of feedback in which a near-field optical element can be maintained within the near-field. Second, the design principles that are essential for integrating the probes and the feedback techniques with the associated technology of scanned probe microscopy on the one hand and far-field optical microscopy on the other.

A. FEEDBACK

The rapidly diverging nature of the near-field means that having some form of feedback to maintain the tip/sample separation is of vital importance when scanning the near-field probe over a surface. Even a small change in the distance to the sample will cause a large change in both the intensity and dimensionality of the near-field light spot. Such variations can significantly degrade the performance of imaging and patterning systems based on the near-field. The feedback is also necessary to prevent the probe tip from crashing into the sample during the approach and scanning. An effective feedback mechanism must give reliable topographic information about the sample and should be independent of the optical imaging parameters.

The proliferation of scanned probe microscopy techniques has produced a number of feedback methodologies which are all being adapted in one form or another to suit the needs of near-field optical imaging. These include electron tunneling (STM), optical tunneling (PSTM), ion conductance (SICM), both normal force (AFM) and lateral force (LFM) sensing and capacitance measurements. Furthermore, there are specialized methods that have been designed specifically with NSOM in mind to achieve feedback using optical means.

1. Electron Tunneling

The STM [90], being the first of the scanned probe microscopy techniques, is an obvious choice for a feedback sensor. There are two main drawbacks of this methodology, however, which have thus far restricted its general acceptance. First is the requirement for a conducting sample which would not allow the examination of biological material, and second is the very strong axial sensitivity of the STM which imposes constraints on the stability of the system and complicates the design. Furthermore, STM has extreme sensitivity to electrical disturbances which requires extensive shielding. Nonetheless, in situations where the sample is naturally conducting, or when the sample can tolerate a thin, semi-transparent conducting overcoating such as gold or platinum-iridium, tunneling can provide an ideal form of distance regulation. In these cases, a small voltage is applied to the metal coating surrounding the near-field aperture and, when the tip is close enough to the sample, the current tunnels across the gap and into the sample where it is monitored and used to adjust the height of the gap.

Tunneling was first used by Durig et al [91] to halt the approach of a probe as it came into the near-field. Lieberman and Lewis [92] and Hartmann et al. [93] have built instruments which are stable enough to produce STM images with a near-field probe while simultaneously recording the near-field optical information. Details of the construction of such instrumentation are provided below. It should also be mentioned that tunneling has been observed from dielectric materials placed on metal films. In one such experiment microwave fields on the surface induce tunneling currents with the aid of microwave induced field harmonic generation [94]. Nonetheless, non-conducting materials are much better tracked by using force sensing methods.

2. Normal Force

The most general purpose technique for regulating the distance between the near-field probe and the sample is to sense the attractive and/or repulsive forces that arise when the tip is brought into close proximity of the sample [95]. This is done by scanning a sharp stylus at the tip of a tiny lever arm over the surface at distances of up to several hundred angstroms. Very fine cantilevers capable of sensing pico -Newton forces [96] are now readily producible. The interaction between the tip and the surface (Van der Walls, coulombic, magnetic, etc.) flexes the arm slightly. The tiny deflection that occurs in the cantilever as a result of these forces is detected and used as a feedback to regulate the distance. This deflection is typically detected by reflecting a laser beam off the cantilever and monitoring its deflection with a position sensitive detector. Optical interferometric techniques are also used. The crucial requirement for such a technique is that the spring constant of the lever be such that it will flex in response to variations in the surface forces (i.e. changes in topography) and not break or deform the surface being scanned. With the probes available today, scanning force microscopes have been used to image almost any conceivable surface.

The difficulty in applying force feedback to near-field optics lies in preparing a subwavelength aperture at the tip of the microcantilevered structure needed for force sensing. One example of a near-field optical probe which is suitable for force distance regulation is the microfabricated silicon apertures produced by Tortense et al [46]. These apertures are integrally fabricated onto thin, flexible silicon membranes which closely resemble commercial silicon force sensing cantilevers. A spring constant of 34N/m allows the membrane to deflect without damage to either the probe or sample as the aperture makes contact with the surface. Force imaging with such a probe is also possible although the spring constant is too stiff to allow imaging of soft samples. Near-field imaging in a PSTM mode with the tip of a silicon nitride force cantilever has been reported [97]. This is based on the transparency of the silicon nitride which picks up the evanescent field and allows it to propagate beyond the tip and into a detector. In addition, such cantilevers have recently been used as sources of scattered light for near-field imaging [98].

We have shown that glass micropipettes can be bent near the tip to produce a cantilevered structure provide an excellent atomic force imaging probe [99]. For the initial experiments with position sensitive detection of normal force (see Figure 19 A), the bending of the tip was accomplished with a microflame and a small mirror was glued to the cantilever in order to allow the sensor to be inserted into conventional force microscopes. In a subsequent development [100] we replaced the microflame with a focused CO_2 laser which permits fine control of the bending operation and allows quartz cantilevers, which are more resilient, to be bent. Such a cantilevered quartz pipette is shown in Figure 17. An additional development was the replacement of the glued mirror by an integrally polished reflecting surface (see Figure 18). In terms of their force sensing capabilities micropipettes can be tailored to the imaging problem at hand. Specifically, they can be prepared with a wide range of force constants, with tips that can be sharp or blunt depending on the degree of the perturbing force that the surface can endure, with high aspect ratio tips for imaging tall structures and they have the capability of having materials inserted into the hollow structures for a variety of applications. One such application is NSOM in which a fluorescent material can be deposited in the tip of the bent micropipette for simultaneous force and NSOM imaging and ion sensing. In addition the same technologies have been used to bend the tip of single mode optical fibers. These fibers effectively light to be transmitted around the bend while permitting the preferred imaging mode of normal force sensing. The procedure for achieving such elements has recently been perfected and work is underway to demonstrate the singular capabilities of such multifunctional imaging elements.

3. Lateral Force

A force technique which permits the use of straight micropipette and optical fiber probes is the measurement of the frictional forces that arise between the flexible tip of a straight probe and a surface. This is done by laterally modulating the tip at or near its resonance frequency and measuring the damping in the vibration as the tip approaches the surface. Two implementations of this technique have been independently developed and demonstrated by Toledo-Crow et al [101] and Betzig et al. [102] and more recently a simplified implementation of monitoring lateral forces with a straight pipette has been demonstrated by Shchemelinin et al. [103].

Vaiz-Iravani and coworkers use a sophisticated differential optical detection system to monitor the vibration amplitude off the side of a pipette tip [101]. In this scheme (Figure 19 B), a laser beam is divided by a Wollaston prism whose axis is at 45 degrees with respect to the laser polarization into two orthogonally polarized beams with a small angular separation. A microscope objective is then used to focus the two beams onto the side of the pipette with a linear separation of approximately 100 microns. The oscillation of the pipette tip introduces an unequal phase shift to the two reflected beams. When the reflected beams are then recombined by the Wollaston prism the phase shift will rotate the polarization of the reconstructed beam at the frequency of the pipette oscillation. The magnitude of this rotation is measured by passing the beam through an analyzer and using a lockin detection at the oscillation frequency. The detected signal can be made linearly proportional to the amplitude of the modulation by adjusting the lateral position of the Wollaston prism across the beam.

In Betzig et al's scheme, shown in Figure 19 C, the light emanating from the near-field aperture is used to both image and monitor the vibration of the tip [102]. A portion of the light is directed by a beam splitter through a small pinhole and onto a photomultiplier. The spatial modulation of the probe thus produces an intensity modulation in the light passing through the pinhole whose amplitude is dependent on the spatial modulation amplitude of the probe. The amplitude and phase of this modulation is monitored with a lock-in amplifier. When the probe begins to encounter the frictional surface forces the amplitude of the modulation will be damped and a phase shift will be observed. Either of these signals may be used to monitor the strength of the damping force on the probe tip. The disadvantage of this technique is that the monitoring signal is detected through the sample, limiting its application to transmission NSOM schemes.

Rudman and Schmeztmellian (Figure 19 D) have developed a technique which works with a reflection system and requires no complex alignment [103]. These workers simply focus a laser onto the tip of the probe with a low power objective and monitor the shift in the diffraction pattern with a position sensitive detector. The detected light is actually reflected off the sample simplifying the alignment procedure. Sensitivities of several angstroms were obtained with this method.

Lateral force systems have the advantage that straight probes may be used, simplifying the fabrication and transmission of the optical signal if aperture NSOM is to be employed. Nonetheless if imaging of soft or rough samples is to be accomplished effectively lateral force methods lateral forces have to be minimized in order not to distort the images. Furthermore, the experimental implementation of such an imaging protocol requires lock-in detection which slows down the imaging process. Finally, lateral force techniques do not work well in liquid environments where the lateral vibration motion of the tip is strongly damped. Using a cantilevered structure to monitor normal forces has the advantage of greater force sensitivity and some inherent protection of the tip since even if the feedback system fails to accurately track over some feature the tip may flex upwards and not be damaged. In addition, the recently introduced non-contact imaging modes that accurately image delicate samples can be readily implemented with normal force sensors.

4. Ion Conductance

Hansma and coworkers [104] have demonstrated an ion conductance imaging technique which may be readily adapted for near-field optical feedback. An electrolyte is injected into the near-field aperture that also bathes the sample. A voltage is applied to the probe generating a small current from the ions diffusing out of the tip under the influence of the electric field. When the aperture is brought close to the surface the flow of ions into and out of the aperture is restricted, reducing the current and increasing the effective resistance of the tip. The resistance becomes significant as the tip/sample distance is reduced to less than the aperture diameter, which is precisely the preferred distance for near-field optical imaging. This technique has been well-developed for patch clamping and performing elecrophysiological measurements on biological membranes [105] and is responsible for stimulating the development of the glass micropipette electrodes that we have adapted for near-field optics. An ion conductance feedback technique is particularly well suited for biological applications where it is often desirable to keep the sample in an environment which is as close to ambient as possible. Hansma and coworkers have produced topographic images with submicron resolution both with glass micropipettes [104] and microfabricated silicon [47] apertures. Bent micropipettes are ideal for this form of scanned probe microscopy.

5. Optical Tunneling (PSTM)

The frustrated internal reflection technique described above (see Figure 9), in addition to being a near-field imaging technique in its own right, may also be used to provide topographic feedback information so long as the sample has relatively uniform dielectric properties. When a near-field aperture tip is placed within the evanescent field present above the sample, a fraction of the light proportional to the field strength at that point will couple into a propagating mode in the tip. So long as the corrugations in the surface are of subwavelength dimension, maintaining a constant field strength should give a good approximation of the surface topography. A second wavelength may be simultaneously transmitted through, or collected by, the aperture to provide spectroscopic near-field information independent of the sample topography.

The extent of the evanescent field and the height of the tip tracking can be adjusted by varying the angle of incidence and wavelength as described above . Longer wavelengths, in addition to increasing the extent of the field, are advantageous because they can be far removed from the frequency of the imaging light, reducing interference during image formation. These long wavelengths also afford protection against bleaching for any contrast enhancing fluorescent dyes used in the sample.

6. Capacitance

Scanning capacitance microscopy has been demonstrated by Matey and Blanc [106]. We have used such capacitance signals as a feedback method for near-field lithography [107]. Capacitance imposes similar restrictions to tunneling in that it requires a conducting sample and conducting probe but the interaction has a longer range than tunneling making it easier to work with although less precise.

7. Reflection Interferometry

The light emitted from the tip of the near-field probe has been used by Bozhevolnyi et al [108] as a mechanism for tracking the surface (see Figure 19 E). These workers used cross polarized detection to monitor the interference between the light reflected from inside the tip of an NSOM fiber probe and the light emitted from the tip, reflected from the surface and coupled back into the fiber. The idea of using cross polarized detection is based on the assumption that the polarization conversion is most efficient near the tip of the probe. This allows the weak signal reflected from the sample to be detected while rejecting most of the light reflected from along the fiber probe. Usin this technique, these workers were able to monitor interference fringes out to several microns from the sample.

8. The Near-Field Dependence Itself

The exponential nature of the near-field of a subwavelength aperture can theoretically be used by itself to regulate the distance between the aperture and a sample without the need for an independent sensing technique. This method was investigated in Jerusalem by Lev Lubovsky [109]. Applying a small (several nanometer) vertical dither to the probe will produce a modulation in the strength of the near-field interaction of the probe/sample interface. This interaction is strongly distance dependent and can be used as the basis for determining the distance between the aperture and the sample. By dithering simultaneously at two different frequencies with different amplitudes it may be possible to determine the exact distance independent of the absolute interaction strength. Experiments to verify this hypothesis are currently underway in our laboratory.

9. Confocal

An optical method for tracking sample surface profiles and monitoring tip/sample separation has been developed by Hrynevych et. al. [110]. These workers obtain very high axial sensitivity by using a variation of a confocal microscope arrangement shown in Figure 19 F. In this setup, two confocal pinholes are used, one places slightly above the image plane and the second slightly below it. As the sample height is varied the image, and corresponding optical signal, will come into focus first at one plane and then at the other. By monitoring the signal differential, height variations as small as 1nm can be detected with this technique. Both the sample surface

and the near-field optical probe position can be monitored while the probe is scanning in order to accurately track the surface. This technique has a lateral optical resolution only as good as a classical optical system so the actual recorded profile information represents an average of the surface over an approximately half micron wide region. If there are no sudden, sharp surface height variation, however, this technique can provide a simple, non-intrusive method for probe feedback.

10. Contact Mode Nsom Without Feedback

Initial NSOM results in our laboratory were in fact obtained by painfully bringing a micropipette tip into contact with a surface watching it flex and then monitoring the light at each contact point [111]. With a straight probe this was next to impossible to accomplish since most of the tips in the operation rapidly were destroyed. With cantilevered micropipettes or fibers such an approach of contact mode NSOM is very feasible. In fact contact mode AFM has been the technique of choice in AFM imaging. However, in AFM a feedback technique is required not only to bring the tip to the surface but also to measure the deflections of the cantilever that mimics the topography of the sample. As can be seen in Figure 17 a bent near-field optical element can be visually brought in contact with the surface using a well-integrated optical microscope that is an essential component in NSOM but has been given somewhat less emphasis in AFM. Once in contact, scanning the sample and monitoring changes in the intensity of light due to index of refraction changes would readily give an NSOM image.

11. Summary of Present Acceptance of Feedback Mechanisms

The three lateral force techniques described above, or variations of them, have achieved the widest acceptance among today's near-field optics researchers. This stems from the fact that lateral force detection is relatively easy to implement because it works well with both the tapered optical fiber and micropipette probes that are commonly used today. Nonetheless, in general for imaging lateral forces have to be minimize as noted above and thus, elements that are capable of feedback without lateral force distortions seem to us to be the future elements of choice in NSOM.

B. THE INTEGRATION OF NEAR-FIELD, FAR-FIELD AND SCANNED PROBE MICROSCOPIES

1. General Design Principles

In this section we consider an overview of the constraints that must be addressed in order to construct an effective near-field optical microscope system. Basically NSOM instruments can be designed to work either in reflection or transmission. In both of these modes the principle of reversibility allows for either illuminating or collecting through the near-field element (see Figure 20).

Vibration Isolation

Vibration isolation is crucial in any system designed for scanned probe microscopy since the probe tip is scanned in close proximity to the surface. This requires the instrument to be well-isolated from mechanical and acoustical vibrations [112]. These principles have been well-studied and the general conclusions are that the microscope has to be as small and as rigid as possible in order to avoid the coupling of external disturbances.

Approach Mechanisms and x-y Scanning

A standard question that has to be addressed in the construction of any such microscope is the mechanism used to bring the probe within the near-field. This requires a method that allows for travel over relatively large distances with high resolution as the probe approaches the surface. One method that is generally employed is a small stepper motor with a lever reduction system to increase sensitivity. In spite of the availability of such methods for several years a particularly important development that we and others have incorporated into near-field microscopes is the Burleigh inchworm [113]. This device allows for essentially unlimited translation of any tip with 2nm steps. The advantage of this device is that it is hollow shafted and this simplifies the insertion of such elements as optical fibers for illumination and collection of light.

The fine x,y and z scanning is done with cylindrical piezoceramic scan tubes that are now standard in all scanned probe microscopies. The scan ranges depend on the size of the tube and the applied voltages. A standard 1 inch (2.5cm) tube gives a 10 μ full-scale, xy deflection and 1 μ axial extension with a 250 V bias. Tube scanners are available with scan ranges of >100 μ and such scanners can be readily attached to the hollow central core of the inchworms that were originally designed for ultrahigh vacuum applications.

Overlapping fields of view

In all scanned probe microscopies it is very beneficial to integrate a more conventional form of imaging that allows for a view of the probe tip with respect to the sample. In scanning tunneling microscopy attempts in this direction were initially centered on integrating this microscope into a scanning electron microscope where the resolution generally is comparable to the field of view of the STM. Similarly in near-field optical microscopy it is incumbent to have the ability to place the subwavelength optical element at a point in the sample where one desires the high resolution that this microscopy provides. The SEM solution is not practical for near-field microscopy since it completely undermines the unique features of NSOM to work under ambient conditions, without the destructive effects of electron beams. Therefore a principal driving force in the instrument development has been schemes that build a near-field optical instrument within the overall constraints of a conventional light microscope. One of the problems in this integration is related to the constraints imposed by the use of the tubular piezoelectric scanners since these scanners require a long tube in order to obtain a large scan range. This long axial extension of the piezo tube makes it difficult to bring an objective lens close to the sample. One solution is to scan the tip instead of the sample, although this causes a number of secondary problems which will be discussed below. Other ingenious approaches involve placing the lens entirely inside the tube scanner [114,115]. Another, option is to use a tripod scanner [116]surrounding a microscope objective and this is described below.

2. Transmission NSOM

An instrument that has been reproduced in an number of laboratories is seen in Figure 21 [51]. The NSOM head sits above an ordinary (Zeiss Axiovert) inverted microscope. The sample stage of the microscope is removed and in its place a vibration isolation system is built on either side, straddling the microscope. The instrument is built in a closed loop form to maximize its rigidity. The near-field optical probe is glued to a threaded insert which is screwed into a mount on the piezo-electric ceramic tube scanner. The piezo is glued directly to the axis of a hollow UHV Burleigh inchworm. The sample rests on a 16mm diameter, 150μ thick glass cover slip. The cover slip is inserted into a Teflon sample mount between two thin o-rings and held tightly by a threaded insert. The long working distance objective of the microscope is corrected to look through the thickness of a cover slip and focuses on the top surface of the glass where the sample is placed. The sample mount rests in a machined x-y stage with 2mm travel for fine positioning of the sample with respect to the pipette. The whole assembly opens for easy placement of the sample and replacement of the tips.

The optical signal for NSOM imaging is acquired through the conventional far-field inverted microscope. For standard transmission NSOM light is fed into the pipette tip from the rear by means of a thin optical fiber inserted down into the very tip of the pipette as indicated in Figure 21A. Alternatively, an epi-excitation technique may be used to produce light from a fluorescent plug grown inside the tip of the micropipette as is seen in the picture in Figure 21B. In addition to the intensity advantage this provides (see above), this method does away with the need to bring an external fiber into contact with the micropipette probe and thus removes a potential source of mechanical instability.

This system provides a very flexible integration of a number of scanned tip microscopies in addition to NSOM while allowing for the conventional optical microscope to be used with all the flexibility that is available to it. For example, this allows the positioning of the micropipette over a region of interest by viewing through the conventional microscope while the pipette tip is scanned by the cylindrical piezoelectrical fine positioner. The same system is capable of simultaneously obtaining NSOM images through the aperture at the tip of the micropipette while generating tunneling images from a tip in the metal coating that surrounds the pipette [92].

These results will be discussed below. Thus, the microscope can be used in far-field and near-field optical imaging and with tunneling not only as a feedback technique but also to generate simultaneous images.
The microscope has also been used with a system to measure ion conductance feedback, as described above.

The same microscope has also been used in an epi-illumination scheme with the subwavelength, fluorescent, microplastic light sources described above. This approach to NSOM is schematically described in Figure 22. A laser beam (dotted line) is reflected off the dichroic mirror in the far-field microscope and focused by the microscope objective through the sample and onto the micropipette tip. The emitted light (solid line) passes through the sample, is collected through the same objective and is transmitted through the dichroic mirror onto the photomultiplier.

One disadvantage of the combination of the above instrument with the epi-illumination scheme is in the mode of collection of the light emanating from the tip. The objective lens of the microscope collects over a large field of view which includes the pipette tip and the surrounding sample. Any autofluorescence in the sample contributes to the background and degrades the image. Further difficulties with the above instrument also include image artifacts which arise due to the scanning motion of the pipette. With epi-excitation fluorescent tips the problem lies in the difficulty in producing a perfectly uniform illumination spot. This is particularly troublesome with coherent laser excitation where interference produces a speckle pattern. As a result of these variations in the strength of the excitation, the intensity of the light source varies from point to point in the image. A similar problem exists in standard transmission NSOM due to the non-stable coupling between the inserted fiber and the pipette tip. Small translations of the pipette during the scanning apparently result in the excitation of different optical modes inside the pipette. This can result, under appropriate conditions, in significant changes in the transmitted intensity.

The resolution of these problems is obviously to hold the probe fixed in space and translate the sample to achieve the desired scanning. The disadvantages of this technique are the potential reduction in scanning rate due to the increased mass of the sample and the difficulty in bringing the lens close to the surface as discussed above. Holding the pipette still is also advantageous for epi-excitation fluorescent tips since there is now no need to defocus the excitation to cover the entire scan range. Thus, low intensities of the incident laser can be used since the laser can be focused to a diffraction limited spot on the tip of the pipette instead of defocussing to cover the entire scan range. In addition, only the sample region in the immediate vicinity of the tip will be exposed to the excitation. This will reduce damage to the sample and cut down significantly on the background fluorescence.

Further advantages of keeping the subwavelength point of light fixed is the ease of integrating such an instrument with methodologies of confocal microscopy [117]. This will allow for better rejection of the out-of-focus light since the near-field is only a surface effect and light from other optical planes degrades the image. However, the major advantage in this design is the fact that only in such a scheme is force sensing easily integrated into the microscope.

A design of a sample scanning near-field microscope head developed in our laboratory is seen in Figure 23. The microscope consists of three plates hinged at one end and separated at the other by two Burleigh inchworms. The lower plate contains the microscope objective and rests in place of the microscope stage. The middle plate contains the sample scan system which consists of a tripod piezo scanner positioned around the microscope objective on which the sample rests. The scan system allows both fine scanning and coarse sample positioning by using an inertial translation mechanism. The upper plate contains a second piezo scan system, concentric with the first, to hold and position the probe. The upper plate also houses the AFM optics (diode laser and position sensitive detector) for both shear force and normal force detection. The upper inchworm is used to move the top plate with respect the middle on for the tip/sample approach while the lower inchworm translates the upper two plates as a unit with respect to the lower plate allowing automated sample focusing. The fine vertical positioning of the inchworm based system coupled with the sample scanning mechanism enables confocal optical sectioning of the sample simply by incorporating a pinhole at the focus of the microscope objective. A photograph of the NSOM head in place above an inverted optical microscope is seen on Figure 23B. Supplemental microscope optics for reflection imaging has been placed above the head in this picture.

An alternate design that is in the literature is by Betzig and coworkers. These workers insert one cylindrical piezo into another larger cylindrical piezo (see Figure 24). The tapered optical fiber is inserted into the small piezo in order to dither the tip. The dithering of the tip is employed in the lateral force scheme developed by these workers as described above. The sample is placed on the larger piezo and is scanned relative to the tip. An approach mechanism that is not shown is used to bring the tip in close proximity to the sample. The advantage of this design is its compactness. The disadvantage is that it is limited to employing the pinhole based shear force scheme which is affected by the transmittance of the sample.

3. Reflection NSOM

In order for the advantages of NSOM to be fully realized it is important to design NSOM instruments that can incorporate the possibility of imaging in reflection. This is crucial for imaging opaque samples. Ideally one would like to illuminate and collect through the same probe. This would be helpful in the design so that the illuminating probe does not obscure the view of the collection optics or the collection optics does not obscure the placement of the probe. In practice however this is not possible because of the strong back reflection of the light from the subwavelenth region of the probe would swamp signal in this geometry. The exception to this is the fiber laser probe discussed above.

In place of this ideal geometry two approaches that have been used are to either illuminate through the tip and collect the light reflected and/or scattered to the side or to illuminate from the side and collect the light through the probe place above the sample (see Figure 20). The difficulty of course is that the tip and the collection optics both have to lie on the same side of the sample.

For such imaging there have been a variety of unique designs. The first reflection instrument was that of Fischer who used an aperture that were produced in a metal coating deposited on a watch glass. Since Fischer used a flat aperture he did not encounter the strong back reflection that is normally seen in a tapered probe and thus was able to perform a reflection experiment by transmitting and collecting the light through the same aperture. However such flat apertures have limited applicability.

An obvious method for collecting the reflected light off a sample that is illuminated with a near-field optical probe is to place a long working distance objective at an angle relative to the surface. This was first reported by Clime et al. [118] (see Figure 25).

An interesting approach to reflection NSOM involves the choice of a large, long working distance objective lens for the conventional light microscope in which a hole is bored for the near-field optical tip [119]. Such an approach has been demonstrated by Suzuki et al [120] who produced such an objective and inserted an STM tip into the hole (see Figure 26). This allowed both the sample and the tip to be viewed from above. Replacing the STM tip with a near-field optical probe would allow the light that is reflected and scattered off the surface to be collected with a relatively high efficiency. The light that is lost by blocking the central part of the objective is a small percentage of the area of the lens.

An alternate technique is to place the entire near-field probe beneath the microscope objective. This is readily accomplished with the cantilevered pipette or optical fiber probe whose tip can be less that 50μ in length. Using an objective with a 5mm or larger working distance also allows uncantilevered fiber probes to be inserted at an angle. By mechanically bending the thin section of the fiber near the tip with a radius of curvature of several millimeters the entire fiber may be inserted while still maintaining the characteristics of a straight probe. This technique has been effectively implemented [121]. The difficulties in working so close to the objective can be removed by replacing the conventional microscope objective with a large reflecting objective which can have significant working distances. An example of an instrument using this technique will be presented in the cryogenic section below.

We have been able to collect reflected light for NSOM with sufficient efficiency by using micro-lensed fiber optic [122]. Such a fiber, held in a fixed position relative to the near-field probe, may collect light with a numerical aperture as high as 0.5. It may be possible to place a number of fibers surrounding the tip from all sides

to further increase the collection efficiency. Although this technique can give extremely good light collection efficiency it does not provide an imaging capability and as noted above it is important to have the capability to simultaneously image the sample and NSOM tip.

Finally, an approach that allows illumination and reflection through the same probe is the fiber laser probe described above. In this case the back reflection does not swamp the signal but rather provides a carrier signal which is modified by the changing boundary conditions at the tip and is amplified by the lasing medium of the fiber.

4. Optical Detection

An important consideration in building a near-field optical system is the type of the optical detection scheme that is employed. Obviously, based on the light signal that are available from subwavelength apertures or light sources any detection scheme has to be capable of sensing individual photons and should have a high quantum efficiency for detection of the light. There are three possible choices that fit into this criteria. These are photomultiplier tubes (PMT), avalanche photodiodes (APD) and charge coupled device (CCD) camera. In principle the serial imaging of NSOM does not require a CCD but when spectral imaging is involved a CCD coupled with a monochromator is beneficial. Thus, the most common system in use today that can detect single photons is the PMT and this detector coupled with photon counting detection systems is the most prevalent in NSOM systems. APDs are gaining popularity for several reasons. They have considerably greater quantum efficiencies, like CCDs, in the visible and near infrared (70 - 80% in comparison to <20% for PMTs) and they are more compact and less susceptible to noise than PMTs. Their principle drawback however is in the size of their detector area. This requires careful alignment so that the light probe is accurately imaged onto the active detector area. For ultimate in speed and for spectral ranges that extend into the deep ultraviolet, the photomultiplier is the detector of choice.

5. Far-Field Light Collection Angle And Efficiency

The total light collection efficiency both for transmission and reflection NSOM, while very important, is not the only factor in determining the quality of the near-field image. As a result of the directional sensitivity that exists in the propagating far-field signal, using the largest numerical aperture available does not necessarily give the most information. Calculations indicate that under some conditions the propagating light is directed from the surface at large angles [19] as was described above. Also the interaction with the near-field probe may redistribute the energy in the far-field while the total integrated intensity may not change significantly. Thus, collecting all the emitted light with the highest numerical aperture objective may not gather all the available information. We have seen this effect experimentally when the same image collected with a higher numerical aperture objective had lower contrast.

6. PSTM Schemes

Instrumentation for imaging near-field frustration of the local evanescent field produced above an interface by total internal reflection has been developed in a number of laboratories [123, 124, 125, 126]. Typically the light is introduced into a glass substrate on which the sample is placed by means of a prism. An etched or pulled optical fiber probe is used to frustrate the evanescent wave produced by internal reflection and converts it into a propagating component which is guided by the fiber to a detector. In many of the experiments with this method the approach was readily controlled by monitoring the onset of the frustration which has an exponential response. The technique's requirements for micromovement and vibrational stability are identical to conventional NSOM.

Two ingenious suggestions to experimentally achieve the principles of PSTM using standard silicon nitride force cantilevers have been made by van Hulst et al [127]. In the first of these suggestions (see Figure 27) an evanescent wave is launched on a surface using the standard prism method discussed above and a force probe is brought into the evanescent field and some of the energy in this field is coupled into the tip of the force probe. This radiation which is coupled into the force tip is then imaged with a lens onto either a photomultiplier or a CCD as the force sensing method scans the topography of the surface. Simultaneous force and PSTM images have been

generated with this method [126]. A second approach suggested by these workers is to generate an evanescent wave in the tip of a silicon nitride cantilever and then to frustrate this wave as the tip of the force sensor comes into contact with surface features. van Hulst et al [128] have generated images with both these methods although the lateral resolution that is governed by the geometrical and optical characteristics of the force tip have still not reached that which can be obtained with conventional NSOM. This latter method does overcome one of the difficulties in PSTM which requires a transparent dielectric sample in which an evanescent wave can be effectively propagated along the surface.

7. Near-field Plasmon Interactions

The experimental constraints of interacting a tip with a propagating surface plasmon wave is in many respects similar to what is required in PSTM. In fact in a particularly exciting paper Hansch and coworkers have described an instrument in which they measured localized quenching of surface plasmons using a tunneling tip acting as a near-field optical probe. In this experiment a prism was coated with silver and a surface plasmon wave was launched by total internal reflection of a using either a HeNe or a HeCd laser as shown in Figure 28. The coupling to surface plasmons reduces the overall reflected intensity. Thus, when the tip approaches the surface and scatters the plasmons the reflected intensity is increased and this is monitored by a photodiode. These workers were able to obtain simultaneous tunneling and surface plasmon near-field images of the surface and obtained a resolution of several nanometers.

8. Modified Scanning Tunneling Microscopes

Scanning tunneling microscopes may be modified to allow optical interactions between the probe and the surface by the insertion of a high numerical aperture lens placed in close proximity to the tunnel tip. This allows one to direct light onto the tunneling junction and monitor the local electrical effects [129, 130], or conversely, to collect light created at the junction by the tunneling electrons [65]. The instrumental requirements here are similar to what is required in reflection NSOM but force feedback is not, of course, needed to control the z position of the tip. In addition non-linear effects have also been investigated with these instrument. The effects include rectification of laser light by the nonlinear aspects of a tunnel junction [130], In this instrument the voltage across the tunnel junction generates difference frequencies in the microwave regime with infrared lasers impinging on the junction. Other workers have also built similar instruments for investigating the generation of higher harmonics when rf fields are applied between a tunneling tip and a sample [131].

9. Cryogenic NSOM instruments

Scanning tunneling microscopy at cryogenic temperatures is now a routine technique, however workers are just beginning to develop near-field optical microscopes suitable for low temperature work. Imaging at cryogenic temperatures requires immersing the entire microscope into a liquid or gaseous nitrogen or helium environment which greatly complicates the design. A recent publication by Grober et al [132] describes a reflection NSOM instrument developed specifically for work inside a dewer (see Figure 29). The instrument uses the shear force feedback technique developed by Shchemelinin et al [103] described above, with all the feedback optics located outside the dewer. The far-field collection optic is a Schwarzchild reflecting objective and is located inside the dewer with all the rest of the optics and detection system positioned externally. The far field light is transmitted through a window at the base of the dewar and the feedback light enters and exits through the side windows. The sample is held on a cylindrical piezo that is connected to a translation stage driven via a small stepper motor with a feedthrough into the dewar. The fiber is fixed in place above the objective and beneath the sample.

NSOM imaging in a cryogenic environment is further complicated by the need to avoid introducing any heat source near the tip or sample which could cause evaporation and bubbling of the liquid coolant. In order to prevent this from occurring it is necessary to reduce the input power into the near-field probe from the normal operating level where input intensities are kept just below the level which would burn off the coating of the probe. Thus, the signal levels available for cryogenic imaging are lower than in other situations. The best resolutions that have been achieved are 0.2 μ. Nevertheless, this is better than what could be obtained with conventional optics due to the difficulty of introducing a high powered objective within the confines of a dewar.

V. NEAR-FIELD IMAGING RESULTS AND DISCUSSION

All the image contrast mechanisms that are familiar to conventional optical microscopists are also available in the near-field regime. This includes all of the single photon excitation methods, which are associated with refractive index [133], polarization [144], fluorescence [134] and differential and interference techniques [145], and many of the non-linear optical techniques such as two photon fluorescence [135], second harmonic generation [136] etc. Near-field optical imaging is also fully compatible with all developed optical staining and sample preparation techniques. A particularly exciting and unique aspect of these near-field achievements is that it has also been shown that optical near-field probes exist with the capability of simultaneously imaging with multiple channels of force, tunneling, conductance and even ion sensing. This simultaneous imaging capability is already yielding exciting comparative results which is surely going to be crucial to future achievements in the applications of near-field optics.

A. EARLY NEAR-FIELD IMAGING

1. The First Results

The first approaches in near-field optics led to a series of images obtained during the next decade which were generated without feedback. This required a great deal of effort in the approach of the near-field aperture without crashing the probe and destroying the aperture. Nonetheless super-resolution was certainly demonstrated in these first pioneering attempts at near-field optics. These first attempts at NSOM could readily achieve 250 nm resolution with visible light and on good days resolutions of between 100 and 150 nm could be obtained. All of these images were obtained on extremely high contrast test structures but they clearly showed the possibilities of this newly emerging technique. To obtain a resolution that was close to 0.25 μ even on high contrast structures with a lens instead of a subwavelength hole would require the most sophisticated lenses available which cost at least over $1 K dollars. Nonetheless, at this stage in the NSOM development the field was only exciting to those individuals committed to the success of the technique. In a few short years that have elapsed since then, the field has rapidly evolved and spread over many centers throughout the world with conferences held on the exciting new results being obtained daily in laboratories that span physics, chemistry, biology and materials research.

Some of the first results that demonstrated the resolution of NSOM in comparison with standard techniques that were available at the time such as scanning electron microscopy and optical microscopy were performed by Harootunian et al. [40]. These comparative measurements used a knife edge test and examined the same edge with these microscopies, optical, NSOM and SEM. The edge was produced by depositing aluminum on glass. Such a test of resolution is standard in all microscopies that are based on a linear response functions of the imaging beam with the sample. The results are shown in Figure 30. The lower two traces in this figure are respectively obtained with SEM and NSOM. Both traces clearly show the sharp edge with a similar response and this was a very good indication of the resolution potential of NSOM. This data indicated that the edge was not perfectly sharp and had a 60 nm slope which explains the breadth of the SEM line scan.

The NSOM trace in this case was generated using light that was apertured by a pipette tip and this subwavelength point of light was placed in the near-field of a sample by detecting a tunneling current. The light passing through the sample was collected by the lens of a conventional optical microscope with a numerical aperture of 0.5 and focused onto a detector. The next trace in this figure is a conventional far-field image of the edge as it is scanned under the same microscope lens that collected the light using conventional illumination. For comparison a calculation is displayed at the top of the figure which is the theoretical response of the system with a 1.4 numerical aperture and in this calculation the edge is barely detected.

Another worker who was active during this early period of NSOM was Fischer [38] who was then at the Max Plank Institute fur Biophysics at Goettingen. An interesting series of images were obtained in Fischer's first paper in which light that was propagating with s and p polarization through an aperture in a flat screen and onto a glass hemisphere which reflected the light back through the aperture. Significantly greater contrast was detected with p polarized light since this polarization induces a larger dipole in the aperture.

A number of workers beginning in 1988 also began to obtain near-field images using frustrated internal reflection schemes [123,124,125,126]. This technique has the advantage that it provides essentially a topographic rendition of the surface and thus tracks the surface as it images. Figure 31 A shows a gray scale contour map of the surface of an indented sapphire sample taken by Paesler et. al. [137] with a PSTM. The indentation extends to a depth of 250 nm below the surface and the resolution of surface features is approximately 50 nm. Figure 31 B shows a PSTM image of a 1 micron period SiN grating taken by Van Hulst [138]. The exponential decay of the evanescent field allows this image to be obtained with a vertical resolution of approximately one Angstrom and a lateral resolution of 30 nm.

Care must be taken when interpreting PSTM images since, in addition to the evanescent surface waves, the probe can also pick up radiated waves far from the surface. This radiation will be emitted from any surface corrugations on the order of a wavelength that is present. For example Figure 32 [126] shows PSTM line scans above the same grating shown in Figure 31 B at increasing distances from the surface. Each line scan that form the y axis of this figure is at a different height relative to the surface. As is evident from the image, the far field radiation interferes to produce a repeating grating like structure at large distances from the surface. Scanning at this distance can produce a PSTM-like image containing no near-field information.

Several years went by in which images were being obtained by dedicated aficionados. NSOM was in fact the first scanned tip microscopy since research at Cornell began in late 1979. Nonetheless the world of scanned tip microscopy experienced an explosion with the advent of the scanning tunneling microscopy. This development led to a world wide effort to develop ever simpler methods of such scanning microtip microscopes and NSOM gained quietly from these efforts without many in the scanned tip community realizing that it existed. As technologies developed it became technically possible to solve many of the problems of NSOM. The fruition of this integration has within the last two years resulted in the new probes discussed above and feedback methodologies discussed above which have resulted in the daily flood of exciting results that flow from the many centers in the world that have entered the field of near-field optics.

2. Imaging With Improved Probes

The next step in the development of near-field microscopy was the integration of new probes aimed at overcoming the problem of the intensity of light that can be obtained from a subwavelength point. Two of the important advances in this area are the use of the optical fiber instead of the pipette as a passive aperture and active pipette based light sources. These probes allowed workers to examine samples of more general interest.

A selection of images have been obtained with optical fibers is shown in Figure 33. In this Figure a SEM image (A) is compared with a conventional far-field optical micrograph (B) and near-field micrographs (C and D). The resolution that is apparent in the unprocessed near-field image (C) is approximately 50 nm. After Fourier deconvolution higher spatial frequencies are present. This near-field image was obtained without feedback. This is permitted by the relatively large signal that allows images to be acquired sequentially as the aperture approaches the near-field.

Images have also been obtained with active pipette light sources again without feedback because of the large signal strengths that can be obtained from such sources. In this image, seen in Figure 34, colloidal gold balls with a diameter of 40 nm are visible. These balls are used as a standard contrast enhancing mechanism in transmission electron microscopy of biological materials and this should be an important point of comparison in future demonstrations of NSOM resolution as applied to biological samples.

An important aspect of imaging without feedback is that there is a dramatic increase in both the signal and the resolution when the probing aperture enters the near-field. This is a characteristic of a subwavelength aperture in which there is an exponential increase in the signal upon entering the near-field.

B. NEAR-FIELD IMAGING WITH FEEDBACK

In order to make effective use of near-field imaging it is incumbent to incorporate a feedback mechanism to track the surface. This is necessary for two reasons. First, to maintain a constant probe intensity due to the exponential variation in the near-field intensity in the vicinity of the probe. The second reason is to both allow a rapid approach into the near-field and to protect the probe from crashing into the sample. An additional benefit of the feedback is that it allows the generation of simultaneous topographic imaging for a comparative study in order to better understand the effects of near-field contrast.

1. Tunneling Feedback

Simultaneous NSOM Imaging

Figure 35 shows an example of simultaneously acquired tunneling and optical image using a hollow, gold coated micropipette as both a near-field aperture and a tunneling probe. The image is of a 3.6 μ square region of a chrome film with small defects. In the tunneling image (Figure 35 A) a number of defects can be seen scattered over the surface. The transmission through the sample as a function of pipette position (Figure 35 B) shows an almost perfect correlation with the tunneling image both with regard to the position of the defects and to their shape. In addition, the presence of two imperfections in the lower right hand region of the image are clearly indicated in the optical scan even though they are barely apparent in the tunneling image. The reason these imperfections are not clear in the STM scan is due to a convolution of the outer diameter of the pipette with the rough grain structure of the sample which prevents the tip from tracking into these very small depressions. Nevertheless, the difference in optical contrast shows up very clearly in the NSOM image. This highlights the advantage of having simultaneous and complementary imaging techniques.

The tunneling and NSOM images in this example are shifted laterally by approximately 0.2 μ since the tunneling image is generated by a random protrusion of the gold coating lying somewhere on the circumference of the pipette while the optical image is obviously centered with the aperture. The diameter of the pipette aperture, which was approximately 0.2 μ in this case, determines the resolution of the optical image. The actual response to the pipette passing over the sharp well- defined edge of one of the holes is shown in normalized, superimposed line scans extracted from both the tunneling and optical images in Figure 36. The shift in the images in now clearly evident. The rise in the optical signal (from 10% to 90%) occurs over approximately 60nm which is significantly less than the pipette aperture diameter. This occurs due to the convolution of the circular pipette geometry with the sharp edges of the high contrast structure used as our test sample. In addition, it is probable that the energy distribution in the exit pupil that is the pipette aperture is not uniform. The STM images, coincidentally, also show a similar response which is determined by the effective radius of curvature of the outer pipette diameter at the tip and the actual protrusion from which the current tunnels, which limits the response to coarse surface features.

Simultaneous tunneling and near-field optical imaging with an etched optical fiber probe has also been demonstrated by Hartmann et. al [93]. After coating the side of the fiber, these workers covered its front surface with a thin, semitransparent PtC coating and imaged a test sample of coated salt crystals as shown in Figure 37. Since the tunneling came from the front of the probe there is no lateral displacement between the two images. Recently, similar results have also been obtained with a pulled fiber that was gold coated [139]. These workers obtained simultaneous tunneling and collection NSOM of microfabricated gratings.

Simultaneous Plasmon Imaging

Figure 38 shows an image of simultaneously acquired near-field plasmon interactions and tunneling data as reported by Specht et. al [26]. In this experiment surface plasmons were launched on an evaporated silver layer on the surface of a prism with an attenuated internal reflection scheme similar to PSTM. A tungsten tunneling tip is then brought into contact with the silver surface, scattering the surface plasmon wave (see Figure 28). This increases the intensity of the reflected wave and probes the local plasmon strength. Figure 38A is a tunneling image of the surface showing the silver grains and a small indentation in the film produced by pressing the tungsten tip into the surface. Figure 38 B and C are the near-field optical scans of the plasmon scattering signal taken at a constant height of 3 nm and 10 nm respectively. Figure 38 D is an image recorded in a hybrid STM/plasmon mode taken by recording the optical signal while maintaining a constant tunneling current.

Surface plasmon fields have also been studied with tunneling probes by other workers. The effect of the optical plasmons on the tunneling current has been studied by Moller et. al. [[65]] in a configuration similar to the one later used by Specht et. al. The decay length of optically excited surface plasmons has also been studied by Kroo et. al. [[140]] with an STM.

Recently, workers have employed the more conventional PSTM geometry described above to observe direct evidence of the localization of surface plasmons in fractal geometries [[141]]. These workers detected regions of high localized intensity of light corresponding to the dimensionalities and exhibiting the polarization sensitivities that were calculated from established theories of such fractal colloid clusters (see Figure 39). This experiment is one of the first applications of near-field optics in which the resolution of these techniques was required to substantiate established theories on an important physical system.

Tunneling induced optical effects

Localized optical properties of semiconductor surfaces have also been studied by a number of workers with the aid of tunneling induced luminescence [[65]]. This can be used, for example, to study the spectroscopic properties of quantum well structures. An example is seen in Figure 40 in which a scanning tunneling microscope has been used to tunnel electrons directly into excited surface states while recording the localized visible luminescence as described above. Figure 40A is a high resolution optical image of the luminescence emitted when scanning a tunneling tip across a multiple GaAs/GaAlAs quantum well structure. Interfaces between the layers are imaged with a resolution better than two nanometers.

Molecular resolution has been obtained by Berndt et al [[142,143]] by applying a similar technique to fullerenes. These results that were obtained at a temperature of 50 K are seen in Figure 40B have reached that highest resolution with light that has been reported. The diameter of the emission as defined by the translation of the probe is 4 Å. The results seen in Figure 40B show excellent between the location of the individual fullerenes in the STM topography and the photon emission map. The emission appears to arise from inelastic tunneling between the tip and the gold surface on which the C60 molecules sit. Possible molecular electronic states that may be involved in this process are excitonic states or collective electronic excitations.

Other approaches which combine interactions between tunneling effects and electromagnetic radiation are describe above in the instrumental section (IV B8) above.

2. Force Feedback

An important advance in the past two years has been the independent introduction by several groups of lateral and normal force methodologies that can be readily incorporated into near-field optical systems.

Lateral force methodologies has been incorporated into both micropipette and optical fiber probes [[101,102,103]]. Betzig et. al. [[102]] used a transmission technique to obtain 20 nm resolution lateral force imaging of a sample of latex balls. This is seen in Figure 41. Normal force sensing with cantilevered micropipettes as described above, have been effectively used to image a variety of samples. The images shown in Figure 42 were obtained using the standard method of measuring cantilever deflection with a position sensitive detector [[100]]. The image seen in Figure 42A is an image of red blood cells while in Figure 42B shows a scan of a millipore filter in which holes of 0.2 μ are clearly imaged with structure well below this resolution. Finally, in Figure 42 C and D are images of a compact disc surface stripped of its laminated layer and a calibration grid structure.

Simultaneous NSOM / Lateral-Force Imaging

NSOM imaging with micropipettes have been obtained by Toledo-Crow et. al. [85] simultaneously with a lateral force image. These workers used their polarization based split beam interference technique to obtain the images seen in Figure 43 A and B. In this image a human blood smear was imaged with both lateral and near-

field optics. As in the simultaneous tunneling images described above variations and similarities are seen in comparing the force and the NSOM images.

Another example of such simultaneous images has been obtained with an optical fiber [86]. In these images (Figure 43 C and D) a PMMA film has been patterned with electron beam lithography to obtain a regular pattern of 50 nm holes that are readily detected by both force and NSOM imaging.

Vaez-Iravani and Toledo-Crow have also shown that in NSOM all the conventional imaging methods such phase contrast [[144]] and polarization imaging[[145]]. Until these results all the work concentrated on simply recording the amplitude modulation and neglected the effects of phase and polarization on the near-field images that were recorded. The technique which these workers have developed allow the extraction of either pure amplitude or phase information rather than a composite. In order to achieve such imaging the NSOM was configured into a Mach Zehnder interferometer in which a beam from a laser was spit into two components. One was sent through an optical fiber in which the phase of the light was modulated and this beam illuminated the sample. The light collected from the sample was interfered with a reference beam from the same laser and the resulting signal was analyzed using heterodyne detection techniques by feeding back the signal into the modulation of the fiber thus allowing the extraction of pure phase information and generating an interference contrast image. The results of such imaging is seen in Figure 44 in which Figure 44 A is the signal at the modulation frequency, Figure 44 B is at the second harmonic of the modulation frequency and Figure 44 C is the pure amplitude variations mathematically extracted from the first two images.

3. Feedback Induced Artifacts

The use of an independent feedback mechanism to track the surface is crucial to protect the tip and maintain resolution while imaging in the near-field. Nevertheless, due to the exponentially decaying nature of the near-field, tracking roughly corrugated surfaces while scanning can introduce artifacts into the image and complicate the image interpretation. For example, as an aperture passes over a small protrusion in the sample, the reduced distance between the tip and the sample may increase the coupling of the evanescent waves present at the tip into propagating radiation. The sample may thus appear to contain optical density contrast where, in fact, only topographic variations are present.

This phenomenon has been investigated with the aid of tunneling feedback and a micropipette where it is possible to decouple the STM and NSOM images from each other and the extent of the interaction can be accurately determined [[92]]. This can be seen from the line scan across a hole shown in Figure 36 which seems to indicate that the two images are essentially independent of each other. The optical peak corresponding to the hole appears after the tunneling tip has finished tracking through the hole, and thus represents a true variation in optical contrast. Close inspection of the small asymmetry in the optical response, however, reveals that some interaction does take place. As the leading edge of the pipette dips sharply into the hole a small increase in the optical signal can be observed. This is a result of the radiating aperture of the pipette being slightly closer to the metal film that is the sample. The change in height is approximately 35 Å and the corresponding increase in the optical signal is approximately 2% of the maximum transmission recorded when the pipette aperture was positioned directly over the hole. Since this sample has a very high optical contrast, these small artifacts induced by the coupling to the feedback do not interfere and are not even visible in the optical image shown in Figure 35 B. This interaction does have to be taken into account, however, and may well present a problem with lower contrast samples.

4. Near-Field Point Spread Function

Measuring the energy distribution in the near-field of a subwavelength aperture is of both theoretical and practical importance. Calculation of the electromagnetic propagation in the near-field of an aperture is very complex and has only been rigorously calculated for the simple, isolated geometries described above [Section II]. The actual behavior of an aperture under the modified boundary conditions given by the proximity of a sample has never been determined for the spherical apertures which are always employed in NSOM. Knowledge of this distribution would allow precise constraints to be set on the accuracy that is needed for the placement of a probe

during scanning in order to maintain a given resolution. Since the structure of the near-field is dependent on the sample, and thus is not spatially invariant, it is not possible to define a global modulation transfer function (MTF) for a near-field microscope. Nevertheless, knowing the general distribution of the intensity under the conditions at which the image was taken does allow for some mathematical deconvolution after acquisition to further enhance the resolution.

Direct measurement of the point spread function of a near-field aperture have been obtained by scanning a micropipette over a group of small holes of various diameters in a metal film at increasing distances from the surface [146]. A sequence of images at approximately 100 nm intervals is shown in Figure 45. Resolution is maintained over several hundred nanometers and then deteriorates rapidly. The symmetry of the imaged holes indicated that there is no internal structure in the energy distribution within the plane of the pipette aperture.

5. Resolution And Signal-To-Noise In Near-Field Imaging

It is difficult to define a rigorous expression for the spatial resolution of a near-field optical microscope. This arises from both the non-linear transfer function and questions concerning what definition of resolution is chosen. In addition one has to take care in distinguishing true optical contrast effects from topographic variations as discussed above. The response when passing across a sharp edge is commonly used as a first approximation to the probe's resolving capabilities. This response may not be retained, however, when passing over more complicated structures. For example, we measured a 60nm response when passing a micropipette over the edge of a 200nm hole but when two touching holes were imaged with the same pipette they are just resolved by the dip between them according to the Rayliegh criterion [147].

The signal to noise ratios obtained with near-field imaging are currently one of the limiting factors in image quality. Due to the inherently low light levels involved and the necessity of obtaining an image in a reasonable amount of time, NSOM images are generally signal limited in performance by the shot noise at each pixel. The exception to this rule occurs when using epi-illuminated fluorescent probes where the residual fluorescence excited throughout the sample can produce a background limited performance. By carefully aperturing the collection to only detect the tip emission, however, it is possible to obtain a signal limited performance. How long one is willing to wait to obtain an image will generally determine the image quality. This will also affect the image resolution since there is a trade off between the total number of pixels that can be acquired and the integration time at each pixel. With bright probes, good transmission images can often be obtained in a matter of seconds on high contrast samples, while fluorescent imaging, discussed in the next section, can take over an hour for a single frame.

Due to the non linearity of the near-field response coupled with the relatively poor signal to noise ratio when compared to other optical imaging techniques, great care must be taken when using Fourier dconvolution in an attempt to improve NSOM resolution. Improper use of these techniques can introduce spurious spatial frequencies and other artifacts.

It is important to note that all the techniques and instrumentation of near-field optical imaging described in this paper have significant application even where actual subwavelength resolution is unattainable or unnecessary. There are many situations where physical constraints in the optical system prevent one from approaching the diffraction limited resolutions theoretically obtainable with far-field optics. Examples include studies which take place in a vacuum or in cryogenic environments [as described above] where one can not readily approach with a high power, high quality objective. In such circumstances even 0.5μ or 1μ resolution would represent a considerable improvement over what is currently available. Such imaging may be easily implemented by scanning a relatively large near-field probe and may be a simpler solution than attempting to integrate an entire far-field optical microscope into the study. Other examples of the use of near-field like optical elements where lenses could not operate is the application of the ArF excimer laser at 193 nm in the liquid environments of ultramicrosurgery where the deep ultraviolet wavelengths cannot propagate [148, 149, 150, 151, 152]. This will be discussed below in the section on excimer laser near-field lithography.

C. NEAR-FIELD SPECTROSCOPY

1. Imaging With Fluorescence Contrast

Fluorescent staining has long been a standard contrast enhancing mechanism for conventional optical microscopy. Many hundreds of fluorophores have been developed over the years which specifically bind to particular sites in biological samples. Near-field imaging can take direct advantage of this vast array of staining methodologies. The price that is paid for such fluorescence imaging is the additional reduction in the already limited NSOM signal. Nonetheless this lack of signal can be somewhat compensated for by increasing the integration time. One advantage as compared to conventional parallel fluorescence imaging is that serial acquisition of the image only results in bleaching of the particular pixel being interrogated. This is an advantage when a illuminating aperture is used for near-field imaging. This advantage is lost when techniques such as PSTM, collection mode NSOM and epi-illumination methods based on linear spectroscopic phenomena are used for image formation.

The potential importance of near-field fluorescence imaging was realized by our group in the early days of NSOM [153, 154]. In one of the first papers that was published on NSOM it was demonstrated that using an array of apertures that was placed in contact with a film of perylene allowed for the detection of fluorescence through the apertures that were as small as a few hundred Angstroms [153]. These experiments were performed in epi-illumination. That is to say the laser was transmitted through the apertures and elicited fluorescence from the perylene. The resulting fluorescence was detected back through the same subwavelength aperture. A similar study was performed by Fischer [155]. In this study Fischer illuminated a solution of rhodamine through a subwavelength aperture in a metal film and was also able to detect significant fluorescent intensities. Based on our results a calculation was performed that showed the feasibility of fluorescence near-field imaging. This calculation indicated that given the expected exponential decay of the near-field the fluorescence excited from the zone next to the aperture would be exponentially more intense than any fluorescence excited beyond this region. In essence, one of the real advantages of near-field fluorescence microscopy is the lack of interference of out-of-focus light, a feature that many conventional optical fluorescence microscopic techniques strive to achieve.

The next step in such fluorescent imaging was to scan a well-defined fluorescent object which could also be imaged with another methodology. The object that was chosen was a fluorescent perylene grating produced by contact printing of perylene through a mask produced by electron beam lithography. On the resulting fluorescent grating a thin coating of gold was deposited in order to allow for a SEM image and to permit control of the contact between the pipette metal coating and the gold surface. Near-field fluorescence and scanning electron microscopy line scans of the grating are compared in Figure 46. The superb comparison [40] gave us confidence that NSOM would eventually evolve into an superresolution method of fluorescence imaging.

Betzig et al using shear force feedback has presented fluorescent images on fixed cultured cells that were stained with a dye complex selective to the cellular cytoskeleton [156]. The cytoskeleton structure is an integral and important part of most cell architectures. Images were obtained that seem to indicate single actin filaments. For these images a fiber probe was employed together with lateral force feedback. The experiments indicated that the sensitivity of the method was approximately 30 fluorophore molecules for an aperture that was somewhat less than 0.1 μ. The imaging under such conditions took close to one hour. Examples of the images that were obtained on these fixed cells is seen in Figure 47. These cells, which are called fibroblasts, send out thin flat processes in the processes of wound healing. In these processes are found actin filaments which were labeled with a mushroom toxin called phalloidon that was fluorescently labeled. The images seen in Figure 47 are of these actin filaments in such a process. Figure 47A is a conventional optical image while Figure 47B is a confocal image. The shear force and the NSOM images are seen in Figure 47C and D. The optical and confocal images appear to have similar resolution although the confocal image has more sharply defined borders. The shear force image provides essentially no information on the actin fiber while the NSOM image indicates clearly the actin fibers at a resolution that is clearly higher than the confocal image.

Instead of integrating the fluorescence intensity as described above, a more powerful approach is to examine the full spectrum at each point. A test of the potential of this method is a two color fluorescence

experiment in which the emission at each point was detected through two filters with different transmission properties. In this experiment [157] a 68 nm latex spheres stained with different dyes were identified by monitoring the fluorescence spectrum.

2. Low Temperature Fluorescence Imaging

In optical spectroscopy it is advantageous to perform low temperature measurements for several reasons. First, materials at low temperature have a considerably enhanced absorption coefficients. Thus if fluorescence imaging is being employed the increased absorption leads to a corresponding increase in the fluorescence intensity. Second, at lower temperatures there is a considerable reduction in the homogeneous line width of molecular species which increases the resolution of the optical spectroscopic signal. Third, fluorescence intensities are increased at low temperature because of the reduction in the non-radiative pathways which significantly increases the quantum yield of the emitters. Finally, there are a large class of phenomena that can only be observed with low temperature measurements. These include many of the effects seen in quantum well devices and other mesoscopic systems.

There is a growing interest in the development of scanned probe microscopes for cryogenic applications since this combines the ability to perform spectroscopy as a function of temperature alterations. There have been efforts made in integrating cryogenic technologies to other scanned probe microscopes for several years and there is even a commercial version of a scanning tunneling microscope (STM) with millidegree Kelvin capabilities [158]. However, NSOM measurements at low temperatures are only just beginning.

One of the first applications of low temperature NSOM is found in a paper by Keilmann and coworkers [50]. In this work a far-infrared (λ=300μ) NSOM was constructed at 4°K. Basically a conventional aperture scanning NSOM was used inside a liquid He dewar to monitor the effect of localized absorption on the cyclotron resonance frequency of a two dimensional electron gas. This has provided information on defined optical interactions in structures that give rise to the quantum Hall effect.

A subsequent study at low temperature has been a recent paper published by Grober et al [159]. In this investigation a GaAs/AlGaAs quantum wire was studied at 1.5°K. The quantum wire was located within an environment of single and multiple quantum wells and the luminescence from each of these structures could be differentiated by their wavelength. The entire region of the sample being investigated was illuminated with a tunable titanium-sapphire laser and collection mode NSOM was employed with an optical fiber to map the luminescence from various regions of the sample. The instrument used in these experiments was described above. The signal collected through a 0.25 micron probe was 10^4 photons/sec. These low signal strengths are a repeating problem in fluorescence NSOM. It remains to be seen whether NSOM can achieve the resolution of methods such as catholuminescence [160] in which an electron beam or a tunneling tip [161] is used to generate light in localized region of a multiple quantum well/quantum wire structure. The advantage of NSOM in this regard if the resolution problems can be overcome is the optical selectivity of the excitation.

More recently Hess et al [162] took complete fluorescence spectra of the quantum constituents of a multiple quantum well structure. The fluorescence signal was excited by a variety of optical fibers that ranged from 150 nm to 250 nm. These workers found that the luminescence originated only from spatially and spectrally discrete states. A comparison of the near-field, far-field and spatially averaged near-field spectra collected in these experiments are shown in Figure 48. The temperature, magnetic and line-width measurements established that these centers arose from excitons laterally located at interface fluctuations.

3. Chemical Sensing With Fluorescence

Chemical sensing with polymer encapsulated fluorescence sensors at the tip of an optical fiber has been investigated over the last decade [71 XX]. Recently, Tan et al [73] have combined this technology with the methodology of near-field optics for generating a straight tapered glass probe with submicron dimensionality. At the tip of such a probe a pH sensor was photoplymerized as described above. These workers illuminated the sensor

at the tip of the probe through the optical fiber and detected changes in the emission spectrum of the dye molecules at the tip of the probe as the pH of the environment was changed (see Figure 49). Although no images were generated in this study the probe was inserted into a developing fertilized egg in which pH changes were occurring and the changes were detected.

Chemical sensing with sol gel filled micropipette probes has been performed by Samuel et al [75]. In these experiments the probe tip was illuminated externally in epi-excitation and the fluorescent intensity was monitored as a the pH of the environment was changed. Due to the minuscule volume of the sensing region, coupled with the rapid diffusion of ions through the porous sol gel matrix the response time of the sensor was shorter than the response time of the experimental arrangement employed. As noted above such structures for measuring ion concentration have the advantage of permitting conductance to be monitored. In addition, the technology that we have developed of epi-illumination together with the bending of such near-field optical elements will be important for their application in the investigation of cell membranes in aqueous media. These bent normal force probes are also capable of being used for surface potential or charge density measurements [163, 164, 165] and thus, the combination of subwavelength optical ion sensing, conductance measurements, simultaneous normal force measurements and investigations of the electrostatic characteristics of membranes portend this to be a very fruitful application of near-field optics.

4. Fluorescence Lifetime Imaging

An alternate and highly developed method for obtaining spectral information about a sample is to examine the lifetime of the fluorescent emission rather than its spectrum [166]. We have obtained such spatially resolved, fluorescence lifetime, NSOM imaging with a micropipette acting as a light source [146]. A sample with microdomains of two different perylene based dyes was prepared. The region where the microdomains meet is shown in a conventional fluorescent optical micrograph in Figure 50. The fluorescence spot excited by a pipette placed just behind the sample and illuminating it in transmission is clearly visible in Figure 50 A. The field view scanned by the pipette is seen in Figure 50 B in which the pipette is being scanned over the region of interest within the overlapping field viewed of the far-field optical microscope. An NSOM image of the fluorescent intensity is shown in Figure 50 C. The two dyes can be distinguished because of their different fluorescent intensities when excited at a fixed wavelength (488nm).

The fluorescence lifetimes were measured by modulating the laser beam input to the pipette and using a frequency domain phase fluorometry system [167] in place of the standard photomultiplier/photon counting system normally used for NSOM imaging. The phase and amplitude of the fluorescent lifetime signals were recorded simultaneously with the conventional fluorescent NSOM image. The phase signal is seen in Figure 50 D. The actual lifetime of both dyes range between 3.5 to 5 nanoseconds and is dependent on the concentration of the dye. The thickness of the dye layer also effects the lifetime since absorption and re-emission of the fluorescence will extend the effective measured lifetime. The transition between the two dye regions can be seen most clearly in the phase data (Figure 50 D) as a change in the lifetime of the fluorescence. The region where the dyes overlap is also apparent in this data. The results of this test experiment demonstrate that the fluorescent lifetime technique can be effectively coupled with near-field microscopy. Signal strengths are sufficient to probe the local fluorescent characteristics although image acquisition takes many minutes.

Another investigation that has focused on fluorescence lifetime imaging has recently been published by [168]. In this investigation fragments of photosynthetic membrane lacking the physiologically active photosystems but containing antenna pigments were imaged in fluorescence. In addition lifetimes of the fluorescence were recorded using a time correlated single photon counting technique although lifetime images are not displayed. An advantage of this method over the methodology used to generate our lifetime images is the fact that in such a time correlated technique single photon sensitivity can be achieved.

The problems related to signal strengths when acquiring fluorescent near-field imaging may be resolvable by not relying on the interactions between freely propagating light and matter but rather through energy transfer mechanisms which have a very high cross section as will be discussed in the Future Directions section at the end of this paper.

5. Single Molecule Detection

The problem of single molecule detection using fluorescence can be broken down, first, into the microscopic imaging of single molecules and second, into the detection, without imaging considerations, of the presence of single molecule in a particular volume element. The second of these problems has been extensively studied and is briefly summarized here in order to highlight the unique applicability of NSOM to this problem. The essence of the difficulties that are associated with single molecule detection is the problem of identifying when a fluorescent molecule is present in a particular volume element and the difficulty of reducing the volume of this element in order to minimize the background from Raleigh and Raman scattering and autofluorescence.

The resolution of these problems have focused on either introducing innovations in detection or modulating the system or manipulating the excitation. One of the innovative detection techniques is the use of photon correlation methods which employ the principle that as a volume of a sample, which can be flowed passed a probe laser beam, the Raman and Raleigh scattering is a constant for each volume element while the presence of a fluorescent molecule results in a burst of photons [169, 170]. A second method of single molecule detection is to manipulate the sample so that the dimension of the illuminated sample is small and thus, the corresponding constant background is reduced. This has been accomplished either by forming a microdroplet [171] or having a flow method that produces a very thin stream of sample that is illuminated by a discrete laser beam [172]. Finally, in terms of excitation the earliest approach was to use evanescent fields that limited the excitation of a sample positioned over a prism on which the evanescent field was generated [173]. Subsequently, an elegant approach that was used for molecules with very narrow homogeneous linewidths was to introduce these molecules into a matrix that caused inhomogeneous broadening and then applying a very narrow band tunable laser in the tail of the inhomogeneously broadened line to select single molecules [174].

In terms of imaging single molecules the first studies were completed, over a decade ago, by Webb and coworkers[175]. These workers used standard far-field microscopic techniques to clearly detect the presence and the motion of a single molecule in a cell membrane. To accomplish this they focused on a molecule found in the cell membrane called the low density lipoprotein (LDL) receptor. This receptor binds the infamous LDL molecule that has been associated with heart disease. The LDL molecule is a string bag containing lipids which can be replaced by fluorescent analogs of these lipids. The LDL molecule used in the Webb et al. experiments had as many as 35 fluorescent lipid molecules. These studies have answered many questions about the motion of such molecules in membranes.

In the vein of reducing the excited volume by manipulating the excitation NSOM is of course an important new solution that can be applied to both imaging and non-imaging (e.g. flow) methods of single molecule detection. This capability of illuminating subwavelength volume elements integrates well with the ideas described of limiting the excitation spatially in order to reduce backgrounds that generally plague single molecule detection. The first applications of this idea have focused on the problem of detection rather than the more complicated question of how to achieve single molecule resolution with light. Recently several workers have demonstrated that when a near-field optical element that is two orders of magnitude larger than a single molecule illuminates a surface there is enough signal from such a near-field aperture to detect a single molecule [176, 177, 178, 179, 180]. For these studies fluorescent molecules were spin coated onto a glass slide and imaged in transmission. The molecules were deposited using an established procedure which has related the distance of the molecules on the glass slide to the concentration of the depositing solution [181]. In the near-field investigation the molecules were separated by hundreds or thousands of nanometers and thus single molecule detection was accomplished without single molecule resolution. This was naturally also the case in the far-field measurements of Webb et al described above.

In all these studies the proof that actually a single molecule was detected was the extinguishing of the fluorescence instantaneously after a recording time that could extend for as much as 15 minutes. This usually occurred when about 1 million photons were emitted and this agrees well with what has been suggested as the viable number of excitations that a fluorescent molecule can undergo before typically photodestructing. In terms of the spectrum of the fluorescence that has been observed for these molecules that were deposited on a surface it was

noted that the spectra varied from molecule to molecule with the average agreeing with the inhomogeneous broadening found in bulk samples [180].

An additional question addressed [176] was the variable intensity distribution of the excited fluorescence molecules in the field of view (see Figure 51 A). This variation in the intensity distributions could be explained in terms of the dipole radiation pattern of the near-field aperture interacting with the specific orientation of the individual dipoles of the fluorescing molecules. The result of this analysis are seen in Figure 51 C for the electric field components as a function of the ratio of the aperture diameter to its distance from the molecule. A stylized representation of the orientation of the dipoles of the fluorescent molecules seen in Figure 51 A based on this analysis is seen in Figure 51 B.

6. Summary

The above review of the present state of the art of near-field fluorescent imaging indicates that the signal strengths available today are only marginally sufficient for forming images in reasonable times. This points to the importance of continued probe developments to increase the signal strengths. Epi-illumination is one possible solution to this problem and new probes such as the non-linear emitting tips described in section III B and optically trapped particles (see section III D) have the potential to overcome some of the drawbacks of the application of epi-illumination in subwavelength fluorescence imaging.

An interesting idea that could allow conventional lens based fluorescence imaging to enter the realm of resolution of near-field fluorescence microscopy is an approach that has been suggested by Hell [182, 183]. In this approach two lenses illuminate the sample from opposite sides in a mutually coherent and confocal geometry which increases the effective numerical aperture of the microscope. This should increase the axial resolution of a conventional microscope by three to seven times. In addition, further improvements in the lateral resolution can be obtained [184] by introducing a predetermined offset in the focal spots, labeling the sample with a non-linear emitter and ensuring that each mutually coherent illuminating laser beam is below the threshold for exciting the non-linear phenomenon in question. In the overlapping region of the focal spots the sample experiences an intensity that is sufficient for phenomena such as two photon excitation.

VI. INTEGRATION OF SUBWAVELENGTH OPTICAL ELEMENTS INTO FABRICATION AND SURFACE MODIFICATION SCHEMES

A. NANOFABRICATION

The narrative above demonstrates that near-field optics can extend optical imaging and sensing into the nanometer regime. The same can be achieved for optical patterning and materials processing. The technical solutions described above are just as applicable to the problems of near-field lithography. The near-field optical elements used in imaging, i.e. micropipettes and optical fibers are also being used for nanopatterning.

Conventional optical lithography with standard resists often use near-ultraviolet light to expose resists which are subsequently developed with wet chemistry to generate the impressed pattern. Such optical patterning employ sophisticated far-field optical systems in which a mask written at a much lower resolution is projected to give a considerably finer resolution of the pattern on the resist. As with all optical systems the resolution achieved in such patterning is wavelength dependent and diffraction limited. Even the most advanced masking techniques, which use such methods as phase shifting of the light using constructive and destructive interference for improving line definition, cannot achieve resolutions significantly better than the wavelength of light.

Near-field lithography breaks the diffraction barrier in a wavelength independent fashion. It can draw structures with a line width that is determined by the size of the aperture and since these apertures can be nanometers in size near-field optical lithography can draw structures of dimensions that can be achieved today only with electron beam or x-ray lithography. This technology can readily be coupled with methods that use near-ultraviolet exposure and wet developing methods to generate patterns in photoresists. In fact we have demonstrated such a combination using a HeCd laser transmitted through a subwavelength micropipette to expose in the near-field a Shipley photoresist which was subsequently developed to generate the structures shown in Figure 52 A. A combination of a resist that was considerably thicker than the extent of the near-field and a less than controlled development produced a linewidth of 1 micron that was considerably larger than the aperture diameter. The experiment demonstrates that the near-field patterning of photoresists using the standard approach, employed in far-field lithography, of exposing and developing is definitely feasible.

An exciting alternative to this more conventional integration of the near-field with optical lithography is to combine the wavelength independence of the near-field aperture with the singular heatless material removal characteristics of deep ultraviolet radiation [[107]]. This permits direct patterning of a wide variety of materials in a single step with no associated wet developing. The 193 nm emission of an ArF excimer laser is an ideal source for such heatless ablation. Nonetheless, this laser wavelength has provided an unmet challenge in the focusing of such light because of the lack of suitable optical materials in this wavelength regime and the very complex mode structure of the emission. In addition no optical fibers exist that can effectively transmit such laser radiation and this has prevented the potential of using this laser in submicron patterning. A straight hollow micropipette provides a perfect solution to all of these problems.

In spite of the above there were technical challenges to be met before such a pulsed laser could be coupled to a near-field optical system. Because excimer laser light is preferentially transmitted through a straight pipette a shear force tracking system is required that will operate under the stringent conditions of the high peak power of pulsed laser source. Specifically, such a source introduces a shock wave with each firing of the laser and this results in oscillations of the micropipette tip. This can result in crashing of the tip or a loss of the feedback signal if not appropriately accounted for. The technique described above of Shchemelinin et al. [[103]] resolved all of these problems while allowing for opaque samples to be employed.

An example of near-field excimer laser ablation is shown in Figure 52 B and C. In this Figure, two 250 nm lines and a single 80 nm wide line are shown. These lines were ablated in a standard polymer photoresists that are used in conventional wavelength limited resolution optical lithography. However the super-resolution patterns seen here were produced with simply direct ablation and without any subsequent development. An interesting aspect of this result is the observation that even while ablating through a thick layer of photoresist the near-field resolution appears to be maintained. This is understandable in terms of the non-linear effect of the ablation

process which requires a threshold fluence of the laser radiation in order for ablation to occur. Thus as the radiation spreads out from the near-field only the center of the beam has enough fluence to result in ablation. This also results in very sharp wall structures with extremely high aspect ratios.

An exciting aspect of this approach to lithography is the ability of such deep ultraviolet radiation to ablate a variety of materials with considerably different thresholds of ablation. A short list of such materials include beside all sorts of polymers including biopolymers and proteins [[185]], high temperature superconductors, diamond films, metals, semiconductors. Of particular importance in this regard is the fact that the cold ablation process does not destroy the characteristics of the material that remains next to the ablated region. For example, it has been shown that electro-optically active proteins that have been patterned with this method retain their native activity [[186]]. We have also seen similar behavior when superconductors have been ablated with this method and this is seen in Figure 53 which demonstrates that the transition temperature and the slope of the curve as the transition temperature is approached remain unaffected by the patterning of an YBCO high temperature superconductor on an MgO substrate.

Near-field optical lithography is limited by the fact that it is a serial technique. A limitation of all serial methods is that it is impossible to achieve speeds that will compete with the throughput that can be achieved in parallel lithographic methods. With this said it is constructive to compare the speeds achievable with near-field optical lithography and electron beam methods. The nominal writing speed of electron beam writers is 1 MHz. However this does not take into account the time that is required in order to achieve sufficient exposure nor the processing or the developing steps that further slow down the process. In contrast a single pulse of the excimer laser is sufficient to ablate many materials directly. The best excimer lasers today have a repetition rate of tens of kHz. In addition, it is interesting to note recent developments with chopped cw argon ion lasers with extremely efficient doubling to produce wavelengths in the deep ultraviolet that can produce ablation characteristics similar to excimer lasers but with repetition rates in the MHz regime [[187]].

In addition to the laser an aspect of the near-field lithography system that needs to be considered when speed is discussed is the scanning limitations that may be connected with the design of the near-field instrument. The best designs for near-field optical systems currently have the optical element in a fixed xy position while the stage is moved. The stages that are employed in scanned probe microscopies are not suitable for these applications because of their limited scan ranges. Therefore standard nanometer resolution closed look xy stages with millimeters to centimeters of travel have to be employed. These stages have limited scan speeds. Current commercial stages of this type have speeds of 10 mm/sec with 300 mm/sec speeds already on the horizon. Even for a 10 mm/sec stage and a spot size of 100 nm there would be 10^5 spots per second patterned at these speeds.

Another factor that effects writing speed is the limitation on the beam size of the electron beam to a maximum of one micron. This is certainly not the case with near-field lithography in which pipettes can be pulled to dimensions of many tens of microns. Such large diameter pipettes can be used to pattern large areas while the higher resolution patterning can be generated with pipette diameters that are comparable to the super-resolution that is required. In regard to this a characteristic of electron beam writing that is not faced in near-field deep ultraviolet lithography is the problem of electron beam scattering which limits the minimum spot size of the electron beam.

There are many applications for this emerging technology of lithography. In fact commercial instrumentation in this area is already available from Nanonics Ltd. [[188]]. Such a technology can be used in any case where high resolution is required. This includes such areas as prototyping with superconductor, electronic, optoelectronic and optical materials. With regard to optical materials it is important to realize that this form of near-field patterning has the capability of gray level patterning which could have considerable potential in the fabrication of diffractive optical elements.

The instrumentation can also be used for custom production of conventional semiconductor integrated circuits. In addition, the technique is well-suited for the production of x-ray masks and mask repair with both removal of unwanted lines and the photochemical addition of metallic lines is a distinct possibility. There is additional uses for the method to affect highly localized photochemical alteration of surfaces to allow for controlled

growth of materials on chemically modified substrates. Finally, the direct patterning and the highly localized, non-thermal, material removal of the method is also of considerable potential value in a production mix and match environment. For such applications a microelectronic circuit or other device is patterned by accepted high throughput parallel methods and the device after these patterning steps could be deposited onto a stage with highly accurate interferometrically controlled movements. Using such a stage and the pipette tip as a force sensor characteristic features can be extracted with subsequent, nanopipette based excimer laser ultrahigh resolution patterning in specific regions.

This use of deep ultraviolet lasers and lensless optical elements highlights another area besides resolution that lenses fail to perform adequately. This is in the area of ultramicrosurgical applications. An important characteristic of the 193 nm radiation, as noted above, is that it can remove material with ultralow ablation thresholds and with minimal heat deposition. This is crucial in microsurgery. In addition, because of strong absorption in most materials, each pulse of this laser can be controlled to remove as little as 0.1 μ of the surface that is being irradiated. Furthermore, in terms of biological applications, numerous studies have shown that with the 193 nm radiation no mutagenic effects have been observed. Thus such a laser should be ideal for cellular and tissue ultramicrosugical applications.

Nonetheless, until our application of near-field optical elements to the problem, the argon fluoride excimer laser had never been used for ultramicrosurgical applications for a variety of reasons. First, diffraction-limited optics is impossible to obtain in this region; second, even if such optics existed, the large divergence in the beam of this laser makes it impossible to obtain diffraction limited resolution; third, there are no effective fibers for this wavelength; and fourth, the large absorption cross section of most materials at these wavelengths extend to biological fluid and make a lens-based delivery system which has to be placed at some focal distance from the surface to be ablated impractical. The methodologies we have developed enable us to overcome any interference from the surrounding biological medium and deliver the 193 nm laser wavelength directly to a spot in an organ such as an eye.

This has permitted the ultimate in laser ultramicrosurgery available today [148,149,150,151,152]. An example of this application of near-field optical elements is seen in Figure 54 in which a hole is produced in the zona pellucida of a rat egg for improving sperm penetration and inducing early hatching of the fertilized egg in *in vitro* fertilization applications. In this application an ArF excimer laser is transmitted through a pressurize, air filled micropipette. This prevents highly absorbing liquid from entering the hollow cavity of the pipette. The resulting ablation of material is seen in both the optical micrograph and a scanning electron micrograph of the ablated hole. Notice that even at the resolution of the electron microscope there is no observable damage to the surrounding zona pellucida demonstrating the heatless removal of material with this laser.

B. HIGH DENSITY DATA STORAGE

An important area in which the near-field can make a significant impact is the high density patterning of materials for potential memory applications. In principle the resolutions that should be achievable in writing bits of information will provide orders of magnitude improvement in the density of writing and reading with light. For example using 800 nm light, which is currently the standard in read only compact disks and read/write magneto optical storage, densities on the order of up to 0.5 Gbits/in^2 can be achieved whereas using a 50 nm near-field spot of light densities of 60 Gbits/in^2 can be realized. This is more than a two order of magnitude improvement in data storage. Using even smaller spots of light in the near-field densities in excess of 100 Gbits/in^2 can be conceived of.

The near-field optical writing and reading of data using a magneto optical storage medium has recently been accomplished using a fiber optic near-field probe [189]. The smallest bits achieved in this study was 60 nm with a corresponding density of approximately 45 Gbit/in^2 (see Figure 55 A and B). In this study a bit was written as a result of a localized heating of the material to above the Curie temperature (300^0 C) and the resulting formation of a magnetic domain which has a magnetization in a direction opposite to the unaltered surroundings. The data is then subsequently read by a lower power linearly polarized laser beam that is transmitted through the subwavelength aperture of the coated tip of the fiber and is subsequently transmitted through the magneto optical film that rotates the polarization by the Kerr effect. The direction of the rotation is dependent on the orientation of

the local magnetic field. The resulting elliptically polarized light is analyzed using a polarizer in front of a detector that sits in the far field relative to the film.

Another example of high density writing using near-field optics and a photochemical rather than a thermal alteration of a film is seen in Figure 55 C. This figure is an electron micrograph of a pattern that was written in a photoresist using near-field photochemical ablation. This pattern was impressed using the near-field optical lithography system described in the previous section. The pattern is a series of parallel pits. The width of the track seen in this figure is 200 nm with the size of the pits considerably less than this dimension. This pattern was obtained when the sample was scanned at a rate that was faster than the repetition rate of the pulsed laser.

An alternate method that is closely related to the technologies of near-field optics has recently been reported by Hoen et al.[190]. These workers have used a metal coated optical fiber that has been pulled by the methodologies developed by Harootunian et al [40] and have transmitted a pulse of laser light through the fiber in order to heat the tip of a fiber which is in contact with a substrate. The heated fiber tip then indents a pit in the substrate surface representing a bit of information (see Figure 55 D). The read out was then accomplished by the same tapered fiber tip acting as a contact force sensor. The deflection of this sensor was monitored by a fiber interferometer technique. Although pits of 50 x 74 nm^2 have been written the sensitivity of the read out was limited in these experiments to pit sizes of 150 x 300 nm^2. The method has overtones of the method of contact NSOM that we have developed as described above. Such a method which does not depend on mechanical feedback to position the probe and is thus not limited by the mechanical resonances of the system. Therefore the reading speed of 300 kHz is several orders of magnitude faster than the near-field magneto optical investigation.

In order to read or write with high density using near-field optics the medium must be thinner than the extent of the near-field. This is a generic problem when near-field optics, a surface effect, is used to view a bulk phenomenon such as absorption, polarization etc. The limited thickness of the medium which reduces the interaction length has significant impact on the signals that are achievable. This is apparent in the near-field magneto optical experiments where the weak interaction (a 1^0 rotation of the polarization) limits the read out speed.

In order to effectively employ near-field optics for data storage it is important to affect surface phenomena with the near-field optical probe. An example of such a combination is surface modification with light that changes the reflectivity of a surface. An alternate example is based on the work of Chen et al [191]. These workers demenstrated that a film of a photochromic material with a gigantic non-linear molecular hyperpolarizability could be altered photochemically with visible light and read out non-destructively with infrared light using surface second harmonic generation. Such non-linear optical effects can also be readily enhanced by several orders of magnitude by the use of appropriately constructed tips with protruding metal particles [25]. Nonetheless, the ultimate read out speed is going to be limited by the shot noise in the signal from a subwavelength spot of light as discussed above.

If one could combine the speed of Hoen et al [190], the erasability of Betzig et. al [189], and our photochemical alterations of surface effects [191] the appropriate combination of a competitive ultra-high density near-field optical standard may be closer than is generally realized. If the potential of near-field optics for serial reading and writing of information is eventually achievable it will have to lead to a new standard in disc technology. Presently, such optical discs place the active area in the far-field relatively to the optical element. This active area is appropriately protected with coatings to prevent contamination and degradation of the surface. Such a geometry will have to be altered for near-field optical memories with the attendant problems of surface wear that could be a significant limiting factor. Finally, as parallel optical memories are further developed stiff competition should be expected as to the best next generation method for high density information storage and retrieval.

An interesting alternative to conventional probe based near-field optics with considerable potential in optical storage applications is the use of the solid immersion lens described above in section III.D. As noted above the improvement in resolution with this lens is only capable of being used for imaging an object if the base of the lens is close enough to the object for evanescent coupling to occur. This is a possible limitation since the

technique could be limited to fairly flat samples. Nonetheless, in data storage applications, the surfaces are fairly flat and this should not pose a problem. Recently Terris et al. [192] have demonstrated a system for such magneto-optical storage using this solid immersion technology. Using a lens with an index of refraction of 1.83 a spot size of 317 nm was achieved with 780 nm light. Domains were written by heating in the presence of a magnetic field with a pulsed laser and imaged with the same lens (see Figure 55 E). Although the resolution is significantly less than what was obtained above with fiber probes this technique has a significant advantage in that it does not have the problems of scanned probe technology. Furthermore, it is possible to coat the sample with a high refractive index protective layer and use the lens to write and image through this layer as is currently the standard in all optical disk storage techniques. Finally, the speed of the solid immersion method is not limited by the signal limitations of aperture based NSOM.

VII. OTHER OPTICAL NEAR-FIELD APPLICATIONS

A. ULTRAFAST APPLICATIONS

Fundamental questions remain in understanding such interesting physical phenomena as quantum and single electron transport in mesoscopic structures, ultrafast electric field and voltage wavefront propagation at metal-semiconductor interfaces and optical phenomena in quantum confined structures. In order to understand these phenomena it is important to be able to probe the poorly understood local mechanisms that govern these phenomena. Such a lack of understanding arises from the paucity of existing experimental techniques which have not been able to combine the time and spatial resolution that is required for the measurements that are required. The super-fine spatial resolution of near-field optics when combined with the ultrafast time resolution of femtosecond laser spectroscopy is providing for the first time new levels of investigation that were not achievable in these area which require both spatial and time resolution.

To reinforce the lack of suitability of geometrical optical elements to the needs of ultrafast spectroscopy of mesoscopic systems the reader is referred to Figure 56. This figure is based on one that was prepared several years ago by Fork et. al. [193] and compares the history of the spatial resolution of microscopic measurements with light and the temporal resolution of optical pulses that have reached their pinnacle with the discovery of methods to generate femtosecond pulses of light. In this figure it can be seen that in 1990 the highest resolution that could be achieved by diffraction limited optics was 0.5 μ (0.5 x 10^{-4} cm) which is far from the spatial resolutions generally required in order to observe interesting mesoscopic phenomena.

In fact the problem of resolution with femtosecond pulses of light is even worse than what is seen in Figure 56. The difficulties that femtosecond pulses encounter with geometrical optical elements are two fold. First, as an ultrashort pulse traverses, for example, a lens it experiences dispersive effects that broaden the pulse in time. Second, ultrashort pulses exhibit uncertainty broadening ($\Delta E\ \Delta t \geq h$) and thus, their spectra are extremely broad. Therefore, it is impossible to achieve even diffraction limited optical resolution.

These problems notwithstanding ultrafast investigations on mesoscopic structures often require ultrahigh resolution. Consider, for example, the conservative notion that an alteration induced in a material by a femtosecond pulse spreads with the speed of light. At such a speed the area over which the particular phenomenon will spread in a femtosecond is 0.3 μ. In actuality many phenomena in such semiconductor structures spread at considerably less than the speed of light. For example, the initial velocity of an excited electron in GaAs is $\simeq 10^7$ cm/sec which means that in a 6 fsec pulse (the shortest pulse that has been created to date) the electron travels only 6 _. Thus, both in terms of the dimensionalities of the mesoscopic structures and the speed at which the effects caused by the light matter interaction spread, a spatial resolution is required that cannot be achieved even in systems in which diffraction limited optics is possible.

Using micropipettes we have completed preliminary investigations on the simplest scheme of all that could integrate near-field optics with femtosecond pulses and that is to pass a femtosecond laser pulse through the empty void of a glass micropipette. From the point of view of illuminating or collecting femtosecond pulses of light in highly localized regions in space the question is whether the subwavelength, conducting aperture at the tip of the micropipette would alter the characteristics of such light pulses. The question is significant not only in terms of the practical applications of femtosecond near-field optics but also in terms of developing a fundamental understanding of how light is transmitted in spaces which have dimensions below the cutoff frequency beyond which light can only be transmitted with large evanescent losses.

An initial result [57] obtained is displayed in Figure 57. These results relate the observed energy spread of a pulse of 60 fsec (estimated for a $sech^2$ pulse shape) from a colliding pulse mode dye laser emitting radiation at 610 nm as a function of the pipette diameter. In this Figure there are two curves. A heavy solid curve which is the energy spread of the pulse without the presence of the pipette and a curve reproduced with a lighter line that corresponds to the energy spread of the pulse after it passes through the opening at the pipette tip. These results indicate that transmission through subwavelength apertures of the dimension indicated in the figure do not reduce

the energy spread. This indicates, that for such apertures even if further experimentation indicates that the pulse is indeed longer after it traverses the subwavelength pipette tip, it will be possible to apply a reverse chirp to the pulse in order to obtain the desired time resolution. This methodology can only be applied when the chirp affected by the subwavelength optical element is linear.

These workers also investigated the problem theoretically and concluded from their theoretical simulation that the alteration in a 3 fsec pulse as it goes through an aperture that is one tenth the wavelength of the light should spread the radiation in time by more than double the initial 3 fsec pulse width. Thus, the experimental observation of minimal effects on the 65 fsec pulses that was transmitted through apertures that were at most 1/6 the wavelength of the laser wavelength are understandable.

A caveat on these deductions is the fact that modes that are reflected back from the direction of the taper should be once again be reflected into the propagating direction by the next larger step but our theoretical model did not consider the back reflection of these modes. Initial investigations on the effect of these reflected modes indicated that they should make a noticeable contribution on the final solution and our continuing studies are aimed at refining the model in this direction. In addition, it should be noted that dispersion effects due to the penetration of the pulse into the walls were not taken into account.

Future directions in this sequence of experiments will employ the sensitivity of the character of these pulses to external influences in order to understand, using the synergistic interplay between the theory and the experiments in this area, the mechanism by which light is transmitted through structures with subwavelength dimensions in the mesoscopic domain in which there is an interesting mix of classical and quantum effects.

In addition to the above it has been suggested [57] that the micropipette tip could be ideal for cross correlating femtosecond pulses with high spatial resolution. An example of a structure that could be used in this vein is the β barium borate tipped micropipette described above (see section III B). In addition, initial steps have also been taken to grow GaAs in the tip of the pipette [57]. This is an important development that will allow the micropipette tip to be converted into an ultrafast switch that would allow the transmission of a transitory electrical pulse from the outer coating of the pipette to an inner electrode. This will also allow for cross correlating such pulses. Finally, when these characteristics are combined with the force sensing capabilities of such pipettes there will certainly be numerous problems requiring spatial and temporal resolution that could be tackled with such probes.

B. APERTURE ARRAYS FOR STATISTICAL MICROSCOPY AND SINGLE PULSE LASER PERMEABILIZATION

It is in general difficult to conceive of using aperture arrays in near-field imaging. Nonetheless, Palanker and Lewis [194] investigated theoretically a novel suggestion for obtaining subwavelength information by employing an array of holes in a metal plate. The object of their approach was to use statistical methodologies in order to determine the average dimension and the distribution of microdomains in surfaces such as membranes. They considered the statistical distribution of cells on an aperture array with millions of similar holes with each cell or a region of each cell statistically placed over each of the apertures in the array. By imaging the domains through the holes onto a charge coupled device it would be possible to analyze statistically the distribution and the size of the domains. These workers demonstrated that the resolution that could be achieved with such a statistical method could be up to 30 times better than the diameter of the holes in the array. The characteristic of CCD cameras are ideal for such an experiments both in terms of the linearity and the reproducibility of the response. Specifically, regions in which there are imperfections in the plate can be readily removed from the data set.

This paper also introduced an improvement in the methodologies developed by Fisher [38] for producing such arrays of submicron holes. In this improvement an excimer laser is used to ablate the metal coated latex spheres on a quartz substrate by irradiating from below as seen in Figure 58 A. The ablation caused micro-explosions which efficiently blasted off the metal coating in very well-defined regions around the latex balls. An optical image of such a plate is seen Figure 58 B.

Such arrays of apertures have also been used to permeabilize millions of cells with single pulses of an ArF laser [152]. In this series of experiments plant and animal cells were placed in their growth media on this aperture array and a single pulse of the excimer laser was transmitted through the holes and this permeabilized the cells. An example is seen in Figure 59 in which asparagus cells were irradiated. Subsequent to the irradiation aloquots of the cells were removed and exposed to propidium iodide. The cells that were irradiated took up the propidium iodide with greater permeability than the unirradiated cells. A particularly important aspect of these measurements was the fact that these irradiated cells resealed and the resealed cells continued to grow and exhibited permeabilities that were similar to the unirradiated fractions. The resealed cells could be repeatedly permeabilized indicating that the procedure had little effect on the viability of the cells.

The technique overcomes one of the principle problems with laser permeabilization by permitting the production of millions of microbeams to permeabilize millions of cells. In addition, the ability to permeabilize plant cells is a very important attribute since plant cells are notoriously difficult to permeabilize. The next step will be to use this technology to introduce genetic material into cells permeabilized by this methodology.

C. NEAR-FIELD OPTICAL METROLOGY

A particularly exciting challenge that near-field optics together with other scanned probe microscopies can begin to attack is the practical problem of resolving the linewidths that are required for microcircuits with a growing density of features. This field is already facing the challenge of precision linewidth measurements of lines which are <350 nm with an accuracy of 10 nm for the 64 MByte dynamic random access memory. This is compounded by the fact that the walls of many of these structures have slopes of $<3^0$. Thus, the problem at hand, is to not only measure the linewidths but also to sense such steep walls and to detect surface features in valleys that are bounded by such walls. This is already beyond the capabilities of conventional light microscopy and, electron microscopy, even after destroying these chips in order to inspect them cannot detect topography in the valleys that are a part of all microcircuits. It is estimated, that if an all optical technique is employed in the inspection process and the destructive aspects of the electron imaging process is bypassed then millions of dollars would be saved in microcircuit production lines.

Already attempts have been made to apply scanning force microscopy for such precision measurements. Force probes are very fragile and are difficult to produce with the slopes that can probe the deepest recesses of such circuits. In addition the approach of a sharp wall can often confuse the probe in its ability to delineate surface topography and may also result in the breaking of the probe. A combination of a micropipette force probe together with near-field optical imaging has the potential of resolving these problems.

These difficulties are best illustrated in the diagram reproduced in Figure 60. In this Figure linewidths and trench depths that are already being approached in near term designs of microcircuits are displayed in the top half of this diagrammatic representation. In the bottom half of this schematic, a feature is drawn in the bottom and close to one of the sharp side walls of the trench. Such a feature would not be detected by present emulations of sharp silicon AFM cantilevers and this is shown by the AFM response depicted in this diagram. In addition, the probe could be broken due to its inability to sense such a sharp wall without some additional information.

One way to overcome the difficulties encountered by using force alone is to compare this signal with near-field optical information from the tip of the pipette. Since the near-field optical response exhibits an exponential dependence, when the tip of the probe reaches the feature near the sharp wall, the near-field signal from the tip would still be large. This is the case even though the wall provides an AFM signal that would indicate the need to retract the tip. Thus, this synergism of near-field optics and force imaging should permit an interesting interplay that will allow for the detection of features that would be impossible to accomplish with force alone. A preview of such synergism has already been described above when tunneling and near-field optical images are compared. In this comparison (see Figure 36 and associated discussion) it is clear that the exponential nature of the near-field intensity profile plays an important role in the analysis of comparative imaging.

D. IMAGING WITH PIPETTE CONCENTRATED AND APERTURED X-RAYS

Initial experiments have demonstrated the feasibility of imaging with x-rays that are concentrated or apertured with glass pipettes. As noted above [81] experimentally spot sizes of 0.1 μ have already been achieved with such devices. An experiment used to demonstrate such highly confined x-rays is shown in Figure 61. In this result obtained at the Cornell High Energy Synchrotron Source (CHESS) by Steve Hoffman in collaboration with Donald Bilderback, Daniel Thiel and Aaron Lewis the edge of a gold stripe on a silicon substrate was scanned under the pipette. As the data in Figure 61 indicates, the resolution obtained was 1000 ± 100 Å. In addition, to such tests of resolution Bilderback et al [82] have continued these experiments at CHESS to demonstrate imaging with test structures of gold on silicon nitride. The images obtained by these workers are displayed in Figure 62. As can clearly be seen the resolution of the scanning micropipette x-ray technique is similar to what can be obtained with scanning electron microscopy.

Besides such imaging experiments, a radiation source of sub-micron size and highly enhanced brightness can be used to advantage in numerous measurements. In fact , it will add extremely high spatial resolution capabilities to almost any type of existing x-ray experiment. For example, it will allow both transmission and fluorescence spectroscopy like extended x-ray absorption of fine structure (EXAFS) to be carried out with a sub-micron resolution over a sample. The same holds for microtomography and imaging experiments. Since the emittance of the beam for linear taper capillaries is conserved, the smaller spot at the exit relative to the entrance is achieved at the expense of a larger divergence. This divergence requires working close to the capillary tip to minimize source magnification. For non-linear tapers, however, a longer focus away from the tip of the capillary can be achieved. This will allow, in principle, experiments where the samples are both small and positioned away from the tip such as those used in three dimensional tomography and high-pressure cells.

The larger divergence will require special measures in application to diffraction experiments. This may require simply that the capillary be used as an effective pinhole. However, the transmission of a 100 Å diameter pinhole centered on a 100 μ diameter beam of 10^{17} photons, typical to an undulator on a third generation synchrotron source, will still yield 10^{9} photons, a flux comparable to those available at a second generation bending magnet source. In fact Bilderback et al.[82] have already attempted a diffraction experiment with pipette focused x-rays. They achieved with gold foil a sample volume of 5 X 10^{-3} μ^3 which is the smallest single crystal volume studied by x-ray diffraction.

E. OTHER OUTGROWTHS OF NSOM TECHNOLOGY

The techniques and the fundamental concepts of NSOM have spawned exciting new directions some of which have been described above. The breadth of the penetration of these techniques is summarized in Figure 63. These include methods for ultramicrosurgery, methods of single laser pulse perforation of cells, methods for solving intractable problems of focusing x-ray radiation etc. In this section we describe one more extension of NSOM technology that has the potential of developing a whole new area of scanned probe imaging. Specifically, a considerable amount of effort has been expended in generating tapered glass structures in which there is a continuous wire of metal from the large end of the pipette to the very tip. One application of this in NSOM is the generation of optical coax structures by being able to pull metal to the very tip of a pipette coated on the exterior with metal. This was described above in section III A. 4. Such a potential structure was shown in Figure 12F. This same technology can be used to generate a very sensitive thermal probe [195].

To achieve such a thermal sensor the metal filled pipette is coated such that the outer coating makes a point contact at the very tip of the pipette structure. By using an appropriate combination of metals for the inner wire and the outer coating a point thermocouple can be generated at the tip of the probe. The small mass of the thermocouple gives it a miniscule heat capacity resulting in an ultra rapid response time. The response of such a point thermocouple is seen in Figure 64A. In this Figure the thermal voltage response to a pulse of a Nd:YAG laser is shown. A response time of < 1 μsec was obtained and this is orders of magnitude shorter than previous microfabricated thermocouples [196] whose time response have been measured.

These thermal probes can also be used for high resolution thermal imaging. In an earlier work, line scans of thermal gradients were reported by Williams and Wickramasinghe [197] using a coated metal wire tip. An image of the mode structure of the focal spot of a laser beam taken with the micropipette based thermocouple is shown in Figure 64B. This image was obtained by inserting the thermocouple probe into a near-field scanning optical microscope. In this mode the thermocouple was essentially used as an optical detector.

A recent paper describes an alternate approach to thermal sensing [198]. In this approach photothermal spectroscopy was acomplished with femtojoule sensitivity using the micromechanical properties of a silicon nitride cantilever on which was deposited molecules with particular absorption characteristics. By changing the wavelength of the light beam that was incident on the molecules that were coating the cantilever and monitoring the deflection of the cantilever using interferometry it was possible to obtain an absorption spectrum of the molecule in question with sensitivities that could approach the femtojoule level. The authors mention the possibility of the application of such a sensor to near--field optical microscopy if the appropriate structure could be found. The micropipette based sensor discussed above with its force sensing capabilities is an important step in that direction.

VIII. THE FUTURE - SINGLE MOLECULE RESOLUTION

The resolving of single molecules is a challenge that has until now not been addressed in the experiments completed with near-field optics. The best resolutions obtained to date are well over an order of magnitude from the dimensionalities required for single molecule resolution. To achieve this aim, which is a far more ambitions project than simply detecting individual molecules as described above, it will be necessary to make use of more localized electromagnetic phenomenon such as molecular excitons, surface plasmons and other non-radiative optical effects. The very short interaction length of these phenomenon can allow one to excite, detect and manipulate optical interactions with nanometer resolutions.

A. MOLECULAR EXCITON MICROSCOPY

The efficient, localized exciton generation which can be produced in the microcrystal probes described above raises the possibility of the ultimate in near-field optical microscopy: namely, the possibility of resolving single fluorescent molecules. Such *molecular exciton microscopy* (MEM) has been proposed [31] and is schematically depicted in Figure 65. A crystal, protruding from the tip of a coated micropipette and excited from the rear by a laser, serves as a source of excitons. The sample to be imaged is tagged with appropriate acceptor fluorophores whose excitation energy band overlaps the energy level of the donor excitons. The tip is then scanned across the sample at a distance less than the Fərster radius. Each time the crystal passes over an acceptor fluorophore highly efficient energy transfer will occur (see section IIB 3) and the subsequent emission from the acceptor will be detected. Such energy transfer is more efficient by many orders of magnitude than phenomena such as absorption.

The greater the Stokes shift in the acceptor molecule the easier it will be to differentiate the tail of the donor fluorescence from the acceptor signal. The overlap in the emission spectra has the potential to completely obscure the weak signal, particularly when dealing with the very broad emissions of organic molecules. A simple calculation shows that even for a relatively small donor crystal with a volume of $0.1\mu^3$, the large number of emitting molecules within the bulk of the crystal can result in a residual overlap comparable to the expected signal from the acceptor. Using materials with sharper emission lines such as complexes or terbium of europium could relax these requirements. An ideal scenario would have a non-fluorescing donor exciton to gather the energy and transfer it to a fluorescent acceptor, completely removing any background signal. This would be analogous to photosynthesis, where a large collection of non-fluorescing antenna molecules gather the light and transfer it to a single reaction center.

B. LOCALIZED QUENCHING OF FLUORESCENCE

It has been known for many years since the classic experiments of Kuhn [34] that metals can quench the emission of fluorescent molecules. Near-field optics allows this phenomenon to be exploited for imaging purposes. The first experiments in this direction have been performed by a number of groups. In the experiments in which a subwavelength aperture was used to bleach single molecules [177,178] the effect of the metal coating of the fiber tip was observed to quench the fluorescent emission and this affected the lifetime (see Figure 66 A). In addition to these experiments workers have also demonstrated that the emission from ruby crystals can be quenched using a tunneling tip and evanescent excitation [64].

Another proposed scheme for monitoring molecular scale interactions is to attach a few fluorophores to the tip of a probe and monitor the reduction in their emission upon approaching a surface, such as a metal film, which will quench the excitation. In order to realize such a scheme the fluorescent material at the tip of the probe must be small enough so that a significant portion of the material can be brought to within the few nanometers of the metal surface. This is required so that enough of the material will be quenched to produce noticeable reduction in the fluorescent intensity. Such an experiment was undertaken by Lieberman [145] in collaboration with Thomas Jovin and Aaron Lewis. In this experiment a metal coated plastic tipped pipette in which dye molecules was embedded was repeatedly brought into tunneling contact with a partially transmitting gold film. During this cycle of contact and withdrawal of the tip the molecules were excited with the epi-illumination geometry and the

emission lifetime was monitored (see Figure 66 B). As can be seen when the tip was in tunneling contact the emission lifetime was altered.

An alternative technique for monitoring single fluorophores, as proposed by Hansch et al [199], involves plasmon quenching. When a metal tip is brought to within a few nanometers of the surface of the near-field plasmon microscope described above there is a strong reduction in the reflected light due to nonradiative energy transfer of the plasmon energy to the tip. These workers propose to place a single fluorophore above a metal surface at a distance of a few nanometers so the fluorophore will not be quenched directly by the metal. Scanning a metal tip directly over the fluorophore will quench the oscillation of the fluorophore, reducing its scattering cross section to the plasmon field, which should result in a change in the reflected intensity. Whether a single fluorophore which is being resonantly excited by a plasmon field would remain stable long enough to be imaged has not been determined.

IX. SUMMARY

In this review we have surveyed a field that is experiencing exponential growth. At the start of this field in1984 disciplines from biology to microelectronics were set to experience a critical need for increased resolution. NSOM was introduced in the hope that near-field optics could alleviate these crucial problems of resolution including the need to achieve nanometer dimension imaging in ambient environments.

The maturation of NSOM has involved resolving numerous technological challanges. These included the discovery of a reproducible method for producing near-field optical elements that could probe highly invaginated structures, developments to increase the signal strength of subwavelength points of light and the demonstration that these structures make excellent force sensors with multifunctional capabilities. In addition, near-field microscopes have advanced so that they are coming to the ideal of being transparently incorporated into conventional optical systems. Futhermore it is becoming increasingly evident that these microscopes also have inherent confocal imaging capabilities. Such advances have resulted in a growing realization in the scientific community at large of the great potential of this field. This has resulted in an exponential growth of the number of groups that are entering this field of near-field imaging. This is seen in Figure 67 which plots the number of papers published in refereed journals and excluding conference proceedings during the first decade of NSOM.

As NSOM has matured the critical need of resolution has grown. A variety of fields are demaning the resolution that NSOM can provide. This includes: Imaging of single DNA molecules with resolutions that overlap and extend conventional optical techniques; Optical characterization of microelectronic structures for the current and future generation of me nories; High resolution patterning of new materials (eg: superconductors, linear and non-linear optical and electr optical polymeric materials, diamond etc) which is becoming an increasingly important activity both in terms of fundamental studies and practical appplications; Invesitgations of microdomains of ion channels and ion pumps in cell membranes which is becoming an increasingly important challange in the forefront fields of biology such as neurobiology; and The increasing need for optical elements and nanometer dimension non-linear cross-correlators as femtosecond lasers are becoming a widely used characterization tool. Furthermore, the multifunctional imaging of surfaces is going to be crucial in the development of scanned probe microscopies and the optical elements of NSOM are unique in their capabilities in this regard. Finally, the incursion of near-field like optical elements into such areas as x-ray imaging and x-ray concentration and in areas such as the delivery of deep ultraviolet beams of light shows the vitality of the field in transfering its technology to other areas of optics that demand unique solutions to difficult problems. Thus, there is little doubt that near-field optics and its extensions have a very bright and synergistic future in imaging, characterizing and fabricating structures where optics had few possibilities in the past.

Acknowledgements

The authors would like to thank all their coworkers who have contributed to the success of near-field optics since its inception. The names of these coworkers are associated with the references from the laboratories of AL first in the Department of Applied Physics at Cornell University and more recently from the Division of Applied Physics at the Hebrew University of Jerusalem.

FIGURE CAPTIONS

Figure 1. Schematic of the near field of a subwavelength aperture. The beam remains collimated only up to a distance on the order of the aperture dimension.

Figure 2. A letter from John O'Keefe, a pioneer in near-field microscopy on hearing of the recent developments in near-field optics in the Lewis laboratory.

Figure 3. A survey of microscopy as it exists today. The vertical boxes associated with each microscopic technique correspond to the extent of resolutions that are generally obtained with the particular microscopy in question.

Figure 4. Calculations by Leviatan of the spread of the near-field energy density after passing through a thin sub-wavelength circular aperture. The exponential like evanescent decay of the signal strength characteristic of all near-field probes can be seen.

Figure 5. Field calculations inside a tapered slit for s and p polarizations. Significantly greater transmission is observed for the p polarization.

Figure 6. Field calculations of the perturbation of a the near-field radiation emanating from a sub-wavelength slit by a perfectly conducting cylinder of dimensionality that is on the order of the aperture diameter.

Figure 7. Calculations of the enhancement of the near-field intensity as function of the dielectric constant of a perturbating cylinder in the near-field.

Figure 8. Calculations of the far-field radiation pattern as a function of the dielectric constant.

Figure 9. PSTM evanescent field set up. The sample rests on a prism on which an evanescent surface wave is created by total internal reflection. The sharp dielectric probe locally frustrates the internal reflection an allows some portion of the incident light to propagate onwards.

Figure 10. PSTM calculation of an image of the letter "E" under different polarizations of the incident light. The strong dependence on the incident field complicates image interpretation.

Figure 11. Theoretical calculation by Denk and Pohl of the electromagnetic field enhancement in the vicinity of a metallic probe.

Figure 12. Schematic of the basic micropipette structure. A metal film is evaporated along the outer walls and on the front surface of the pipette to produce well defined apertures that can be < 10nm in diameter.

Figure 13. Near-field probes: (A) SEM photograph of a 100 nm micropipette tip coated along the sides and front surface (B) SEM photograph of a 70 nm tapered optical fiber coated only along its sides. (C) Selectively etched fiber (D) Microfabricated tip (E) Coaxial waveguide structure (F) Micropipette optical coax.

Figure 14. Transmission of far infrared light ($\lambda \simeq 200$ μ) through a subwavelength aperture with and without a internal wire. Without the wire (open circles) the power drops to zero promptly after the cut-off diameter is reached. On the other hand with the wire (filled circles) the power is maintained at a nearly constant value even below cutoff.

Figure 15. A. An optical micrograph of a subwavelength fluorescent anthracene filled pipette tip excited externally with several milliwatts of UV light from an argon ion laser. B & C Two views of a fluorescent dye embedded in a plastic that fills the tip of a micropipette under ordinary (B) and fluorescent (C) illumination. D. Second harmonic generation at the tip of a micropipette. E. Electroluminescing micropipette tip. F. Photopolymerized pH sensing dye at the tip of an optical fiber.

Figure 16. A. A schematic of the tapered capillary structure used to collimate x-rays by total external reflection. B. Optical micrograph of an x-ray collimating tapered capillary.

Figure 17. A. A nanopipette to sense surface forces bent at the tip with a focused carbon dioxide laser. B. A bent micropipette touching a surface and visibly flexing the cantilever without breaking the tip.

Figure 18. Electron micrograph of the integral reflecting surface polished into the arm of the micropipette cantilever just above the bend.

Figure 19. Feedback methodologies currently employed for NSOM. A. Normal force feedback B. Interferometric lateral force detection with polarization sensitive optics C. Lateral force detection by observing transmitted light through a pinhole D. Diffraction detected lateral force with a position sensitive detector E. Confocal profilometry.

Figure 20. Modes of operation for NSOM. Transmission imaging: (A) illuminating through the probe, (B) illumination through the sample. Reflection imaging: (C) illuminating through the probe, collecting externally, (D) illuminating externally, collecting through the probe and (E) illuminating and collecting through the probe.

Figure 21. A. Schematic of a tip scanning NSOM head which is positioned in place of the sample stage of a conventional far-field inverted microscope. The stack of plates straddling the microscope provides for vibration isolation for the head. B. Picture of the NSOM head in place above the inverted microscope. A dot of light is visible from a broken tip that is in place.

Figure 22. Schematic diagram of the method used to incorporate the externally illuminated fluorescent tip into the near-field optical microscope.

Figure 23. A. Schematic of a stage scanning near-field microscope with confocal microscopic capabilities. B. A photograph of the NSOM head integrated into an inverted and upright optical microscope.

Figure 24. Schematic of a concentric piezo design NSOM.

Figure 25. Set up for performing reflection NSOM with an obliquely placed objective.

Figure 26. Picture of an STM tip inserted into a hole bored through a long working distance microscope objective.

Figure 27. Schematic for integrated force feedback and PSTM with a silicon nitride cantilever.

Figure 28. PSTM set up for exciting surface plasmons

Figure 29. A reflection NSOM head designed for insertion into liquid helium dewar.

Figure 30. A comparison of line scans of a metallic edge on glass obtained with a SEM, NSOM, with the lens of an optical microscope compared to a theoretical calculation of the predicted response of a microscope with an oil immersion N.A1.4 objective.

Figure 31. A. Topographic image of an indentation in a sapphire surface generated by monitoring modulations in the evanescent wave on a surface using an optical fiber etched to 0.1 μ. B. PSTM image of a grating.

Figure 32. PSTM line scans as function of sample tip separation above a dielectric grating demonstrating the radiated fields.

Figure 33. Images of microfabricated letters A. SEM B Far-field optical C. NSOM using a optical fiber probe D. As in C but with image processing.

Figure 34. NSOM image of 40 nm colloidal gold particles using a fluorescent dye filled micropipette and the epi-illumination technique.

Figure 35. Simultaneous STM (A) and NSOM (B) imaging of ~0.1μ defects in a chrome film using a gold coated micropipette.

Figure 36. Normalized STM and NSOM line scans extracted from the images in Figure 35 across one of the imperfections in the chrome film showing the displacement between the images.

Figure 37. Simultaneous STM and NSOM with a PtC coated etched optical fiber probe.

Figure 38. A. STM image taken of a 600 nm square area on a silver surface. B. Scanning plasmon image of the same area with a tip spacing of 3 nm C. Same as B with a tip spacing of 10 nm D. A surface plasmon image taken while the tunneling feedback was engaged.

Figure 39. PSTM images of local fields in fractal silver colloid aggregates irradiated by light of various wavelengths and polarizations. (A & B) λ = 488 nm with *s* and *p* polarizations respectively; (C & D) *p* polarization for λ = 488 nm and 514 nm respectively.

Figure 40. A. Tunneling induced luminescence in multiple quantum well structures. Scan size 78 X 78 nm^2. B. Simultaneous and photon emission in fullerenes on a gold surface. Scan size 6.5 nm^2.

Figure 41. Shear force imaging using a straight optical fiber of polystyrene spheres with mean diameters of 230 nm (A) and 19 nm (B).

Figure 42. A gallery of AFM images obtained with cantilevered micropipette force probes on commercial scanning force microscopes. A. 50 μ scan of human red blood cells; scale bar = 10μ. B. 0.2 μ holes in a Millipore membrane; scale bar = 2 μ; inset scale bar = 500 nm. C. Pits in a compact disk surface; scale bar = 10μ. D. 10 μ field of a calibration grid. Images A, B & C were collected with a Digital Instruments Nanoscope III and image D was obtained on a Topometrix TMX 2010.

Figure 43. Simultaneous shear force and near-field optical images with a straight pipette of a human blood smear (A, B) and a straight fiber of pits in polymethylmethacrylate (C, D).

Figure 44. Heterodyne interference NSOM image at (A) the fundamental modulation frequency, (B) the second harmonic (C) mathematically extracted image from a and b of the pure amplitude variations.

Figure 45. A sequence of image frames demonstrating the spread of the near-field taken at increasing distances from the sample, starting from contact and extending beyond one micron.

Figure 46. Comparisons of line scans of a grating with 800 nm periodicity obtained using (A) fluorescence NSOM and (B) scanning electron microscopy.

Figure 47. A comparison of a conventional optical image (A) with a confocal image (B), a shear force image (C) and an NSOM image (D) of actin based stress fibers labeled with the mushroom toxin phalloidon complexed to rhodamine.

Figure 48. Near-field, far-field and spatially averaged near-field photoluminescence spectra from a 23 _ single quantum well structure at 696 nm excitation at 2^0K.

Figure 49. Fluorescent emission spectra of an optical fiber sensor (A) Excitation at 442 nm and (B) at 488 nm.

Figure 50. A. A far-field microscopic view of the region of contact between two microdomains of fluorescent pyrelene dyes showing the microscopic illumination of a pipette near-field element. B. A far-field microscopic view of the scanning micropipette. The scan range is approximately 9 μ. C. A fluorescent NSOM image of the region scanned by the micropipette. D. A fluorescent lifetime image of the same region as in C.

Figure 51. A. Near-field image of single molecules of cyanine spread on a surface. B. A stylized representation of the inferred dipole orientation of the molecules. C. The theoretical strength of the electric field components as a function of normalized distance from the aperture.

Figure 52. A. A pattern obtained on a Shipley photoresist using near-field exposure of a HeCd laser. B. 2 250 nm lines patterned by direct ablation on a photoresist. C. A single 80 nm wide line patterned by direct ablation on a photoresist.

Figure 53. Measurements of the transition temperature of a high Tc superconducting film after near-field ablative patterning demonstrating that the properties of the film are unaffected by the patterning.

Figure 54. A. An optical micrograph of the ablation in liquid medium of the zona pellucida of a rat oocyte by an ArF excimer laser transmitted through an air filled micropipette. B. A scanning electron micrograph of the resulting hole.

Figure 55. A. Domain size versus write power for near-field magneto optic storage. B. A 20 X 20 array of domains with a 120 nm periodicity corresponding to a storage density of 45 Giga bits per in^2. C. Photochemicaly altered domains of 200 nm written with near-field ablation. D. Domains physically depressed in a plastic with the tip of a heated near-field probe. E. Domains written and read with a solid immersion lens.

Figure 56. Historical development of spatial and temporal resolution.

Figure 57. Comparison of the spectra of a 65 a fsec pulse of light that was passed though a 100 nm micropipette with the spectrum of the original pulse. No change was observed in the spectrum.

Figure 58. A. A schematic representation of the method used to produce a mask with uniform holes of submicron dimension. B. A light micrograph of one of the plates produced by this method.

Figure 59. Light micrographs of a cell suspension of *Asparagus officinalis*. A. Intact cells before irradiation and B. After irradiation. Notice that after the irradiation the cells have taken up a fluorescent stain.

Figure 60. Schematic representation of the problems encountered in metrology of linewidths of microelectronic circuits.

Figure 61. A line scan of the edge of a gold stripe on a silicon substrate obtained by scanning the sample under a 100 nm x-ray pipette aperture.

Figure 62. Image of a gold structure on silicon nitride obtained with A. Scanning electron microscopy. B. Optical microscopy using a 0.9 numerical aperture lens. C. The unprocessed x-ray image with the same pipette used in Figure 61 and step sizes of 50 nm. D. X-ray image after processing.

Figure 63. A schematic representation of the growth of NSOM and the penetration of its tchnology and fundamental principles in various areas.

Figure 64. A. Response of a micropipette thermocouple to direct laser heating. Dashed-dotted line, the signal from a pin-phhotodiode; dotted and solid lines, the signal from a thermocouple immersed in air and water respectively. The photodiode output follows the temporal nature of the laser pulse. B. Thermal image of an argon ion laser beam focused to a spot in an inverted microscope and imaged with a micropipette thermal probe.

Figure 65. A. Representation of the pipette tip and sample configuration proposed for molecular exciton microscopy. B. Schematic of the set up used for quenching of tip fluorescence by a metal film.

Figure 66. A. Quenching of the fluorescence of a single molecule by the metal coating of an optical fiber near-field probe. B. Quenching of the fluorescence of dye tipped micropipette by a metal film.

Figure 67. A graph showing the exponential growth of near-field optics since the first publications in 1984. Based on papers published in refereed journals.

REFERENCES

[1] McMullan D. *Proc. Roy. Micros. Soc.* **25**, 127 (1990).
[2] O'Keefe J. A., *J Opt. Soc. Am.* **46**, 359 (1956).
[3] Ash A. E. and Nicholls G., *Nature* **237**, 510 (1972).
[4] Pohl D. W., Denk W. and Lanz M., *Appl. Phys. Lett.* **44**, 651 (1984).
[5] Lewis A., Isaacson M., Hartoonian A. and Murray A. *Biophysical J.* **405a** (1983).
[6] Lewis A., Isaacson M., Harootunian A. and Murray, *Ultramicroscopy* **13**, 227(1984).
[7] Lewis A. and Lieberman K. *Analytical Chemistry* **63**, 625 A, (1991).
[8] Pohl, D. W., *Advances in Optical and Electron Microscopy*, Academic Press Ltd. London, England 1992.
[9] Betzig E. and Trautman J. K. Science 257, 189 (1992)
[10] Bethe H. A. *Phys. Rev.* **66**, 163 (1944).
[11] Bouwkamp C. J., *Philips Research Reports* **5**, 321 (1950).
[12] Leviatan Y. J., *Appl. Phys.* **60**, 1577 (1986).
[13] Roberts A., *J. Appl. Phys.* **70**, (1991).
[14] Roberts A., *J. Appl, Phys.* **65**, (1989).
[15] McDonald N. A., *IEEE Trans. Microwave Theory Tech.* **MTT-20**, 689 (1972).
[16] Betzig E., Harootunian A., Lewis A. and Isaacson M., *Appl. Opt.* **25**, 1890 (1986).
[17] Betzig E., Trautman J. K., Harris T. D., Weiner J. S. and Kostelak R. L., *Science* **251**, 1468 (1991).
[18] Sommerfeld A. Academic Press, New York (1949).
[19] Novotny L., Pohl D. W. And Regli P., *J. Opt. Soc. Am.* **11**, 1768 (1994).
[20] Girard C. and Courjon D., *Phys. Rev. B* **42**, 9340-9349 (1990)
[21] Girard C. and Spajer M., *Appl. Opt.* **29**, 3726 (1990).
[22] Girard C. and Bouju X., *J. Chem. Phys.* **95**, 2056-2064 (1991)
[23] Labani, B., Girard, C., Courjon, D. and Van Labeke, D., *J. Op. Soc. Am. B* **7**, 936 (1990).
[24] Reddick R. C., Warmack R. J., Chilcott D. W., Sharp S. L. and Ferrell T. L., *Rev. Sci. Instrm.* **61**, 3669-3677 (1990)
[25] Wessel J., *J. Opt. Soc. Am. B* **2**, 1538-1540 (1985)
[26] Specht M., Pedarnig J. D., Heckl W. M. and Hansch T. W., *Phys. Rev. Lett.* **68**, 476 (1992)
[27] Jackson, J. D., *Classical Electrodynamics*, Wiley, New York (1975) p. 283
[28] van Hulst N. F., Segerink F. B., Achten F. and Bolger B., *Ultramicroscopy* **42-44**, (1992)
[29] Gersten, J. and Nitzan, A. *J. Chem. Phys.* **73**, 3023 (1980)
[30] Denk W. and Pohl D., *J. Vac. Sci. Technol. B* **9**, 510(1991).
[31] Lieberman K., Haroush S., Lewis A. and Kopelman R., *Science* **247**, 59 (1990)
[32] Forster, T., *Naturwissenschaften* **33**, 166 (1946); *Ann. Phys.* **6** Folge **2**, 55 (1948).
[33] Stryer L., *Ann. Rev. Biochem.* **47**, 819 (1978).
[34] Drexhage K. H., *Progress in Optics* **XII**, ed. E. Wolf, North Holland, Amsterdam (1974) p. 165.
[35] Kopelman R., Smith S., Tan W., Zenobi R., Lieberman K. and Lewis A., *Proceedings of the International Society for Optical Engineering (SPIE)* **1637**, pp. 33 (1992)
[36] Young, R., *Physics Today* (**November 1971**) p. 42
[37] Berndt R., Gaisch R., Gimzewski J. K., Reihl B., Schlittler R. R., Schneider W. D. and Tschudy M., *Science* **262**, 1425 (1993)
[38] Fischer, U. Ch., *J. Vac. Sci. Tech.* **B3**, 386 (1985).
[39] Synge E. H., *Phil. Mag.* **6**, 356-362 (1928)
[40] Harootunian A., Betzig E., Isaacson M. and Lewis A. *Appl. Phys. Lett.* **49**, 674-676 (1986)
[41] Sutter Instruments, Inc. 40 Leverony Ct., Novato, California.
[42] Betzig E., Trautman J. K., Harris T. D., Weiner J. S. and Kostelak R. L., *Science* **251**, 1468-1470 (1991)
[43] Reddick, R. C., Warmack, R. J. and Ferrell, T. L., *Phys. Rev B* **39**, 767 (1989).
[44] Ohtsu, M. , S. Juang, T. Pangaribuan and M. Kozuma, *Proceesing of NFO-1*, 131-139 (1993)

[45] Jiang, S., Ohsawa, H., Yamada, K., Pangaribuan, T., Ohtsu, M., Imai, K., and Ikai, A., *Jpn. J. Appl. Phys.* **31**, 2282 (1992).
[46] Tortonese M., Yamada H. and Quate C. F., *Ultramicroscopy* **42-44** (1991)
[47] Prater, C. B., Hansma, P. K., Tortonese, M. and Quate, C. F., *Rev. Sci. Instr.* **62**, 2634 (1991).
[48] Fischer, U. Ch., *Ultramicroscopy* **42-44** (1991)
[49] Keilmann, F. and Merz, R., *Proceedings of NFO-1, Besancon*, Allewell Press
[50] Merz, R., Keilmann, F., Haug, R. J., Ploog, K., *Phys. Rev. Lett.* **70**, 651 (1993).
[51] Lewis A., and Lieberman K., *Nature* **354**, 214-216 (1991)
[52] Lieberman K. and Lewis A., *Ultramicroscopy* **42-44**,399-407 (1992)
[53] Reisfeld, R., Brusilovsky, D., Eyal, M., Miron, W., Burshtein, Z., and Ivri, J., *Chem. Phys. Lett.* **160**, 43 (1989).
[54] Burroughs J. H., Jones C. A. and Friend R., Nature 335, 137-141 (1988)
[55] Baker C. J., Gelsen O. M. and Bradley D. D, *Chem. Phys. Lett.* **201**, 127 (1993)
[56] Piston D. W., Kirby M. S., Cheng H., Lederer W. J. and Webb W. W., *Applied Optics*, **33** 662-669 (1994)
[57] Lewis, A., Ben-Ami, U., Kuck, N., Fish, G., Diamant, D., Lubovsky, L., Lieberman, K., Katz, S., Saar, A., and Roth, M., *Scanning* (in press, 1994)
[58] Betzig E., Grubb S. G., Chichester R. J., DiGiovanni D. J. and Weiner J. S., *App. Phys. Lett.*, **63** 3550-3552 (1993).
[59] Kuck N., Lieberman K., Lewis A. and Vecht A., *Appl. Phys. Lett.* **61**, 2 (1992)
[60] Burroughs, J. H. et. al., *Nature* , **347**, 539 (1990).
[61] Burn, P.L. *et al.*, *J. Chem. Soc., Perkin Trans. 1.*, 3225 (1992).
[62] Greenham, N. C. *et al.*, *Nature* , **365**, 628, (1994)
[63] Moller, R., Albrecht, U., Boneberg, J., Koslowski, B., Leiderer, P and Dransfeld, K. *J. Vac. Sci. Tech. B*, 9 506 (1991)
[64] Pedarnig, J. D., Heckl, W. M. and Specht, M., and Hansch, T. W., NFO-2 Abstracts, Rayleigh, NC.(1993).
[65] Abraham D. L., Veider A., Schononberger Ch., Meier H. P., Arent D. J. and Alvarado S. F., *Appl. Phys. Lett.* **56**, 1564-1566 (1990)
[66] Malmqvist, L. and Hertz, H. M., *Proceedings of NFO-1*, 141-146 (1993)
[67] Ashkin, A., *Science* **210**, 1081 (1980).
[68] Chu, S., *Science* **253**, 861 (1981).
[69] Non-linear particle, *Proceedings of NFO-1, Besancon*
[70] Seltzer, E. H. K., Albrecht, S , Rosin, A., and Horber, J. K. H., European Molecular Biology Meeting on " New Microscopic Techniques for Biology and Medicine: Photonic Microscopies," Heidelberg, May 1994.
[71] Ghislain, L. P., and Webb, W. W., *Optics Lett.* **18**, 1678 (1993)
[72] Arika, Z., "A submicron detector based on photoconductive materials," Masters Thesis (Hebrew University, 1991).
[73] Tan W., Shi Z., Smith S. Birnbaum D. and Kopelman R., *Science* **258**, 778-781 (1992)
[74] Woltbeis, O. S., Fiber Optic Chemical Sensors and Biosensors (CRC Press, Boca Raton, Fl., 1991). Vol 1.
[75] Samuel, J., Strinkovski, A., Shalom, S., Lieberman, K., Ottolenghi, M., Avnir D.and Lewis, A., "A metallized micropipette tip filled with doped xerogel for near-field optical pH sensing," Chemical Materials (in press, 1994).
[76] Lewis, A., "Diffraction unlimited optics," in *Trends in International Optics*, J. C. Dainty, Ed., Vol 2 , Academic Press, New York (1994).
[77] Stern, E. A., Kalman, Z., Lewis A., and Lieberman, K., *Appl. Opt.* **27**, 5135 (1988)
[78] Saitoh, K., Inagawa, K.., Kohra, K., Hayashi, C., Ida, A., and Kato, N., *Jap. J. Appl. Phys.* 27, L2131 (1988)
[79] Pearlman J. S. and Benjamin R. F., *Appl. Opt* **16**, 94 (1977)
[80] Wilkins, S. W., *Nuc. Instrum. Meth.* A **269**, 321 (1988)
[81] Thiel, D. J., Bilderback, D. H., Lewis, A., and Stern, E. A., *Nucl. Instrum. Methods Phys. Res. Sect.* **317**, 597 (1992).
[82] Bilderback D., Hoffman S. A. and Thiel D. J., Science **263**, 201 (1994)
[83] Engstrom, P., Larsson, S., Rinby, A., and Stocklassa, B., *Nucl. Instrum. Methods* **B36**, 222 (1989)
[84] Engstrom, P., Larsson, S., Rinby, A., and Stocklassa, B., *Nucl. Instrum. Methods* **A302**, 547 (1991).
[85] Thiel D. J., Bilderback D. H., Lewis A., Stern E. A. and Rich T., *Applied Optics* **31**, 987 (1992)
[86] Thiel D. J., Stern E. A., Bilderback D. H.and Lewis A., *Physica B* **158**, 314 (1989)

[87] Livins P., Thiel D. J., Stern E. A.and Lewis E. A., *Nuclear Instruments and Methods* **A291**, 250 (1990)
[88] Thiel D. J., Bilderback D. H. and Lewis A., *Rev. Sci. Instr.* **64**, 2872 (1993)
[89] Mansfield, S. M. and Kino, G. S., *Appl. Phys. Lett.* **57**,
[90] Binnig, G. , Gerber, Ch. Weibel, E., and Rohrer, H., *Phys. Rev. Lett.* **50**. 120 (1983),
[91] Durig, U., Pohl, D. W. and Rohner, F., *J. Appl. Phys.* **59**, 3318 (1986).
[92] Lieberman, K. and Lewis, A. , *Appl. Phys. Lett.* **62**, 1335 (1993).
[93] Hartmann, T., Gatz, R., Wiegrabe, W., Kramer, A., Hillebrand, A., Lieberman, K., Baumeister, W., and Guckenberger, R., Proc. of the NATO Advanced Workshop on Near-field Optics, Arc-et-Senans, Oct. 1992, NATO Series E: Applied Sciences, Vol. 242 (Kluwer, Dordrecht, 1993) p35.
[94] Michel, B., Mizutani, W., Schierle, R., Jarosch, A., Knop, W., Benedickter, H., Bachtold, W., and Rohrer, H., *Rev. Sci. Instr.* **63**, 4080 (1992).
[95] Sarid, D. Oxford University Press.
[96] Binnig, G., Quate, C. F., and Gerber, C., *Phs. Rev. Lett.* **56**, 930 (1986).
[97] van Hulst, N. F., Moers, M. H. P., Noordman, O. F. J., Tack, R. G., Segerink, F. B., and Bolger, B., *Appl. Phys. Lett.* **62**, 461 (1993).
[98] Zenhausern, F., O'Boyle, M. P. and Wickramasinghe, H. K., *Appl. Phys. Lett.* **65**, 1623 (1994).
[99] Shalom S., Lieberman K. Lewis A. and Cohen S. R., *Rev. Sci. Instrm.* **63**, 4061 (1992)
[100] Lieberman K., Lewis A., Fish G., Shalom S., Jovin T., Schaper A. and Cohen S. R., *Appl. Phys. Lett.* **65**, 650 (1994).
[101] Toledo-Crow R., Yang P. C. Chen Y. and Vaez-Iravani M., *Appl. Phys. Lett.* **60**, 2957-2959 (1992)
[102] Betzig E., Finn P. L. and Weiner J. S., *Appl. Phys. Lett.* **60**, 2484-2486 (1992)
[103] Shchemelinin A., Rudman M., Lieberman K. and Lewis A., *Rev. Sci. Instr.* **64**, 2528-2531 (1993)
[104] Hansma P. K., Drake B., Marti O., Gould S. A. C. and Prater C. B., *Science* **362**, 641-643 (1989)
[105] Neher, E., and Sakmann, B., *Nature* **260**, 799 (1976).
[106] Matey J. R. and Blanc J., *J. Appl. Phys.* **57**, (5) 1437-1444 (1985)
[107] Rudman M., Lewis A., Mallul A., Haviv V., Turevets I., Shchemelinin A., Nebenzahl I., *J. Appl. Phys.* **72**, 4379 (1992).
[108] Bozhevolnyi S. I., Xiao M. and Keller O., *Applied Optics*, **33** 876-880 (1994)
[109] unpublished results
[110] Hrynevych M., Butler D. J., Nugent K. A.and Roberts A., *Proceedings of NFO-1*, 391-398 (1993)
[111] Betzig E., Lewis A., Harootunian A., Isaacson M. and Kratschmer E., *Biophys. J.* **49**, 269 (1986).
[112] Proceedings of STM-93, American Institue of Physics (1994)
[113] Burleigh Instruments, Inc., Burleigh Park, Fishers, New York 14453.
[114] Gary Valascovic private communication.
[115] Putnam, C. A. J., van der Werf, K. O., de Grooth, B. G., van Hulst, N. F., Segerink, F. B. and Greve, J., *Rev. Sci. Instrum.* **63**, 1914 (1992)
[116] Besocke, K. , *Surface Science* **181**, 145 (1987)
[117] Wilson, T. and Shepard, C., Theory and Practice of Scanning Optical Microscopy. Academic Press, London (1984).
[118] Cline, J. A., Barshatzky, H., and Isaacson, M., *Ultramicroscopy* **38**, 299 (1991).
[119] Lewis A., Isaacson M., Betzig E. and Harootunian A., "Near-Field Scanning Optical Microscopy", United States Patent Number 4,917,462; Issued: April 17, 1990
[120] Suzuki, M., Fujii, T., Onuki, T., Miyashita, M., and Matsushiro, M., Proceedings of STM 1991, *Ultramicroscopy* **22-24**, (1992).
[121] O'Conner S., private communication
[122] Eisenstein, G., and Vitello, D., *Appl. Opt.* **21**, 3470 (1982).
[123] Reddick, R. C., Warmack, R. J. and Ferrel, T. L., *Phys. Rev. B* **39**, 767 (1989)
[124] Courjon, D., Sarayeddine, K., and Spajer, M., *Opt. Comm.* **71**, 23 (1989)
[125] de Fornel, F., Goudonnet, J. P., Salomon, L., and Lesniewska, E., *Proc. SPIE* **1139**, 77 (1989).
[126] van Hulst, N. F., Moers, M. H. P., and Bolger, B., *J. of Micros.* **171**, 95 (1993)
[127] van Hulst, N. F., Moers, M. H. P., Noordman, O. F. J., Tack, R. G., Segerink, F. B., and Bolger, B., *Appl. Phys. Lett.* **62**, 461 (1993).

[128] van Hulst, N. F., Moers, M. H. P., Noordman, O. F. J., Faulkner, T., Segerink, F. B., an der Werf, K. O., de Grooth, B. G., and Bolger, B., *Proc. SPIE* **1639**, 36 (1992).
[129] Akari, S., Lux-Steinger, M. Ch., Vogt, M., Stachel, M.,and Dransfeld, K., *J. Vac. Sci. Technol.* **B9**, 561 (1991).
[130] Volcker, M., Krieger, W., and Walther, H., *Phys. Rev. Lett.* **66**, 1717 (1991).
[131] Michel, B., Mizutani, W., Schierle, R., Jarosch, A., Knop, W., Benedickter, H., Bachtold, W., and Rohrer, H., *Rev. Sci. Instr.* **63**, 4080 (1992).
[132] Grober, R. D., Harris, T. D., Trautman, J. K. and Betzig, E., *Rev. Sci. Instrum.* **65** 626 (1994)
[133] Inoue, S., *Video Microscopy*, Plenum Press, New York (1986).
[134] Pawley, J., *The Handbook of Biological Confocal Micorscopy*, IMR Press, Madison, Wisconsin (1989).
[135] Denk, W., Strickler, J.H. and W. W. Webb, *Science* **248**, 73 (1987).
[136] Freund, I., Deutsch, M., and A. Sprecher., *Biophys. J.* **50**, 693 (1986).
[137] Paessler, M. A., Moyer, P. J., Jalmoke, O. J., Johnson, C. E., Reddick, R. C., Warmack, R. J., Ferrel, T. L., *Phys. Rev. B.* **42**, 6750 (1990).
[138] van Hulst, N. F., Segerrin, F. B., Achten, F. and Bolger B., *Ultramicroscopy* **22-24** (1992)
[139] Garcia,-Parajo, M., Cambril, E., and Chen, Y., *Appl. Phys. Lett.* **65**, 1498 (1994).
[140] Kroo, N., Thost, J.-P., Volcker, M., Krieger, W., and Walther, H., *Europhys. Lett.* **15**, 289 (1991).
[141] Tsai, D. P., Kovacs, J., Wang, Z., Moskovitz, M., Shalev, V. M., Suh, J. S. and Botet R., *Phys. Rev. Lett.*, **72** 4149 (1994)
[142] Berndt R., Gaisch R, Schneider W. D., Gemzewski J. K., Reihl B., Schlittler R. R. and Tschudy M., *Appl. Phys. A.* **57**, 5133 (1993)
[143] Berndt R., Gaisch R., Gemzewski J. K., Reihl B., Schlittler R. R., Schneider W. D., and Tschudy M., *Science* **262**, 1425 (1993).
[144] Vaez-Iravani M. and Toledo-Crow R., *Appl. Phys. Lett.*, **62** 1044 (1993)
[145] Vaez-Iravani M. and Toledo-Crow R., *Appl. Phys. Lett.*, **62** 138 (1993)
[146] Lieberman K., Phd Thesis, Hebrew University of Jerusalem 1992
[147] Lord Rayleigh, *Phil. Mag.* **42**, 167 (1896).
[148] Palanker D., Lewis A., Ohad S., Simon A., Shenkar J., Penchas S. and Laufer N., *Lasers in Surgery and Medicine* **11**, 580-586 (1991).
[149] Lewis A., Palanker D., Hemo I., Pe'er J. and Zauberman H., *Investigative Ophthalmology and Visual Science* **33**, 33 (1992).
[150] Laufer N., Palanker D., Shufaro Y., Safran A., Simon A. and Lewis A., *Fertility and Sterility* **59**, 889 (1993).
[151] Palanker D., Hemo I., Turevets I., Zauberman H. and Lewis A., *Investigative Ophthalmology* (in press).
[152] Turovets I., Lewis A., Palanker D., Gilo H., Vilenz A., Broder J. C. and Lewis S., *BioTechniques* **15**, 1022-1027 (1993).
[153] Betzig E., Lewis A., Harootunian A, Isaacson M. and Kratschmer E. *Biophy. J.* **49**, 262 (1986)
[154] Lewis A., Betzig E., Harootunian A. and Isaacson M., "Fluorescence Near-Field Microscopy," in **Spectroscopic Membrane Probes**, Vol II, ed, L. M. Loew, CRC Press, Florida (1988) pp. 81-110.
[155] Fischer U., *J. Opt. Soc. Am.* **B3** 1239 (1986)
[156] Betzig, E., Chichester, R. J., Lanni, F., and Taylor, D. L., *Bioimaging* **1**, 129 (1994).
[157] Trautman J. K., Betzig E., Weiner J. S., DiGiovanni D. J., Harris T. D., Hellman F. and Gyorgy E. M., *J. Appl. Phys.*, **71**, 4659 (1992)
[158] Oxford Instruments, Old Station Way, Eynsham, Witney, Oxon, England
[159] Grober R. D., Harris T. D., Trautman J. K., Betzig E., Wegschleider W., Pfeiffer L. and West K., *Appl. Phys. Lett.* **64**, 1421 - 1423 (1994)
[160] Christen J., Kapon E., Colas E., Hwang D. M., Schiavone L. M., Grundmann M. and Bimberg D., *Surface Science* **267**, 257 (1992)
[161] Abrahm D. L., Veider A., Schonenberger C. H., Meier H. P., Arent D. J. and Avarado S. F., *Appl. Phys. Lett.* **56**, 1564 (1990)
[162] Hess, H. F., Betzig, E., Harris, T. D., Pfeiffer, L. N., and West, K. W., *Science* **264**, 1740 (1994).
[163] Butt, H-J., *Nanotechnology* **3**, 60 (1992).
[164] Ducker, W. A.; Senden, T. J., and Pashley, R. M., *Nature* **353**, 239 (1991).

[165] Butt, H.-J., Biophys. J. 60, 1438 (1991).
[166] Lakawicz, J. R. in *Applications of Fluorescence in the Biomedical Sciences* eds Taylor, D. L., Waggoner, A. S., Murphey R. F., Lanni, F. and Birgee R. R., Liss Inc. New York, NY (1986) pp 29-67
[167] Gratton E., Jameson D. M. and Hall R. D. *Ann. Rev. Biophys. Bioeng.* 13 105-124 (1984).
[168] Dunn,R. C., Holton, G. R., Mets L. and Xie, X. S., *J. Phys. Chem.* 98, 3094-3098 (1994).
[169] Peck, K., Stryer, L., Glazer, A., and Mathies, R. A., *Proc. Natl. Acad. Sci. U.S.A.* 86, 4087 (1989)
[170] Shera, E. B., Seitzinger, N. K., Davis, L. M., Keller, R. A., and Soper, S. A., *Chem. Phys. Lett.* 174, 553 (1990).
[171] Whitten, W. B., Ramsey, J. M., Arnold, S., Bronk, B. V., *Anal. Chem.* 63, 1027 (1991).
[172] Nguyen, D. C., Keller, R. A., Jett, J. H., and Martin, J. C., *Anal. Chem.* 59, 2158 (1987).
[173] Hirshfeld T., *Appl. Opt.* 15, 2965 (1976).
[174] Moerner, W. E., and Basche, T., *Angew Chem.* 32, 457 (1993).
[175] Barak L. S. and Webb W. W., *J. Cell Biol.* 90, 595 (1981).
[176] Betzig E., and Chichester, *Science* 262, 1422 (1993)
[177] Xie, X. S., and Dunn, R. C., *Science* 265, 361 (1994).
[178] Ambrose, W. P., Goodwin, P. M., Martin, J. C., and Keller, R. A., *Science* 265, 364 (1994).
[179] Ambrose, W. P., Goodwin, P. M., Martin, J. C., and Keller, R. A., *Phys. Rev. Lett.* 72, 160 (1994).
[180] Trautman, J. K., Macklin, J. J., Brus, L. E., and Betzig, E., *Nature* 369, 40 (1994).
[181] Lieberherr, M., Fattinger, C., Lukosz, W., *Surface Science* 189, 954 (1987).
[182] Hell, S. W., European Patent Application 91121368.4 (1990)
[183] Hell, S. W., Lindek, S., Cremer, C., and Stelzer, E., *Appl. Phys. Lett.* 64, 1335 (1994).
[184] Hell, S. W., Opt. Commun. (in press 1994).
[185] Srinivasan R, Braren B, *Chem. Rev.* 89, 1303 (1989).
[186] Haronian D. and Lewis A., *Appl. Phys. Lett.* 61, 2237 (1992).
[187] Srinivasan R., J. Appl. Phys. 72, 1651 (1992).
[188] Nanonics Ltd. 21 Havaad Haleumi, Jerusalem, ISRAEL
[189] Betzig, E., Trautman, J. K., Wolfe, R., Gyorgy, E. M., and Finn, P. L., *Appl. Phys. Lett.* 61, 142 (1992).
[190] Hoen S., Mamin H. J. and Rugar D., *Appl. Phys. Lett.* 64, 267 (1994)
[191] Chen Z., Lewis A., Takei H. and Nebenzahl I., *Applied Optics* 30, 5188 (1991)
[192] Terris, B. D., Mamin, H. J., Rugar, D., Studenmund, W. R., and Kino, G. S., *Appl. Phys. Lett.* 65, 388 (1994).
[193] Fork R. L., Avramopoulos H. and Valdmanis J. A., *American Scientist* 78, 216 (1990).
[194] Palanker, D. and Lewis, A., *Biophys. J.* 60, 1147 (1990).
[195] Fish G, Bouevitch, O., Kokotov, S., Palanker, D., Turevets, I., Liebberman, K., Lewis, A., *Rev. Sci. Instrum.* (in press).
[196] Schrek, E., Hiller, B., and Singh, G. P., *Rev. Sci. Instr.* 64, 218 (1993).
[197] William, C. C., and Wickramasinghe, H. K., *Appl. Phys. Lett.* 49, 1587 (1986).
[198] Barnes, J. R., Stephanson, R. J., Welland, M. E., Gerber, C. H., and Gimzewski, J. K., *Nature* 372, 79 (1994).
[199] Pedarnig, J. D., Heckl, W. M. and Specht, M., and Hansch, T. W., NFO-2 Abstracts, Rayleigh, NC.(1993).

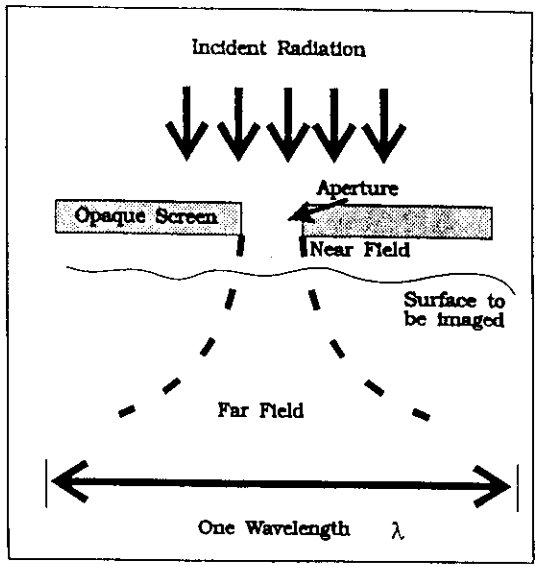

F1

National Aeronautics and
Space Administration

Goddard Space Flight Center
Greenbelt, Maryland
20771

NASA

Code 681

June 14, 1988

Dr. Aaron Lewis
Cornell University
Applied and Engineering Physics
159 Clark Hall
Ithaca, NY 14853

Dear Dr. Lewis:

The New Scientist for 19 May 1988 carried an article on your optical microscope. A friend brought it to my attention, noting that I had described something of the same kind (though without any experimental verification) in JOSA long ago. I enclose the reprint, and would appreciate receiving a reprint of your paper. My address is:

Code 681
NASA Goddard
Greenbelt, MD 20771.

The occultation of a star by the moon yields a somewhat analogous situation. A study of the light variation with time during the occultation allows a fellow with a small telescope to measure one component of the separation of a double-star pair which cannot be resolved with the biggest optical telescope. Occultation by an asteroid gives another large factor in resolution; that is how the rings of Uranus were discovered.

Sincerely yours,

John A. O'Keefe

John A. O'Keefe
Laboratory for Astronomy and Solar Physics

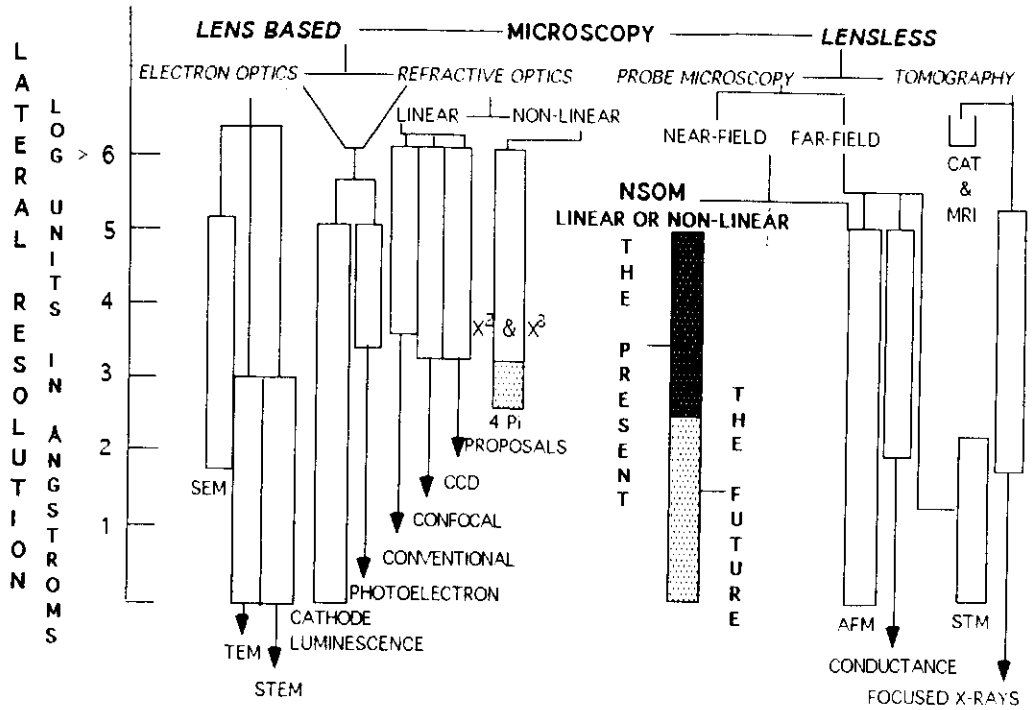

Figure 2

#3

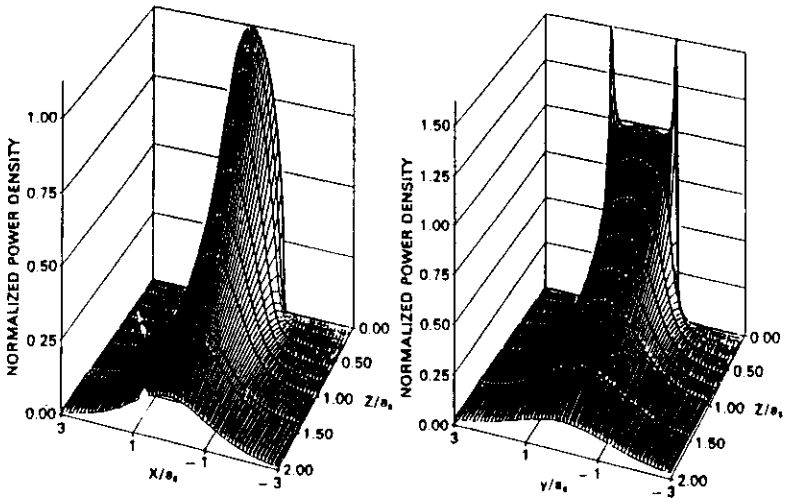
NORMALIZED POWER DENSITY
1.00
0.75
0.50
0.25
0.00
3
1
−1
−3
X/a₀
0.00
0.50
1.00
1.50
2.00
Z/a₀
NORMALIZED POWER DENSITY
1.50
1.25
1.00
0.75
0.50
0.25
0.00
3
1
−1
−3
Y/a₀
0.00
0.50
1.00
1.50
2.00
Z/a₀

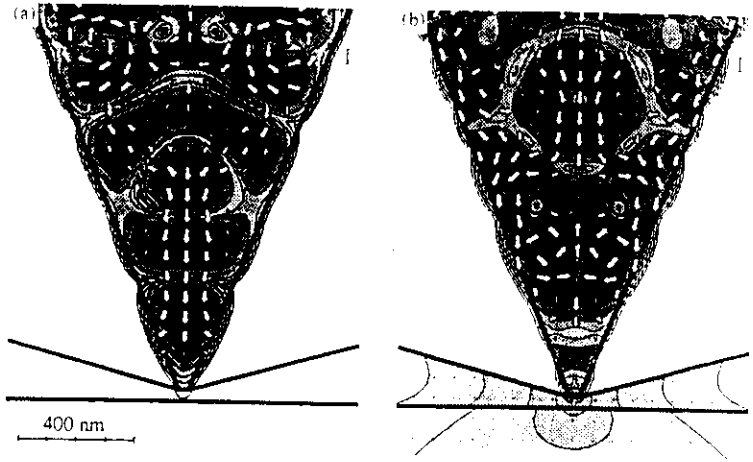
(a)
(b)
400 nm

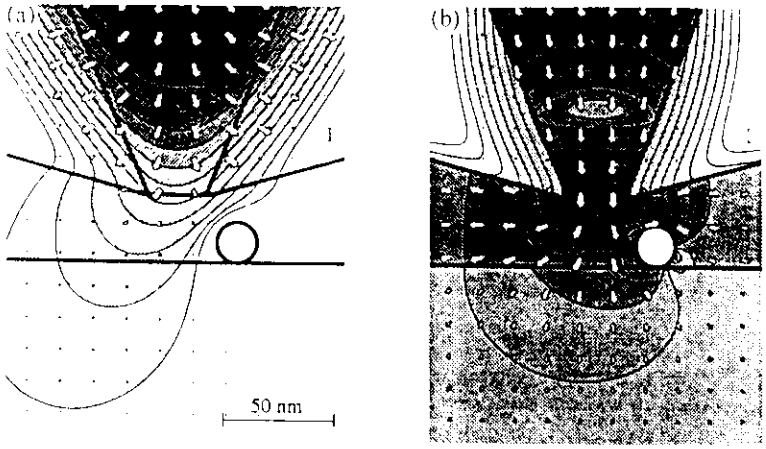
(a)
(b)
50 nm

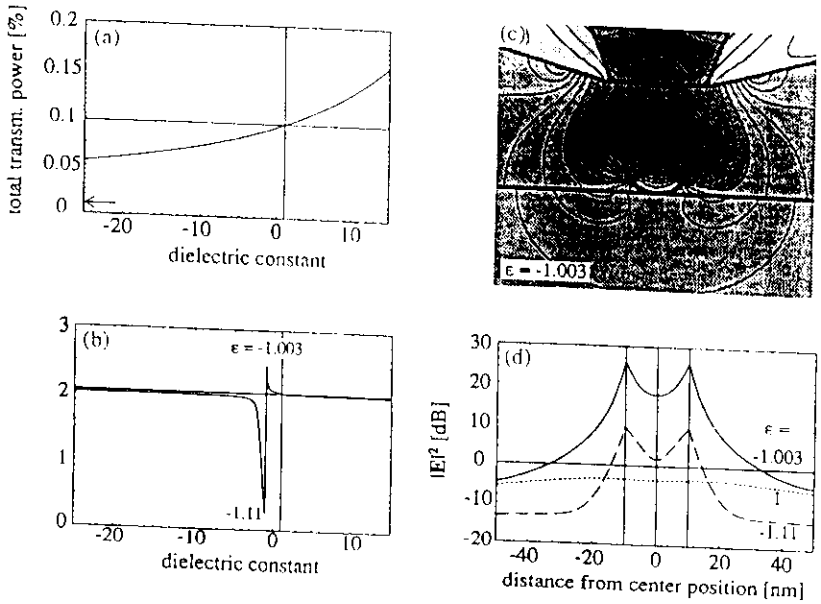
total transm. power [%]
(a)
dielectric constant
(b)
ε = -1.003
-1.11
dielectric constant
(c)
ε = -1.003
(d)
|E|² [dB]
ε = -1.003
-1.11
distance from center position [nm]

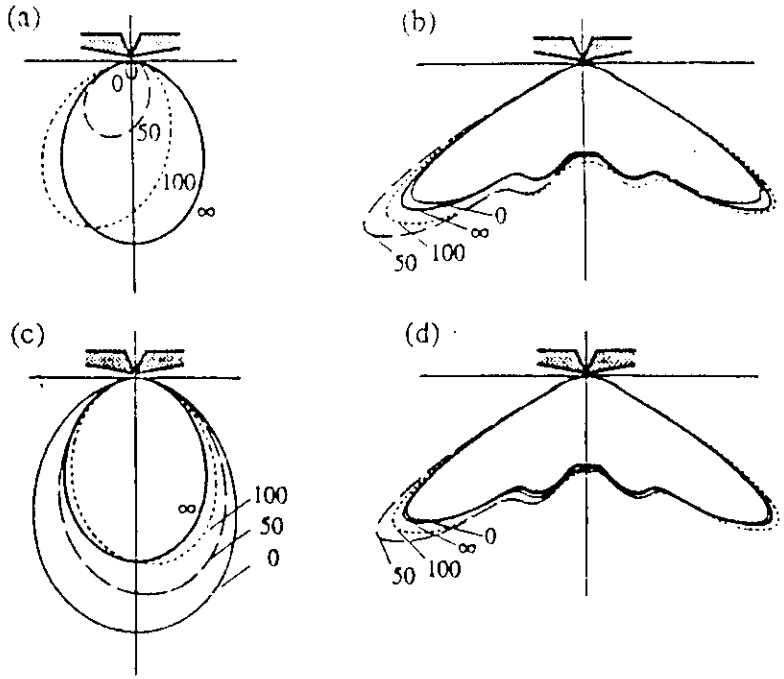
(a)
0
50
100
∞
(b)
0
∞
50
100
(c)
∞
100
50
0
(d)
0
∞
50
100

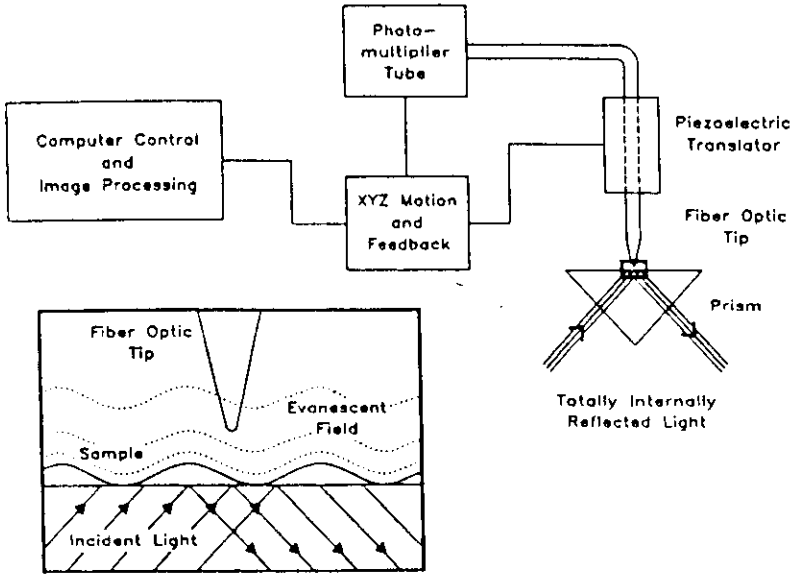
Photo-multiplier Tube
Computer Control and Image Processing
XYZ Motion and Feedback
Piezoelectric Translator
Fiber Optic Tip
Prism
Totally Internally Reflected Light
Fiber Optic Tip
Evanescent Field
Sample
Incident Light

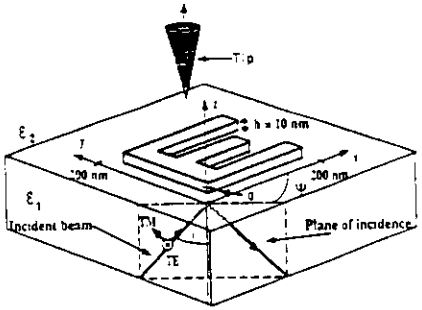
Tip
h = 10 nm
200 nm
200 nm
Incident beam
Plane of incidence
TM
TE

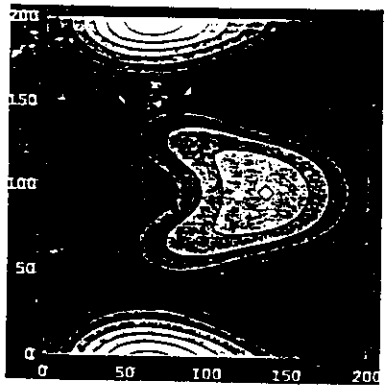
200
150
100
50
0
0
50
100
150
200

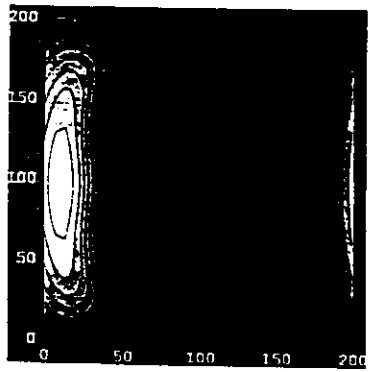
200
150
100
50
0
0
50
100
150
200

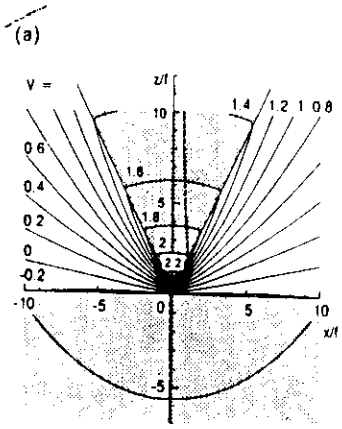
(a)
V =
z/f
x/f
1.4
1.2
1
0.8
0.6
0.4
0.2
0
-0.2
1.6
1.8
2
2.2
10
5
-5
-10

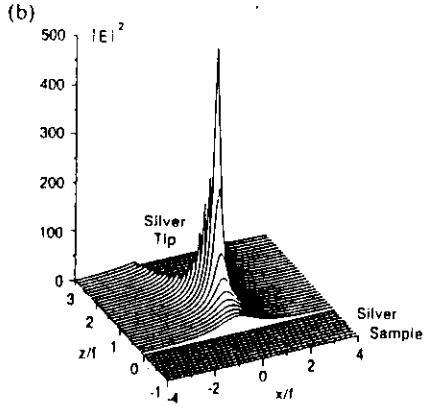
(b)
|E|²
500
400
300
200
100
0
Silver
Tip
Silver
Sample
z/f
x/f
3
2
1
0
-1
-4
-2
0
2
4

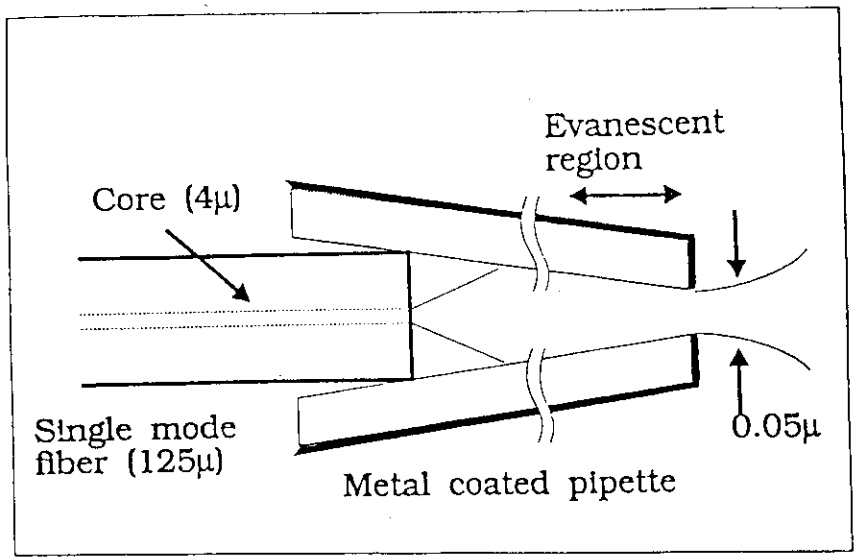
Evanescent
region
Core (4μ)
Single mode
fiber (125μ)
0.05μ
Metal coated pipette

Fig 2

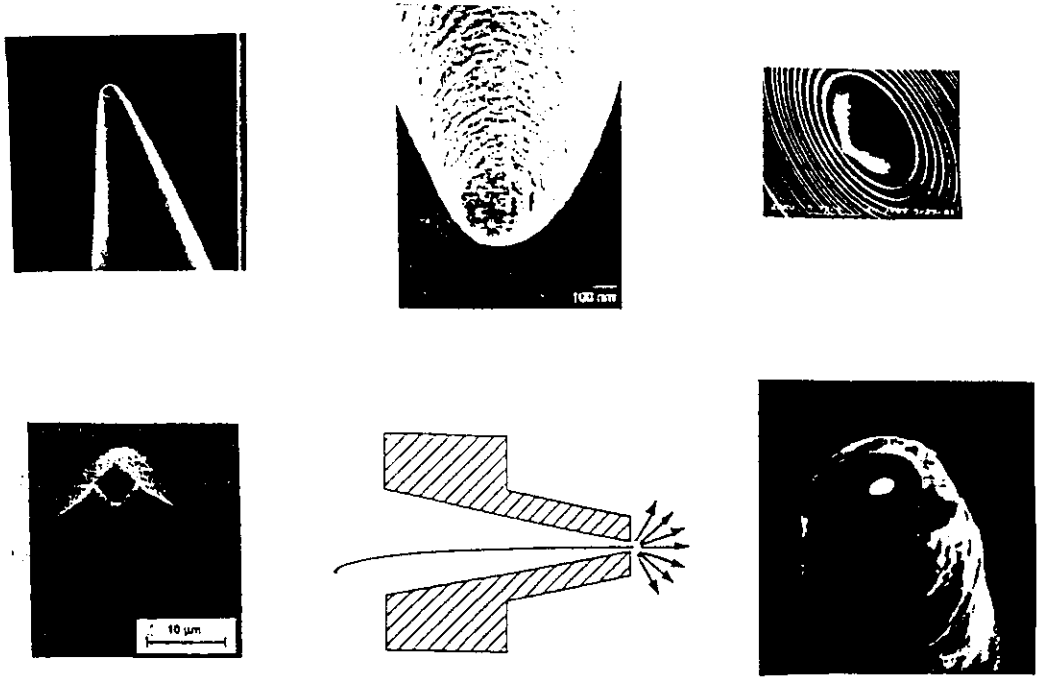
10 μm

Fig 3

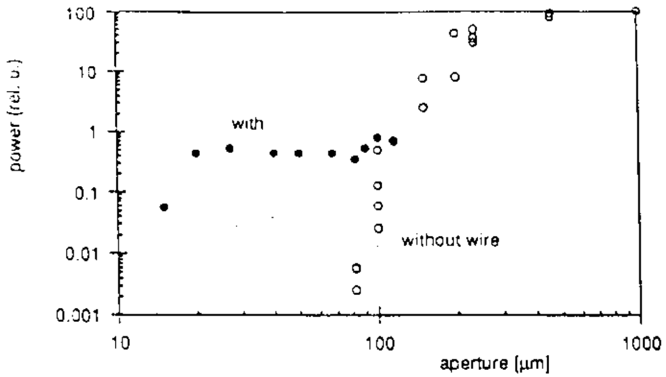
power (rel. u.)
100
10
1
0.1
0.01
0.001
10
100
1000
aperture [µm]
with
without wire

F 12

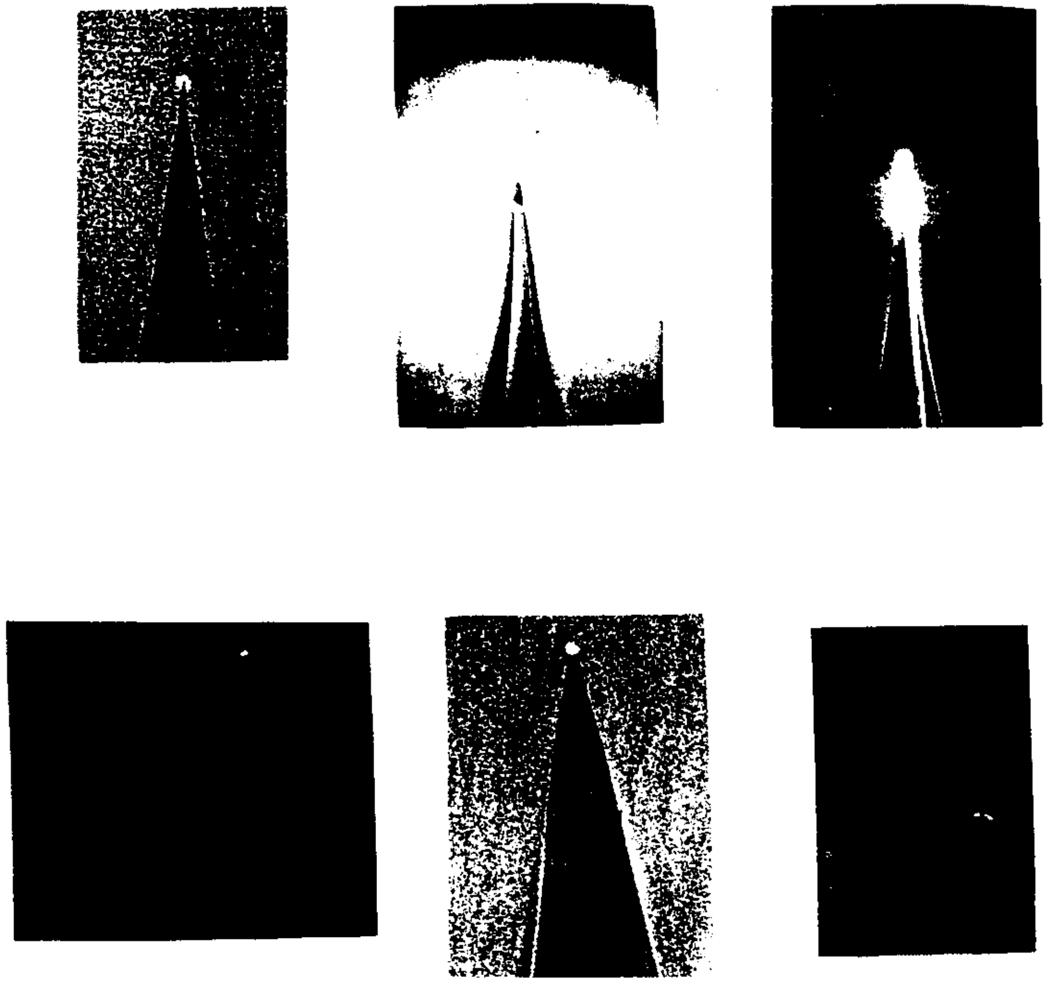

F 13

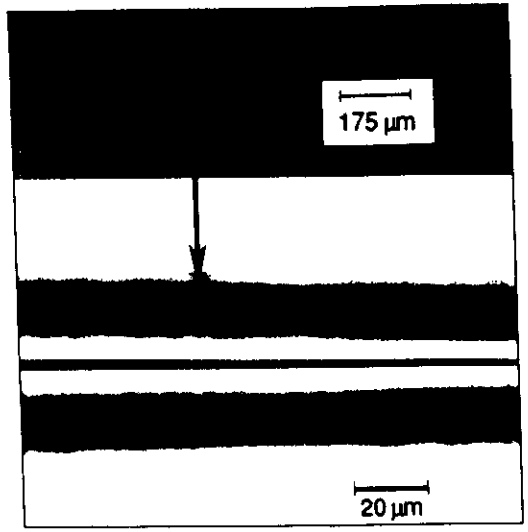

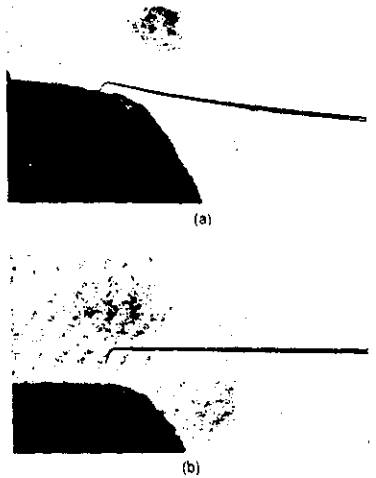

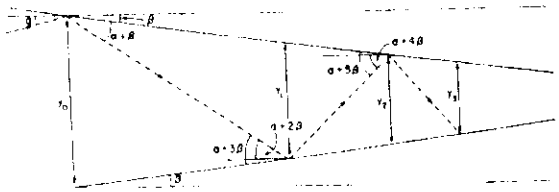

α = angle of incidence with respect to capillary axis
β = angle of capillary taper

Fig. 16

Fig 18

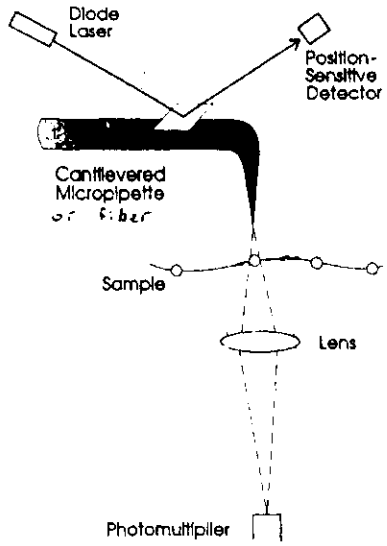

Fig 19a

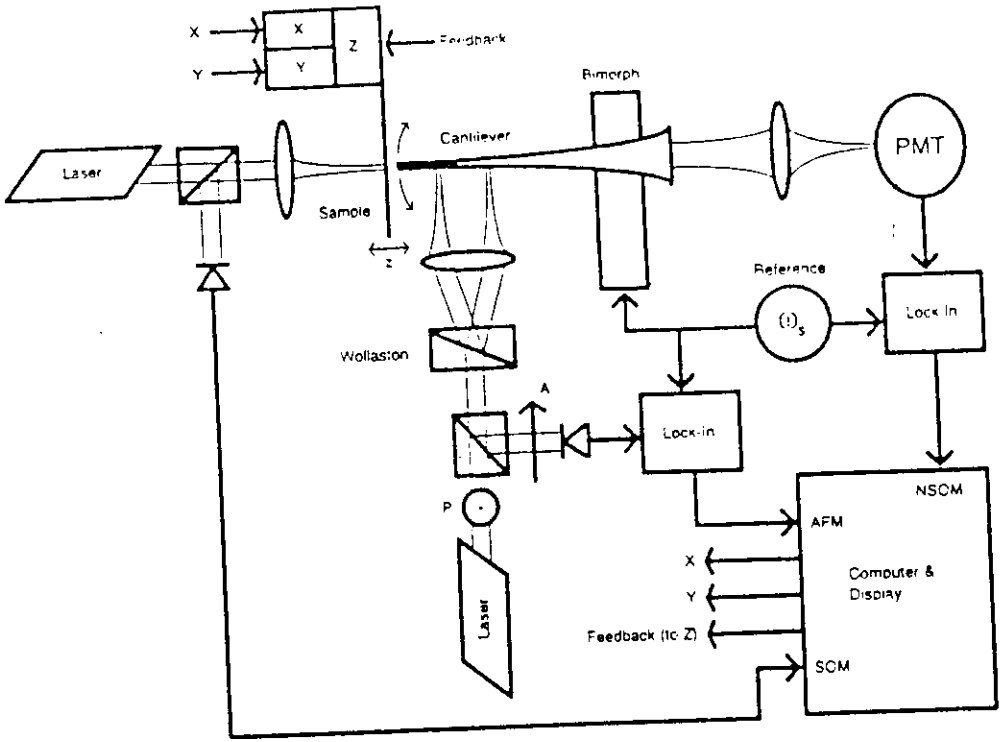
X
Y
X
Y
Z
Feedback
Bimorph
Cantilever
Laser
PMT
Sample
Reference
Lock-In
Wollaston
A
Lock-in
NSOM
AFM
P
Computer &
Display
X
Y
Feedback (to Z)
Laser
SOM

Fig 19B

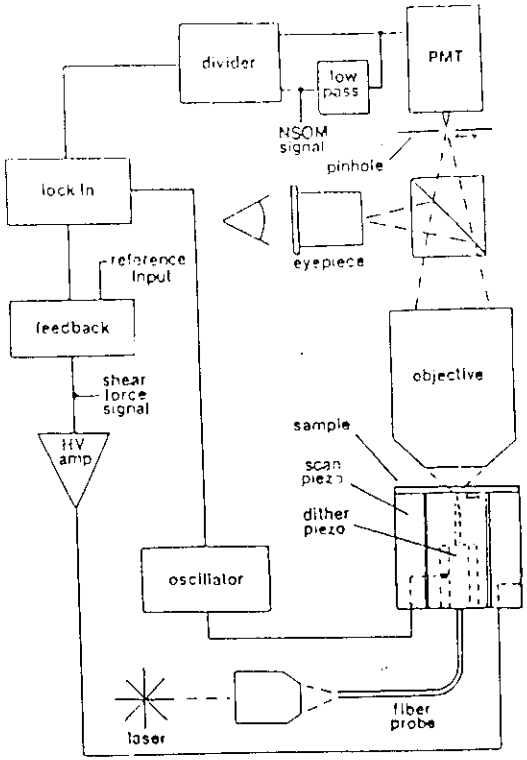

Fig 19C

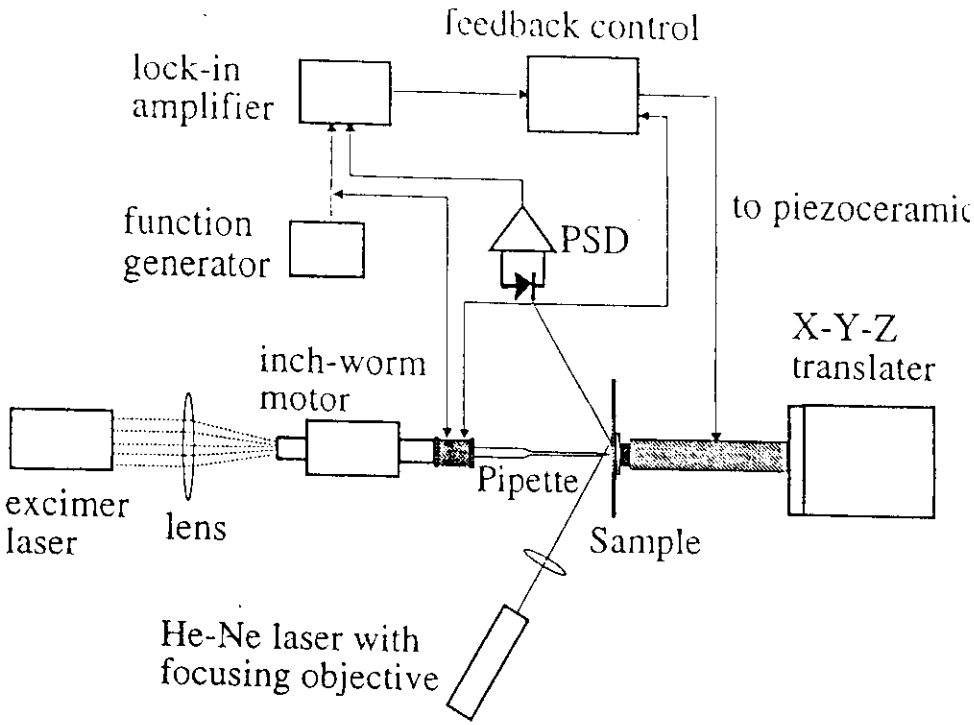

Fig 19D

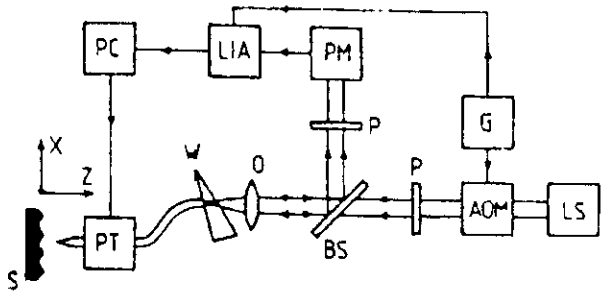

Fig. 19E

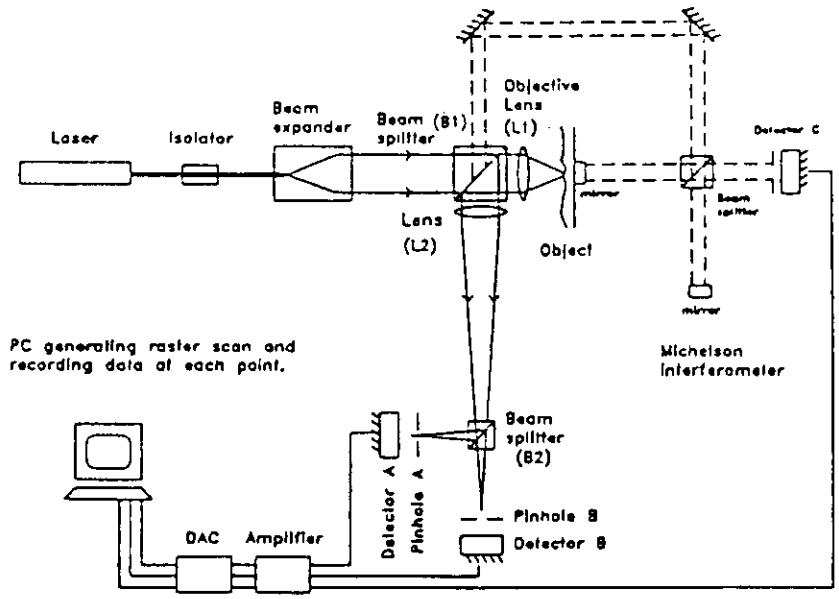
Laser
Isolator
Beam expander
Beam (B1) splitter
Objective Lens (L1)
Lens (L2)
Object
mirror
Beam splitter
Detector C
mirror
Michelson interferometer
PC generating raster scan and recording data at each point.
Beam splitter (B2)
Detector A
Pinhole A
Pinhole B
Detector B
DAC
Amplifier

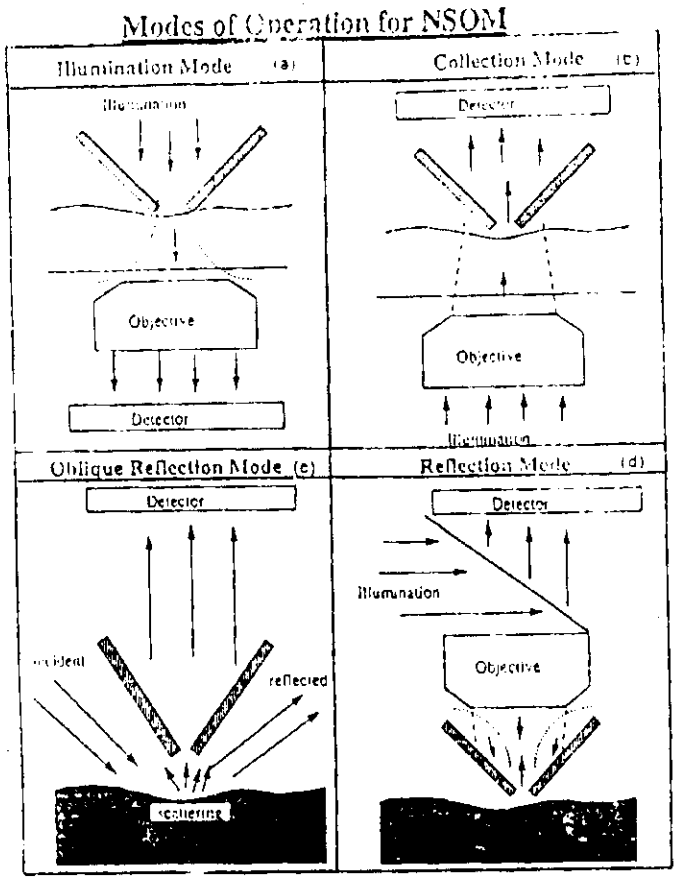
Modes of Operation for NSOM
Illumination Mode (a)
Objective
Detector
Collection Mode (b)
Detector
Objective
Oblique Reflection Mode (c)
Detector
reflected
Reflection Mode (d)
Detector
Illumination
Objective

Fig 20

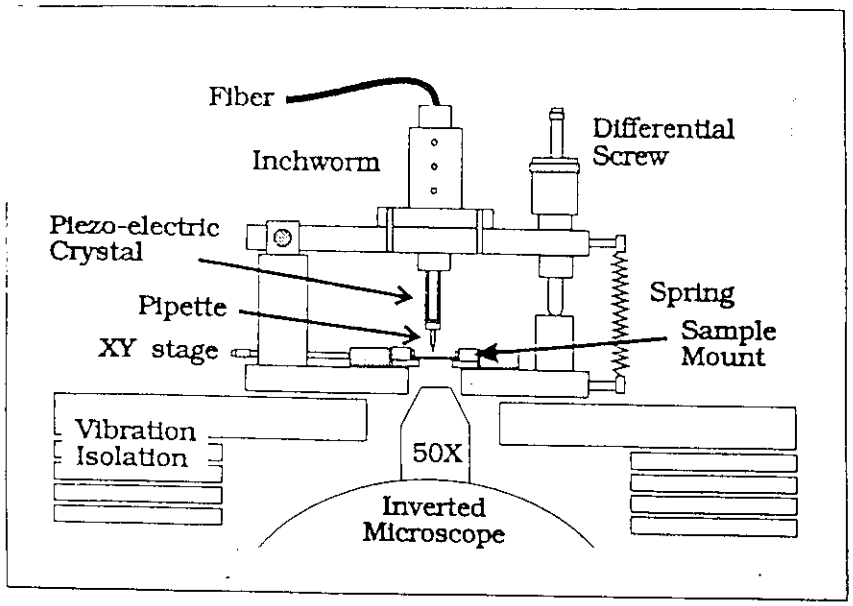
Fiber
Inchworm
Differential Screw
Piezo-electric Crystal
Pipette
XY stage
Spring
Sample Mount
Vibration Isolation
50X
Inverted Microscope

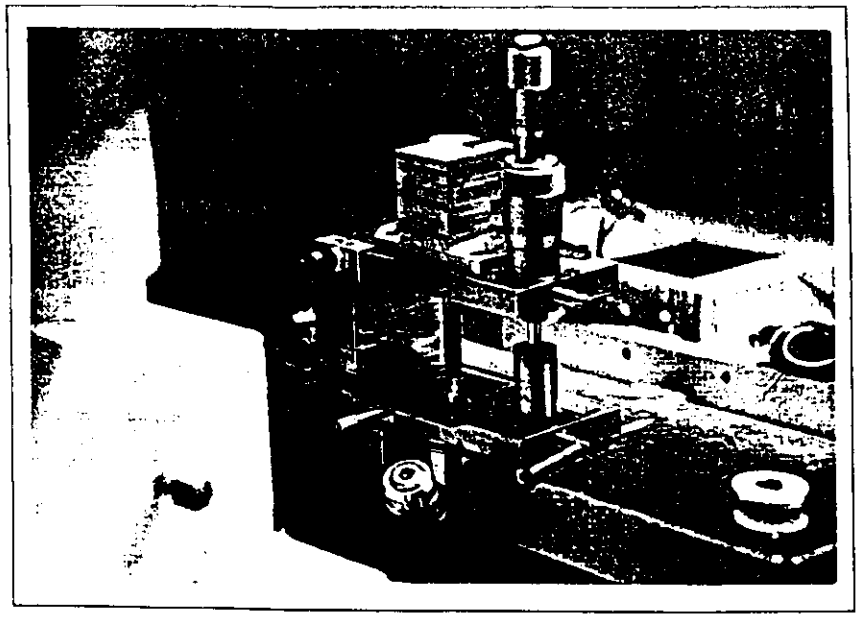

Fig 21

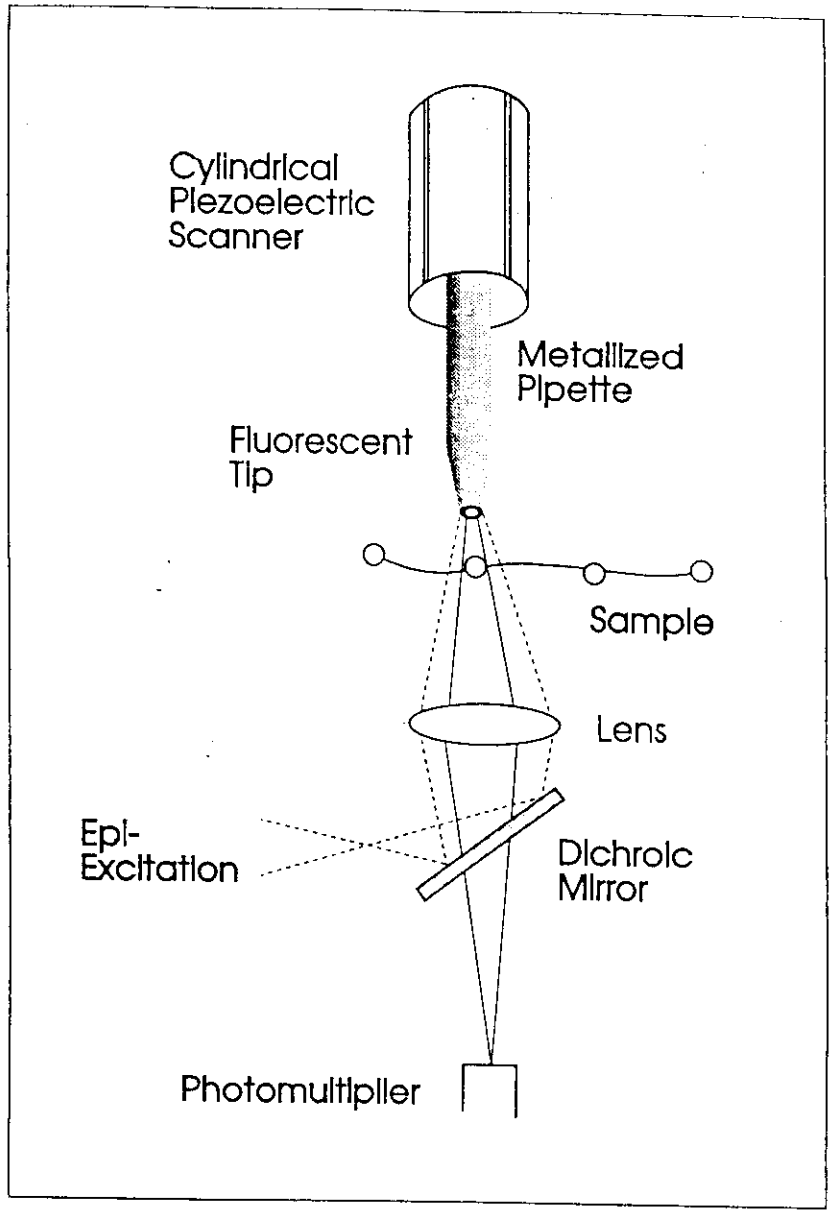
Cylindrical Piezoelectric Scanner
Metallized Pipette
Fluorescent Tip
Sample
Lens
Epi-Excitation
Dichroic Mirror
Photomultiplier

Fig 22

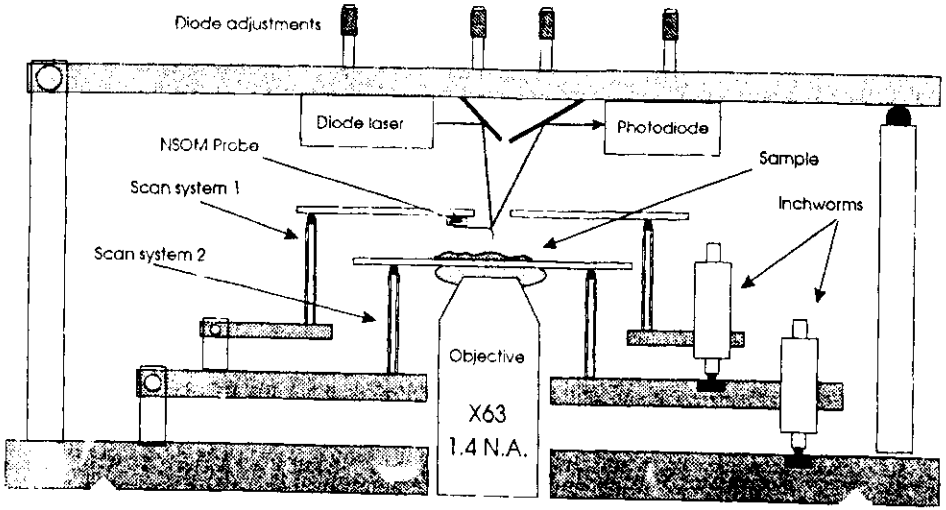
Diode adjustments
Diode laser
Photodiode
NSOM Probe
Sample
Scan system 1
Inchworms
Scan system 2
Objective
X63
1.4 N.A.

Fig 23

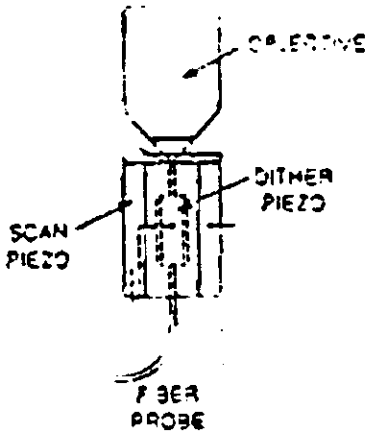
OBJECTIVE
DITHER PIEZO
SCAN PIEZO
FIBER PROBE

Fig 24

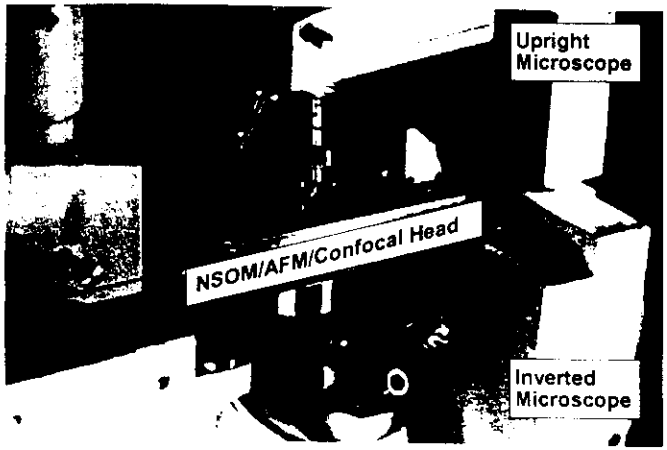
Upright Microscope
NSOM/AFM/Confocal Head
Inverted Microscope

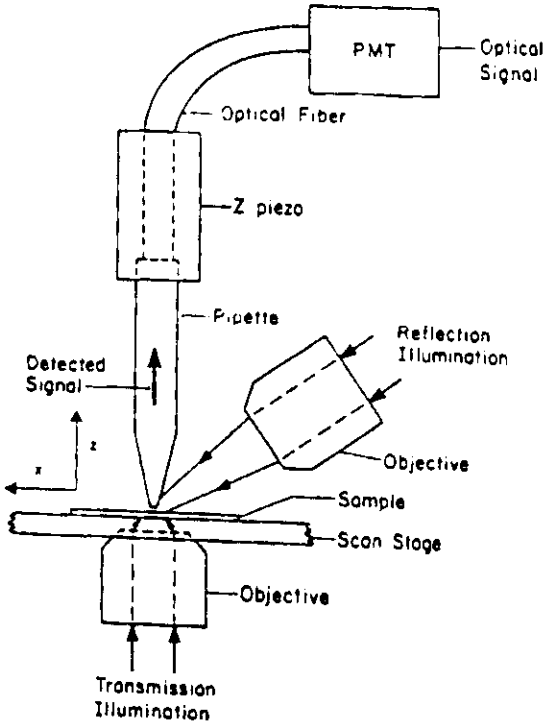
PMT
Optical Signal
Optical Fiber
Z piezo
Pipette
Reflection Illumination
Detected Signal
z
x
Objective
Sample
Scan Stage
Objective
Transmission Illumination

Fig 25

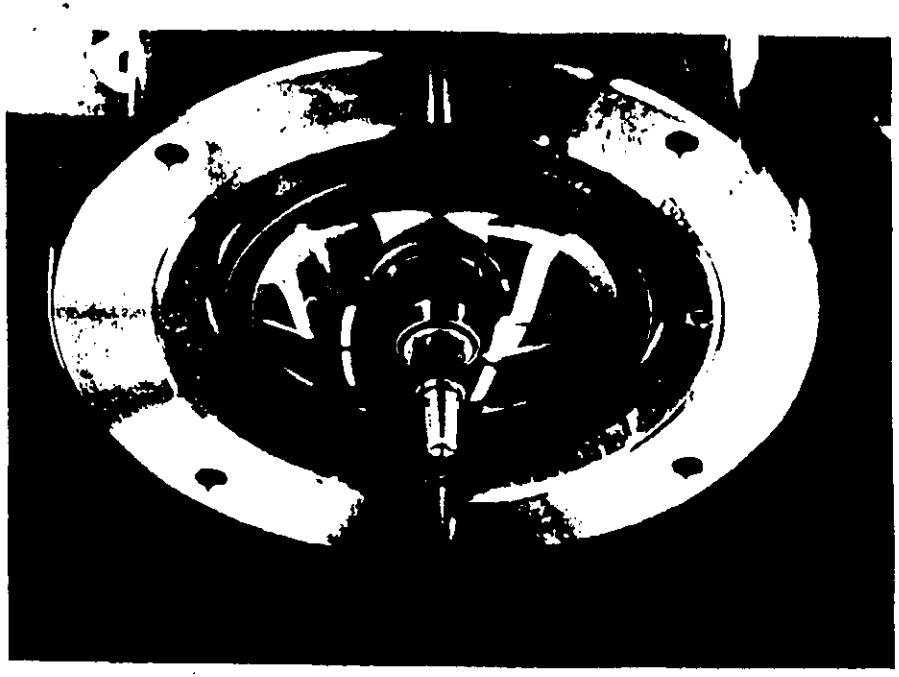

Fig. 26

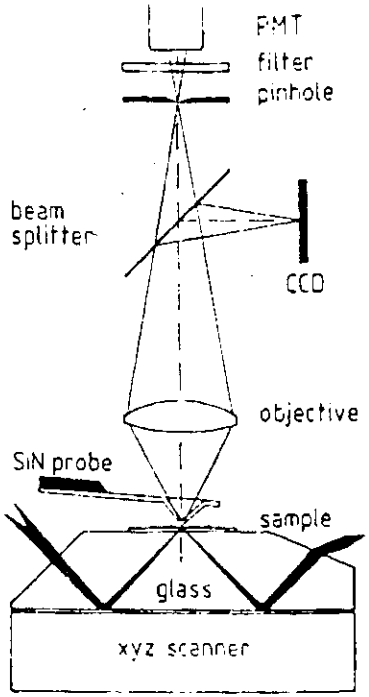
PMT
filter
pinhole
beam
splitter
CCD
objective
SiN probe
sample
glass
xyz scanner

Fig 27

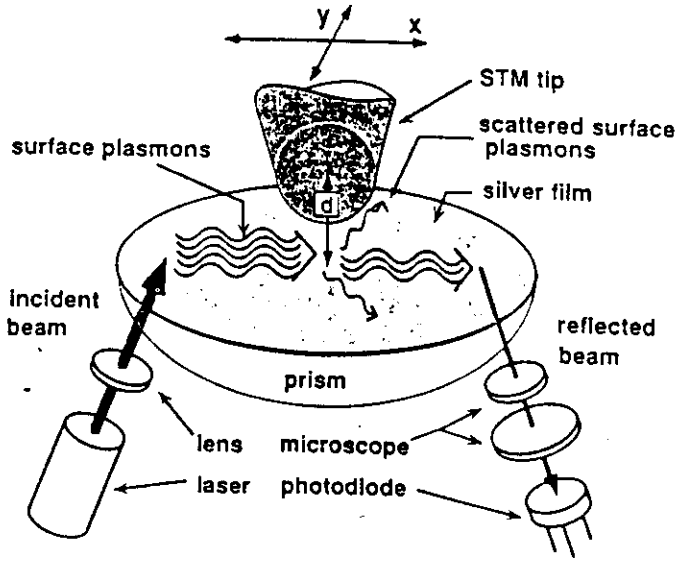
y
x
STM tip
scattered surface
plasmons
surface plasmons
silver film
d
incident
beam
reflected
beam
prism
lens
microscope
laser
photodiode

Fig 28

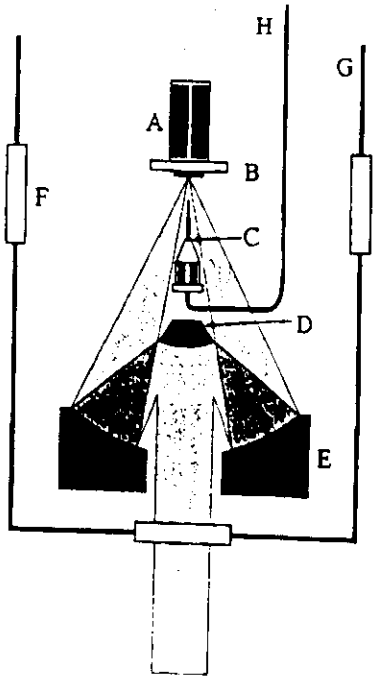
H
G
A
B
F
C
D
E

Fig 29

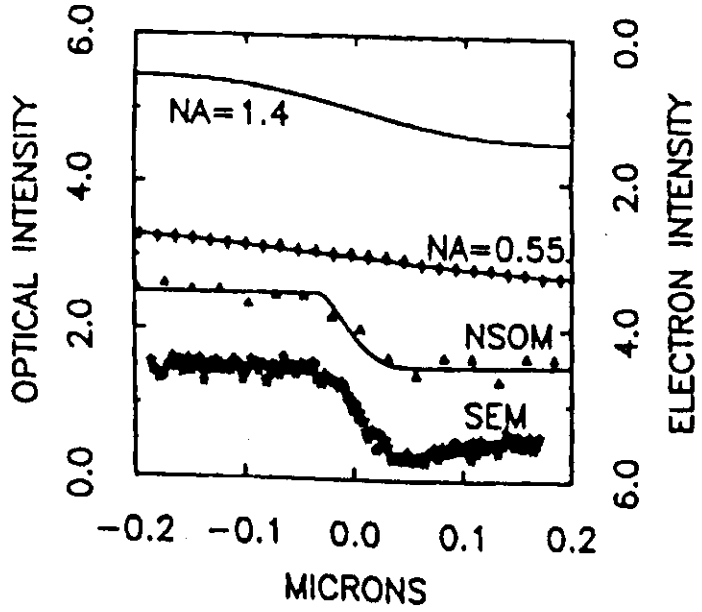
OPTICAL INTENSITY
ELECTRON INTENSITY
NA=1.4
NA=0.55
NSOM
SEM
6.0
4.0
2.0
0.0
0.0
2.0
4.0
6.0
−0.2
−0.1
0.0
0.1
0.2
MICRONS

Fig 30

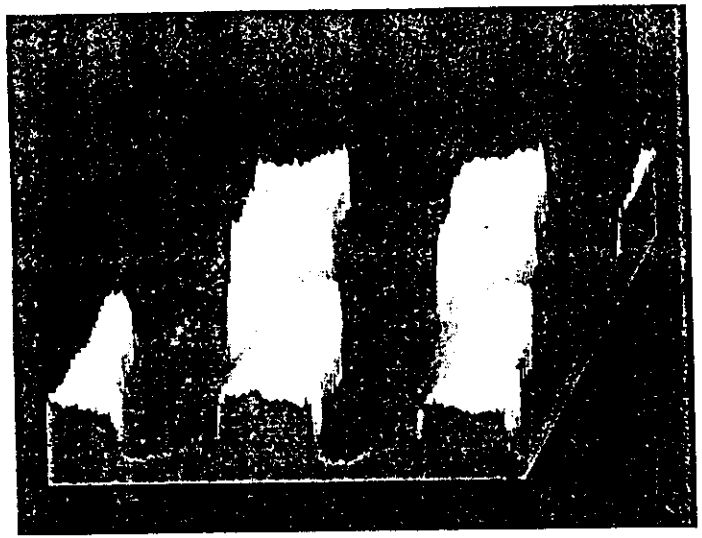

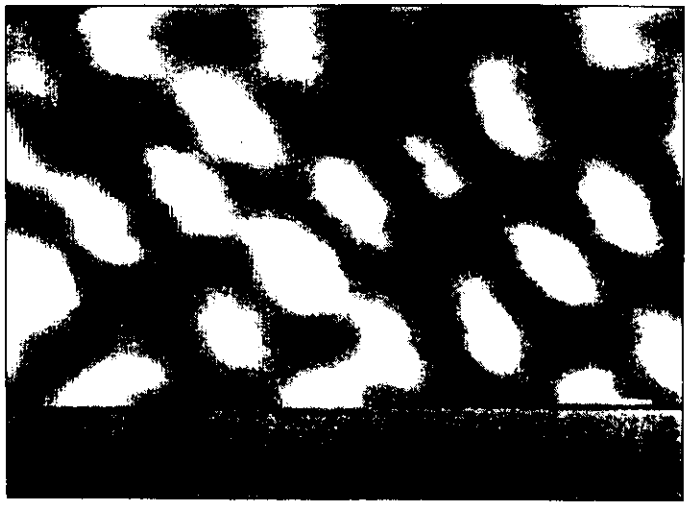

Fig 31

Fig 32

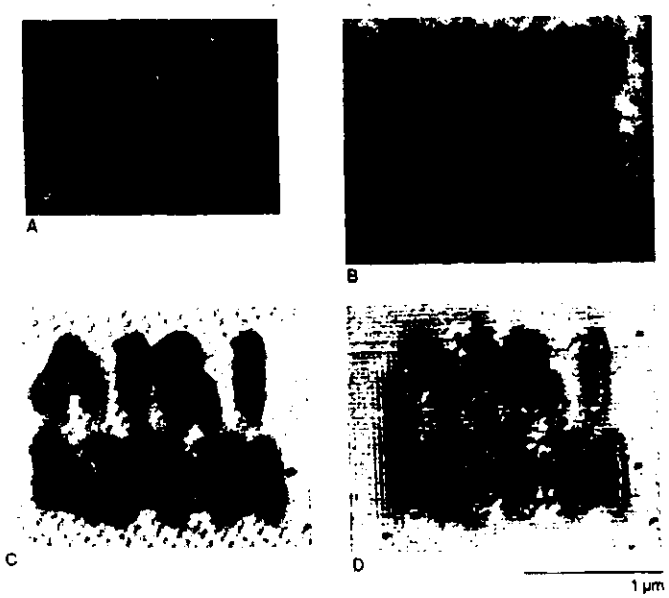

Fig. 33

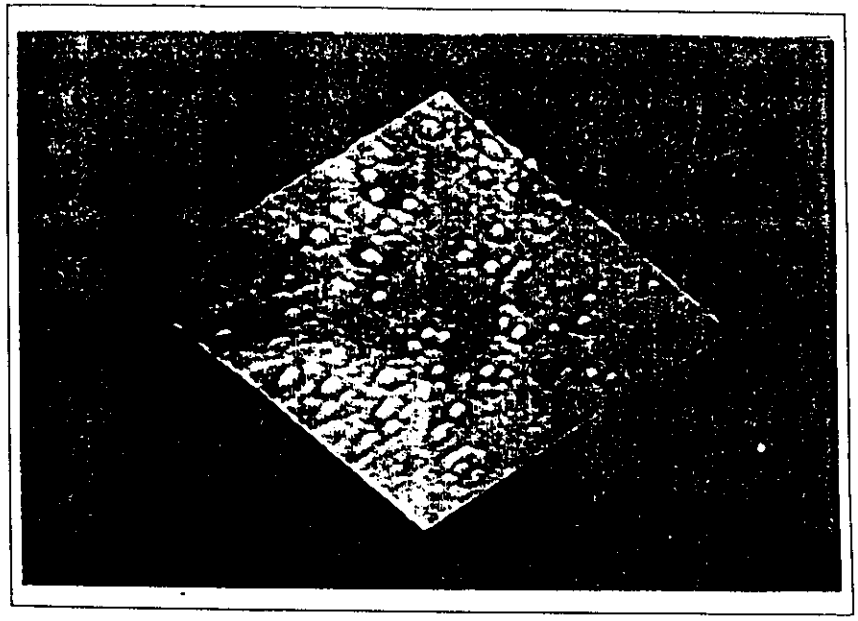

Fig. 56

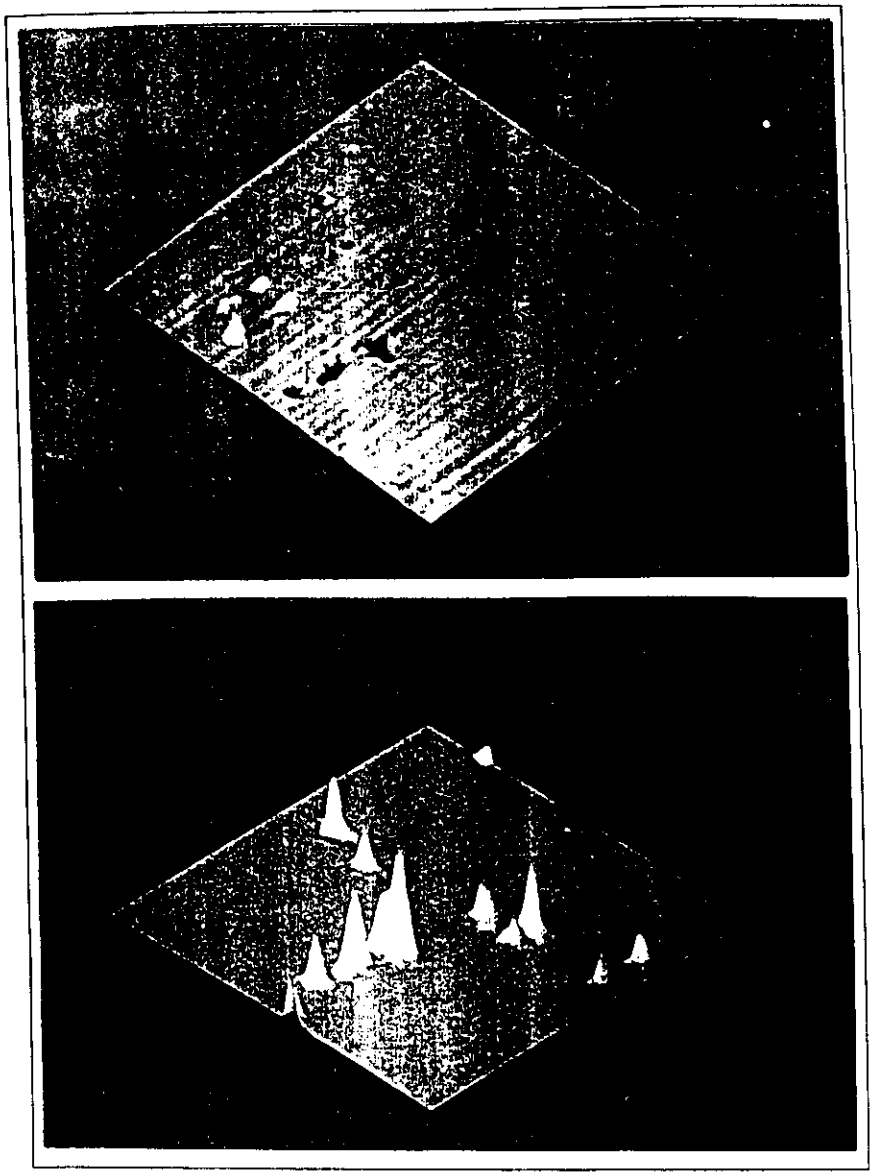

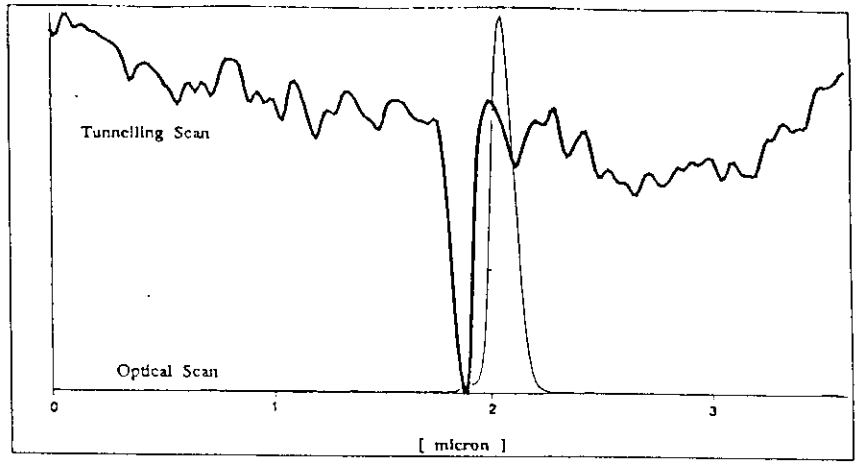

Fig. 35

Fig 36

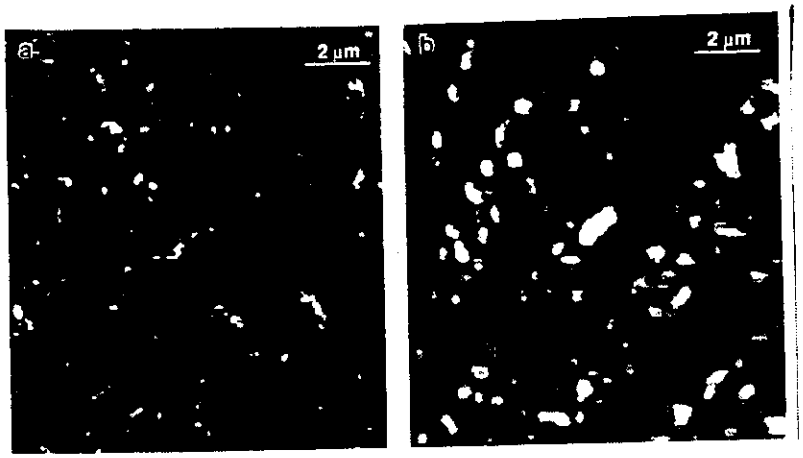
a
2 μm
b
2 μm


(a)
(c)
(b)
(d)

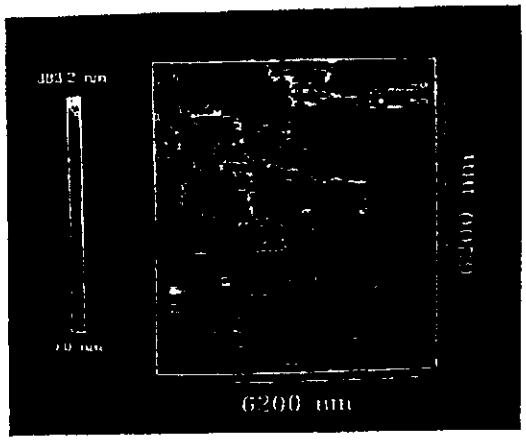

(a)

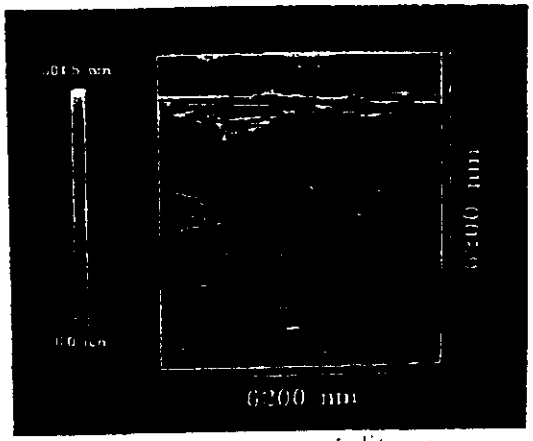

(b)

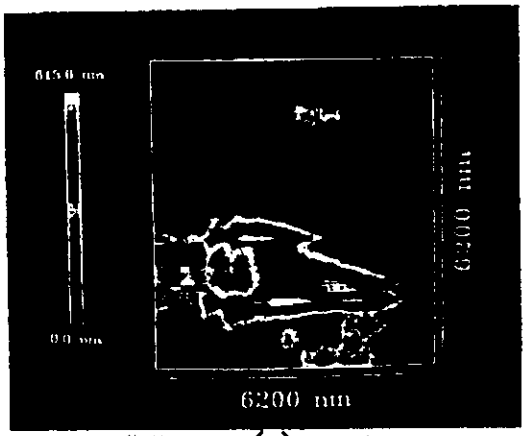

(c)

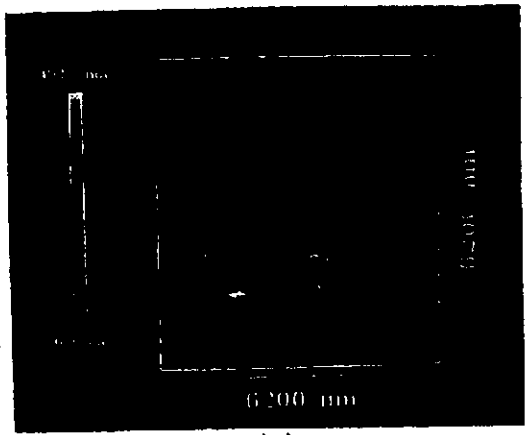

(d)

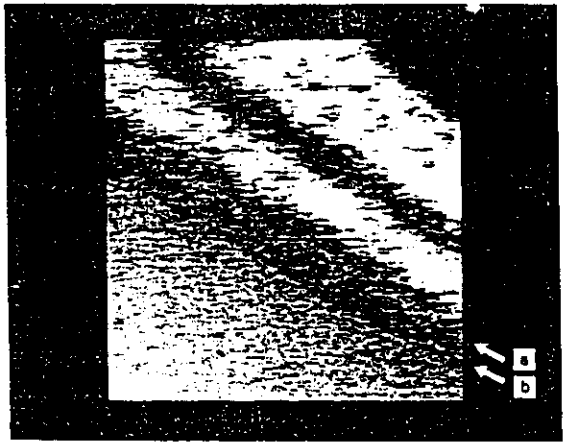

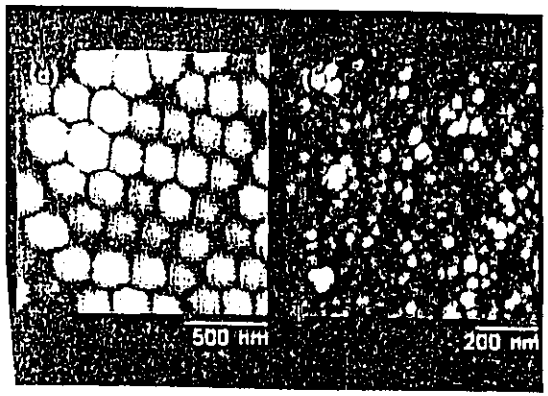

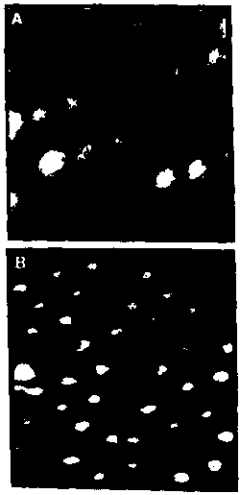

Fig 60

Fig 61

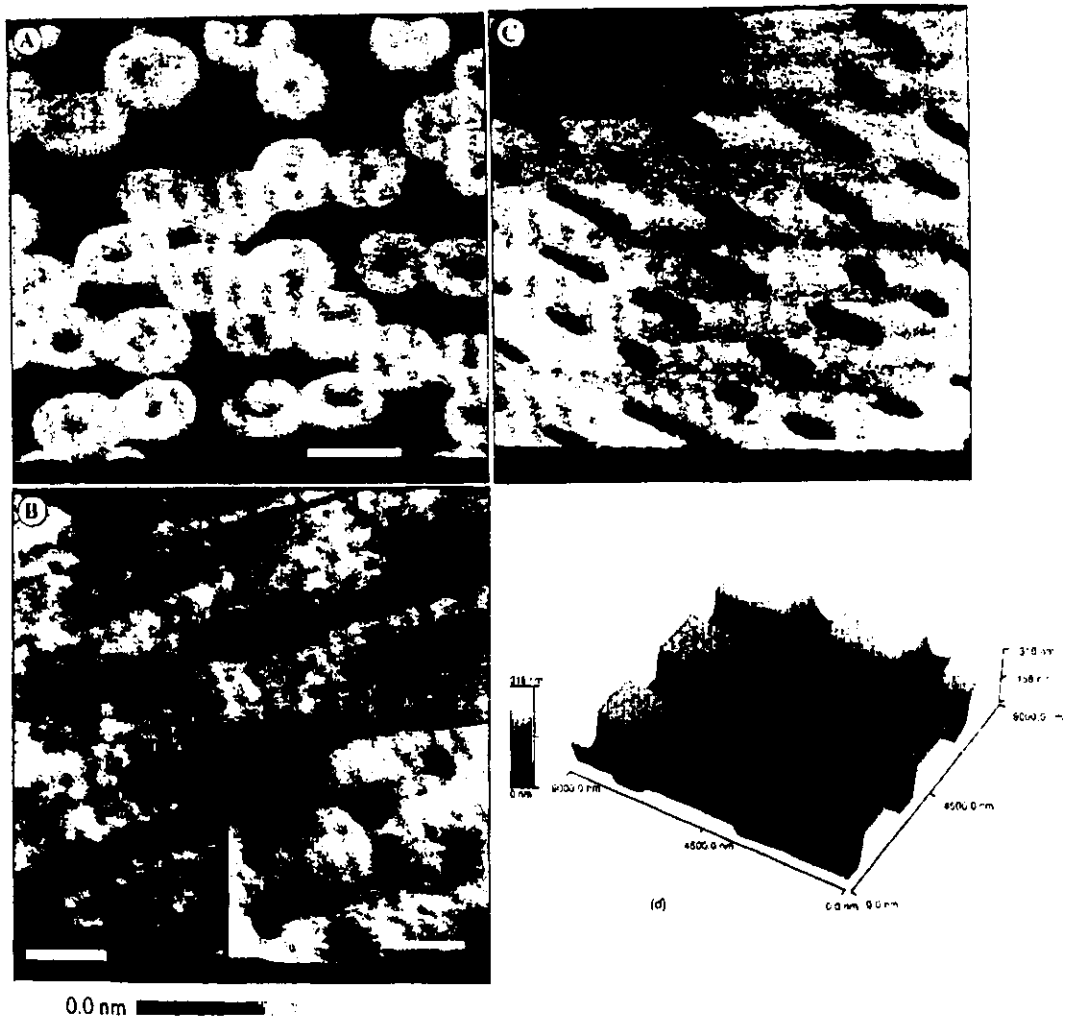

Fig 42

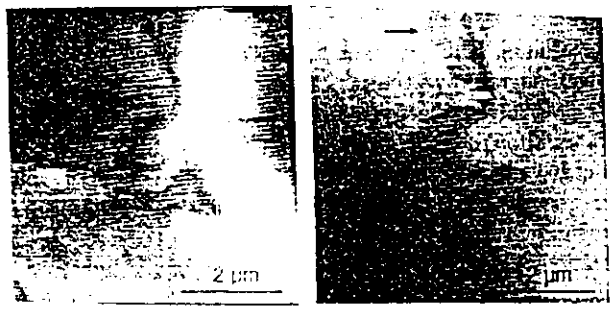

(a) (b)

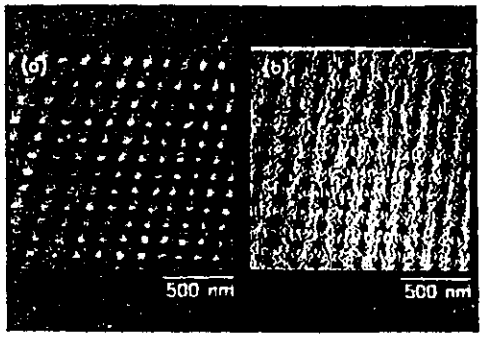

D

Fig 63

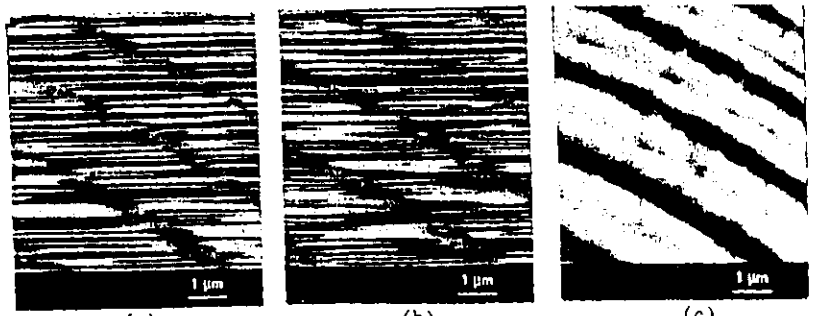

(a) (b) (c)

Fig 64

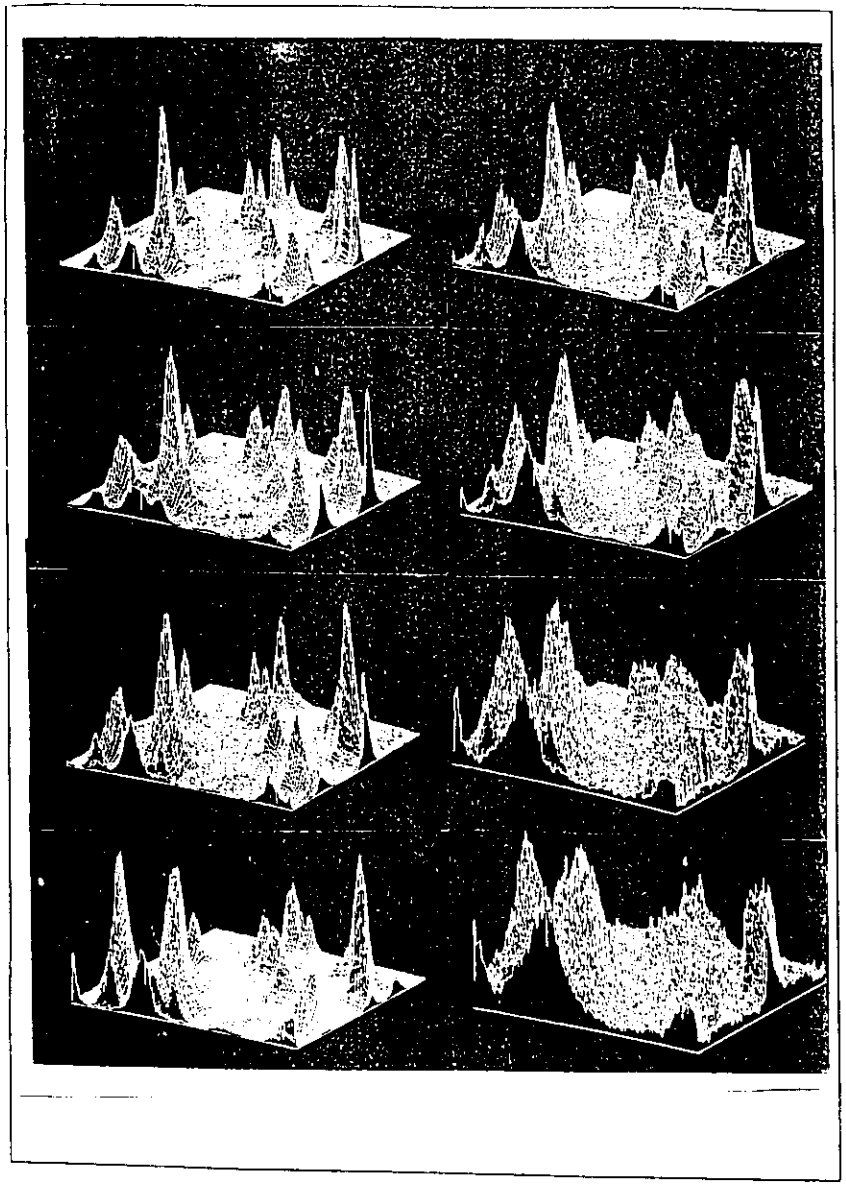

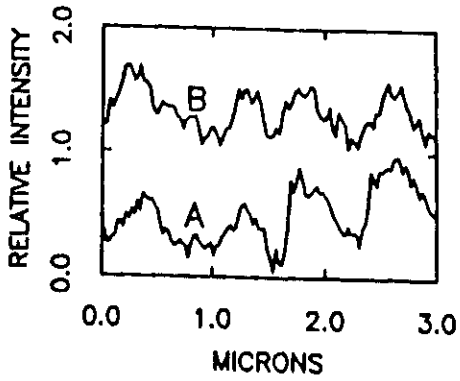
RELATIVE INTENSITY
2.0
1.0
0.0
B
A
0.0
1.0
2.0
3.0
MICRONS

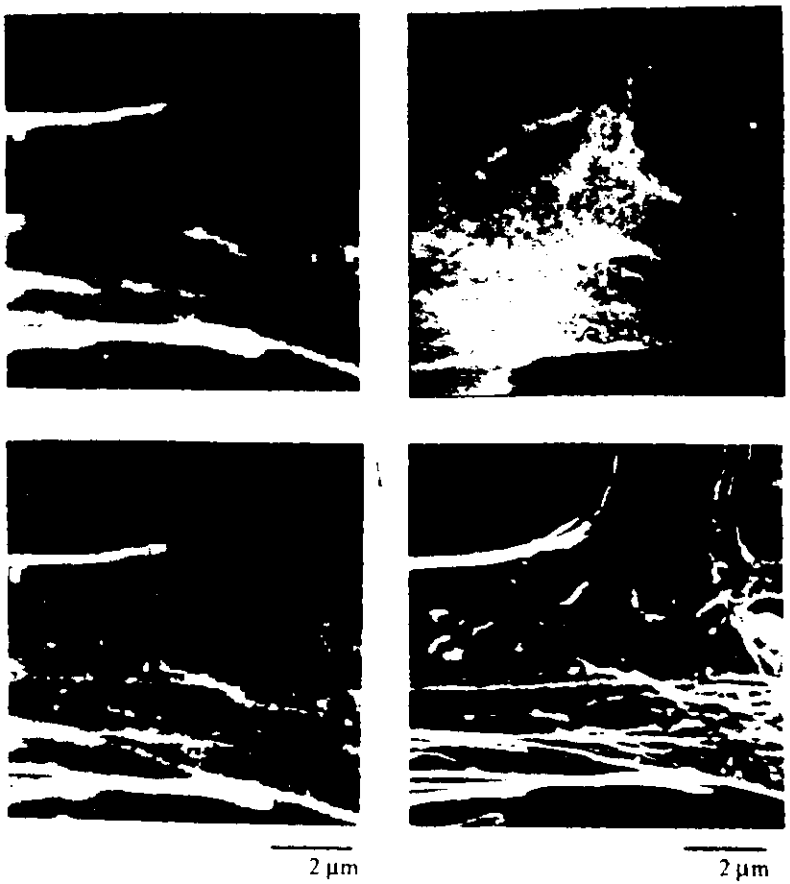
2 µm
2 µm

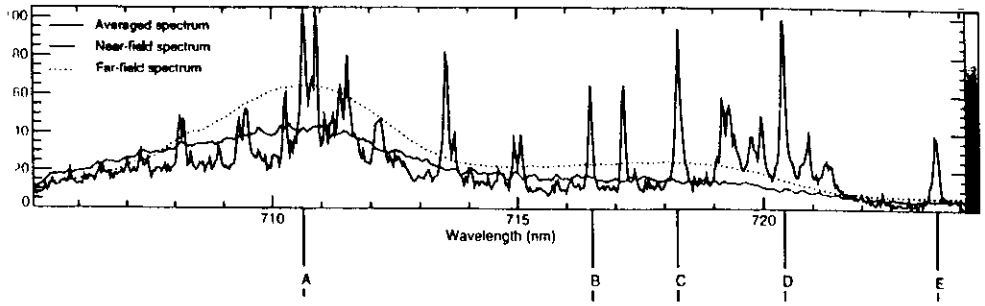
Averaged spectrum
Near-field spectrum
Far-field spectrum
100
80
60
40
20
0
710
715
720
Wavelength (nm)
A
B
C
D
E

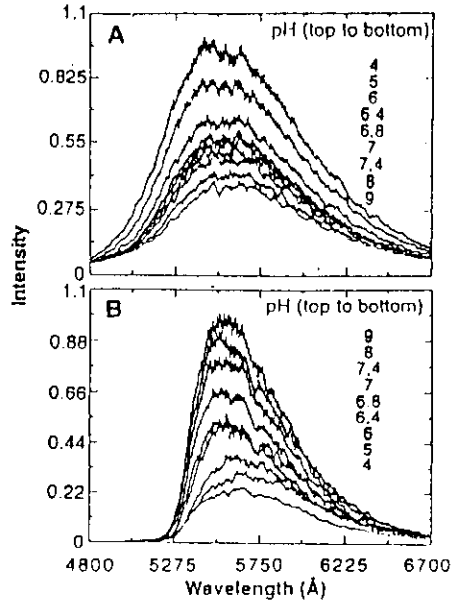

Figure 49

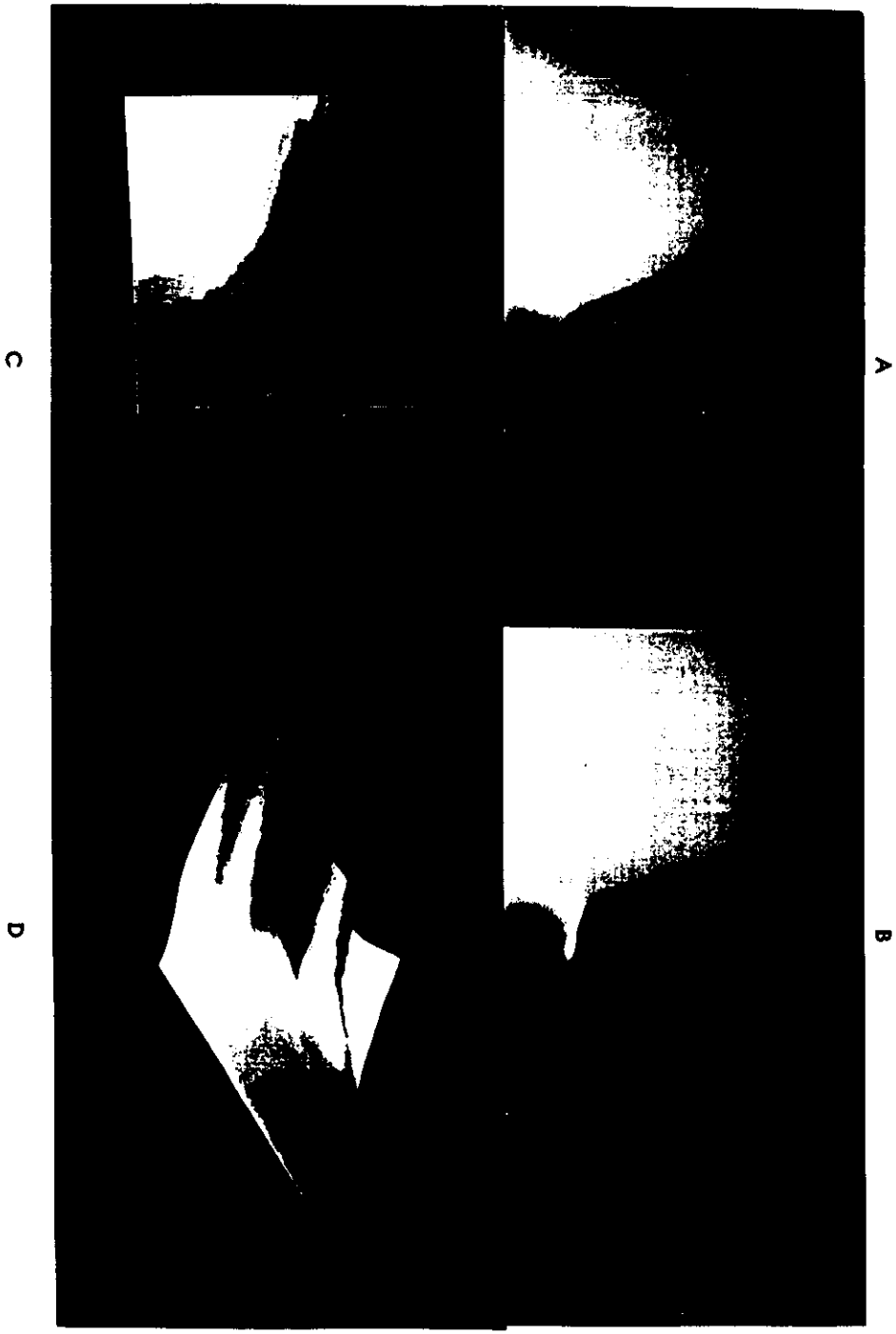

Figure 50

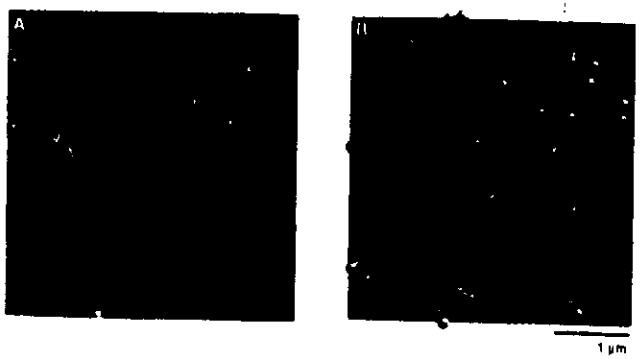

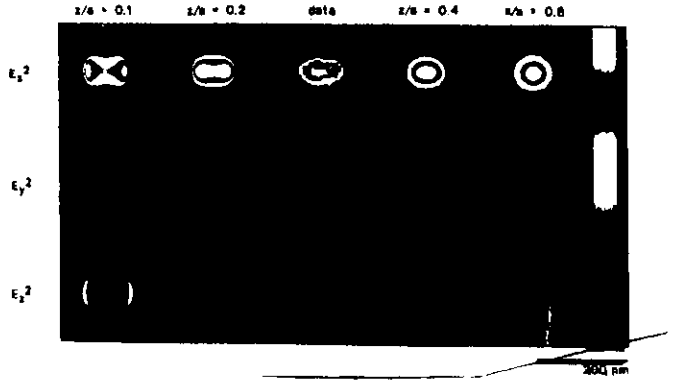

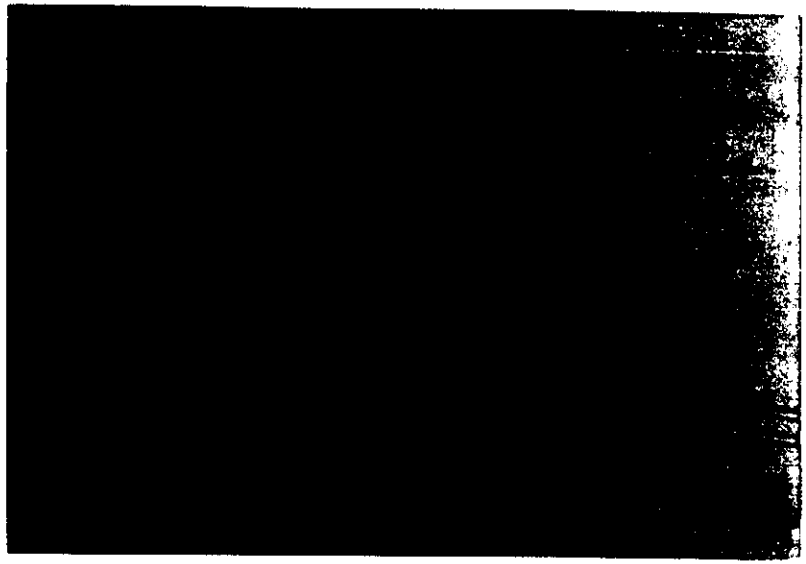

Two 150nm lines

An 80nm line

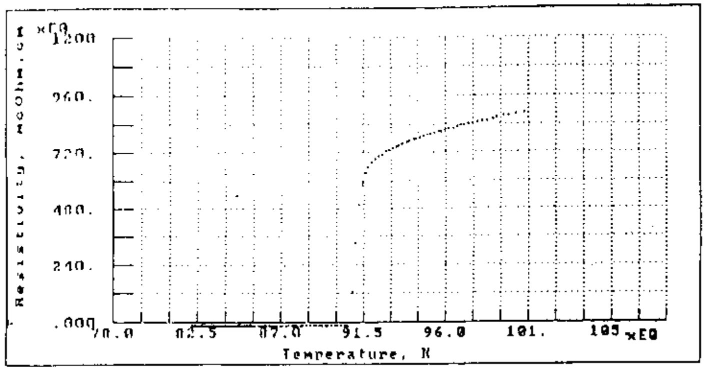

Resistivity, mOhm.cm
×E0
1200
960.
720.
480.
240.
.000
78.0
82.5
87.0
91.5
96.0
101.
105
×E0
Temperature, K

F 43

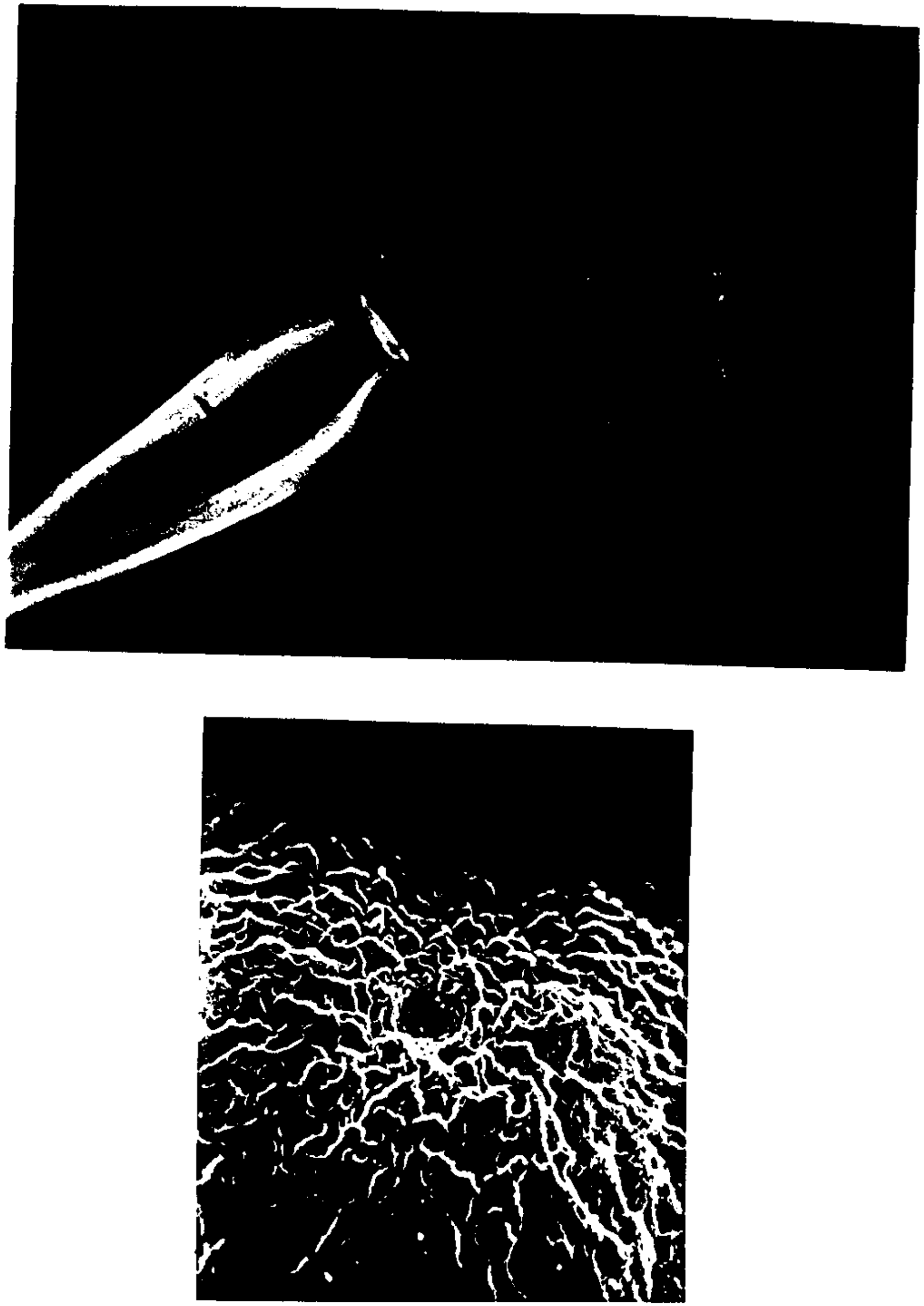

F 34

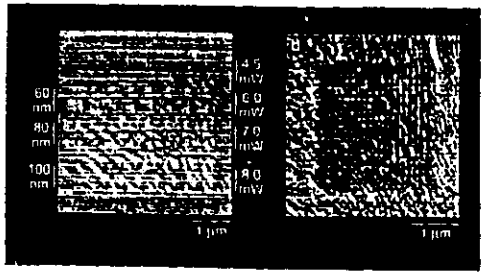
60 nm
80 nm
100 nm
45 mV
60 mV
70 mV
80 mV
1 μm
1 μm

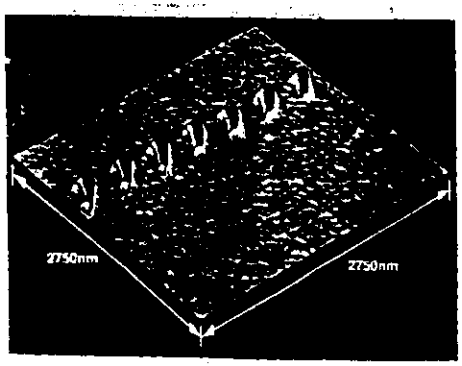
2750nm
2750nm

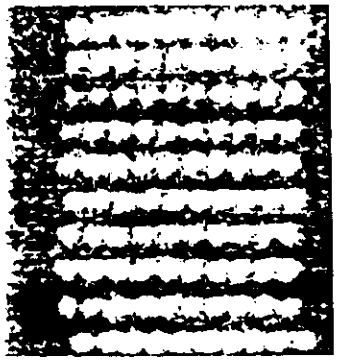
1 μm

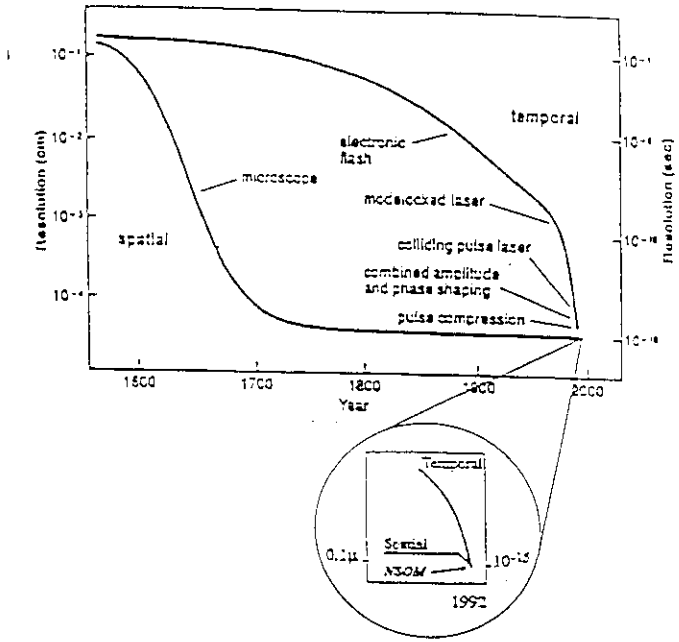
temporal
electronic flash
microscope
modelocked laser
colliding pulse laser
combined amplitude and phase shaping
pulse compression
spatial
Resolution (cm)
Resolution (sec)
1500
1700
1800
1900
2000
Year
Temporal
Spatial
NSOM
0.1μ
10-15
1992

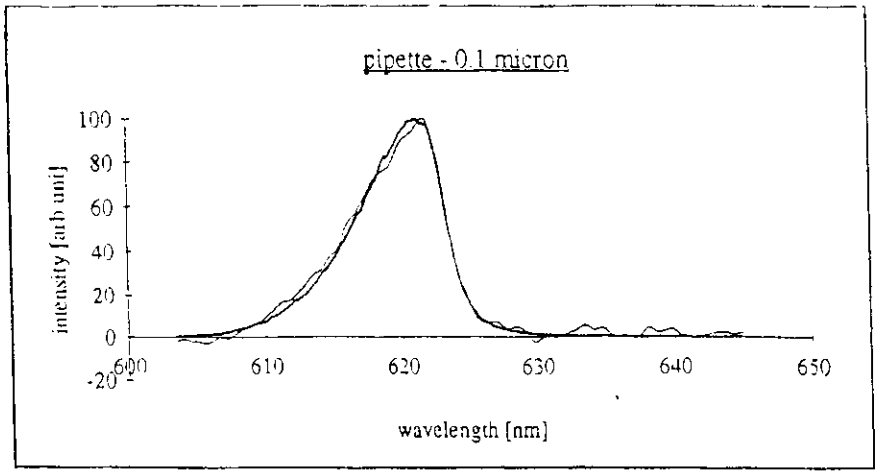

Figure 57

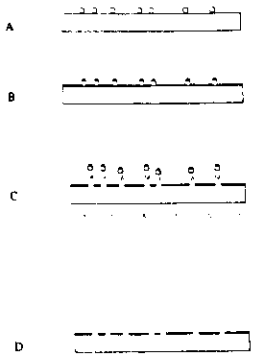

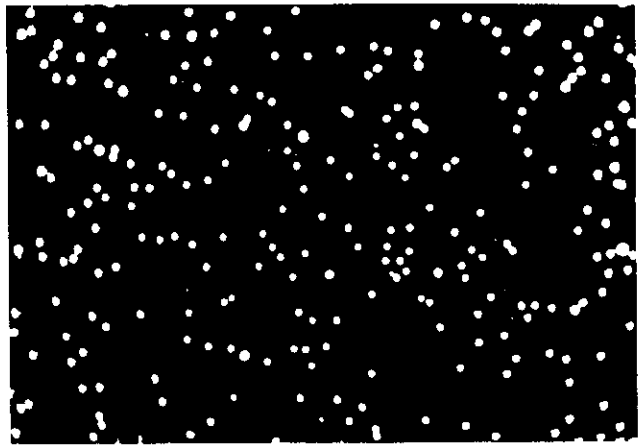

Figure 58

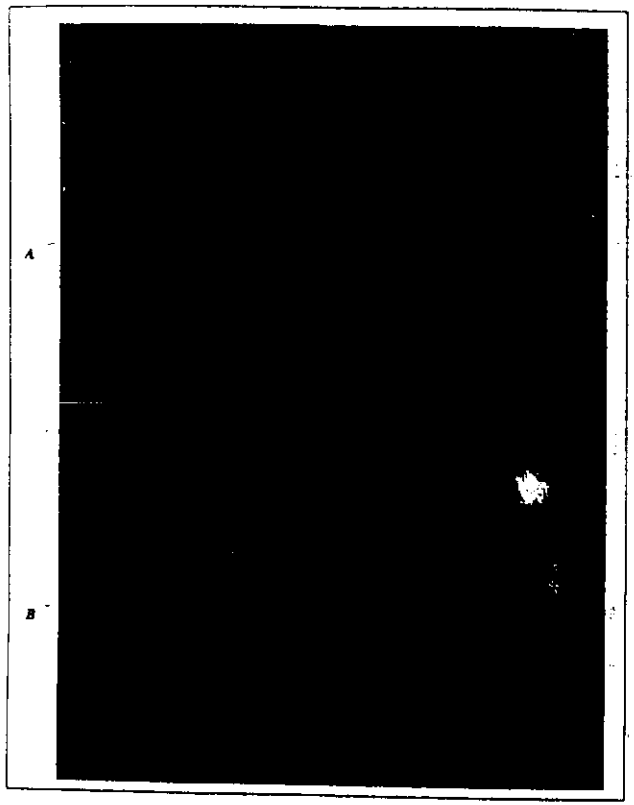

Nanopipette Measurement of Trench Line Width

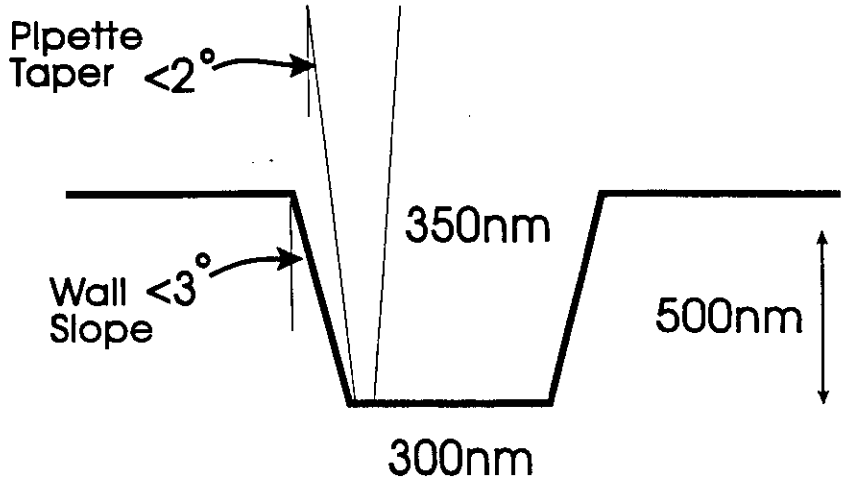

Near-field Resolution of Edge Features

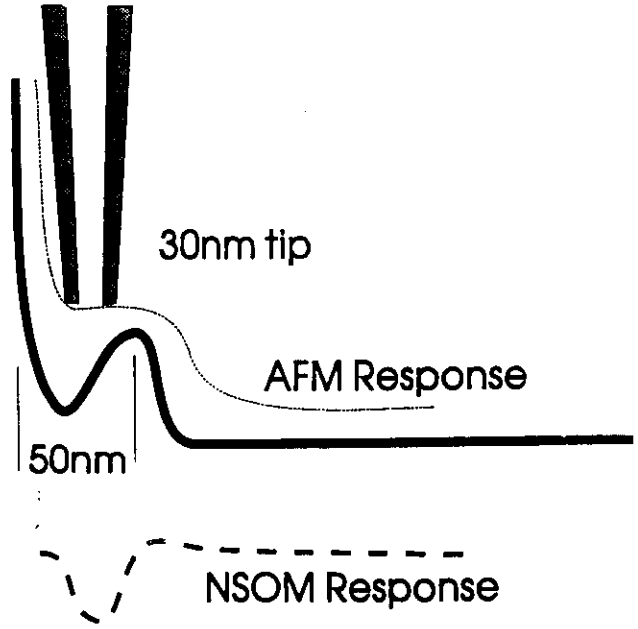

Accurately Monitors Aperture/Surface Separation

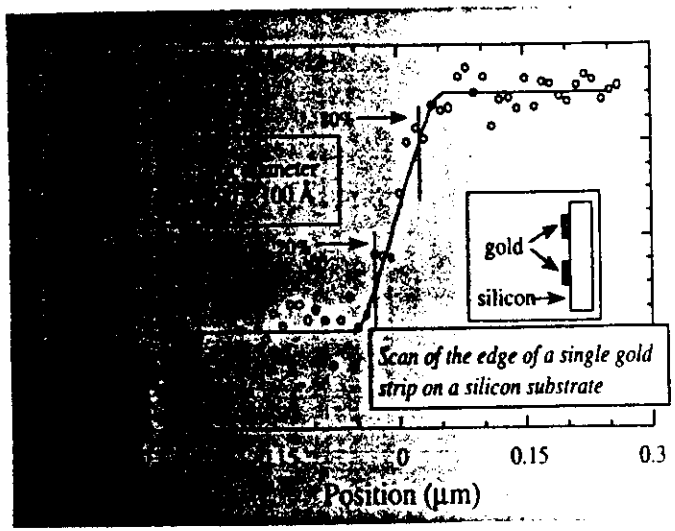
80%
20%
gold
silicon
Scan of the edge of a single gold strip on a silicon substrate
0
0.15
0.3
Position (μm)

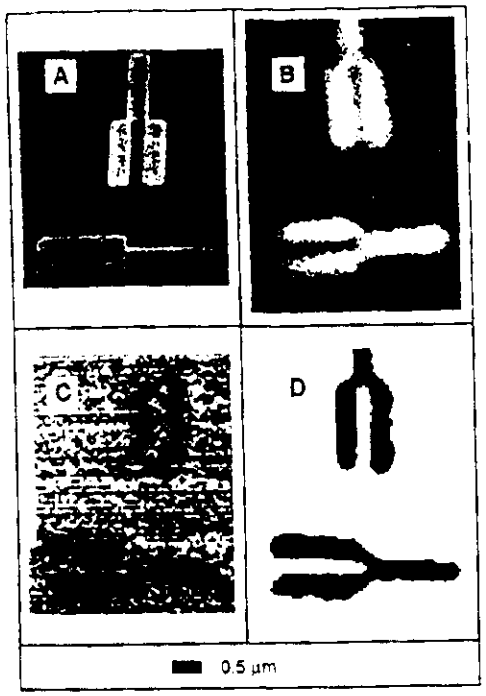
A
B
C
D
0.5 μm

Fig 61

Fig 62

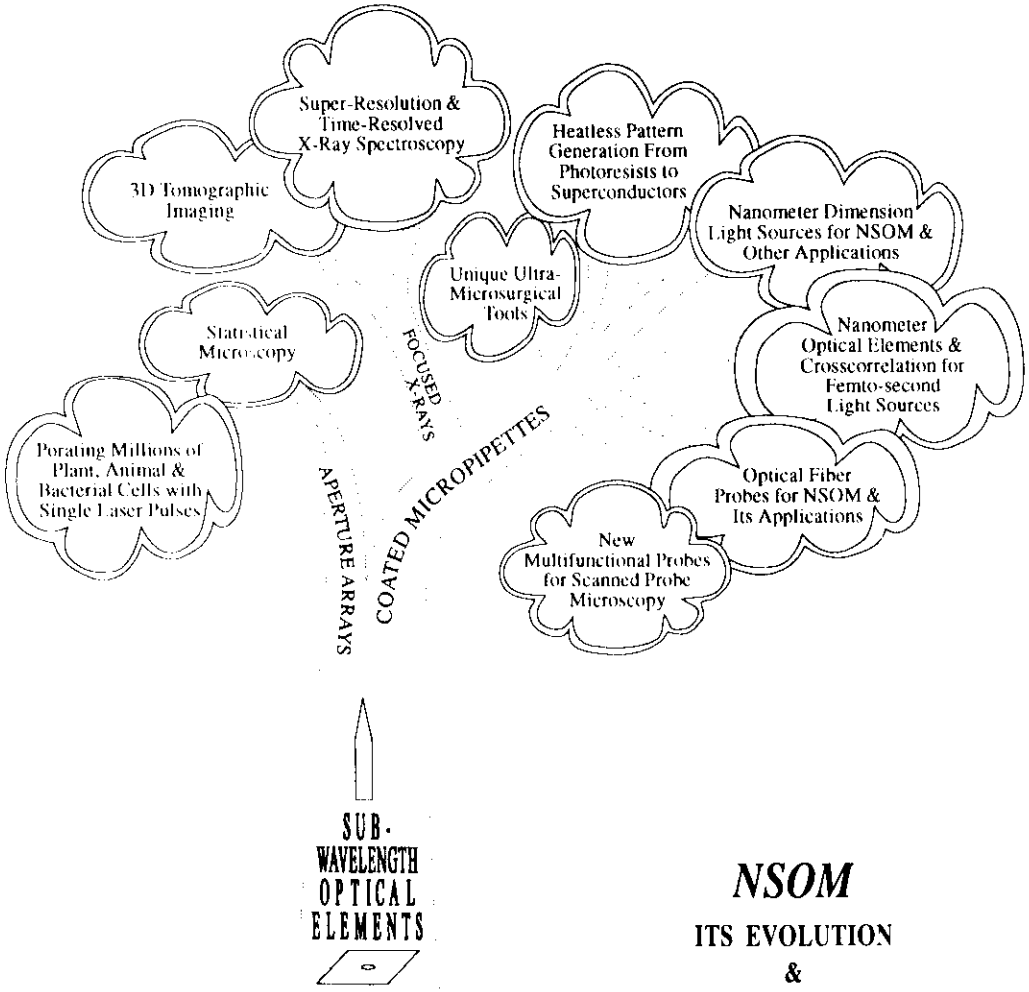

NSOM

ITS EVOLUTION
&
GROWING CONTRIBUTIONS

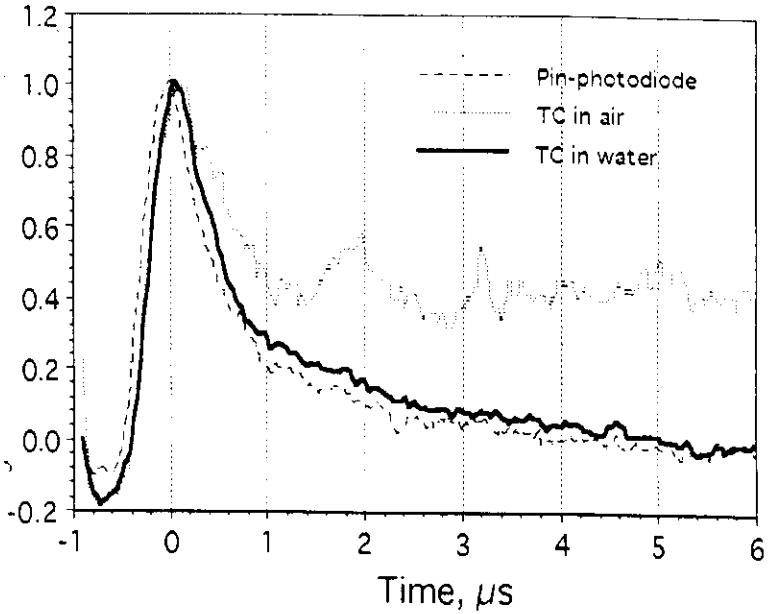

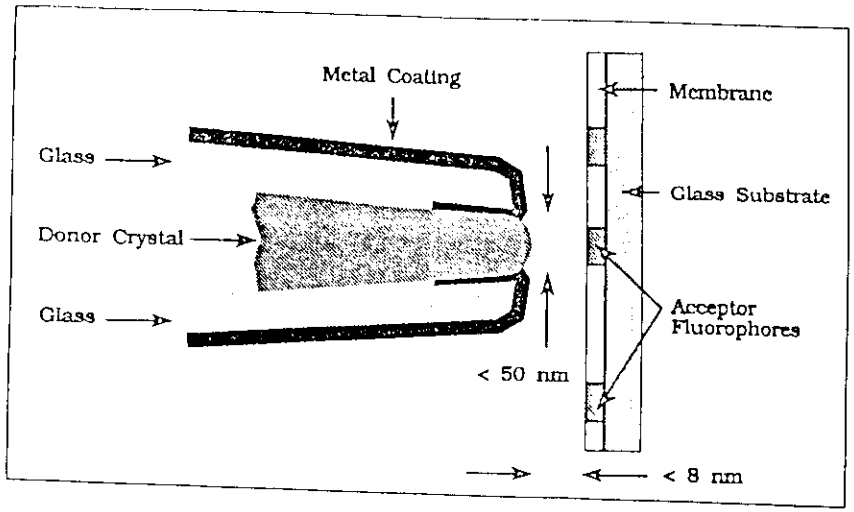
Metal Coating
Glass
Donor Crystal
Glass
< 50 nm
Membrane
Glass Substrate
Acceptor
Fluorophores
< 8 nm

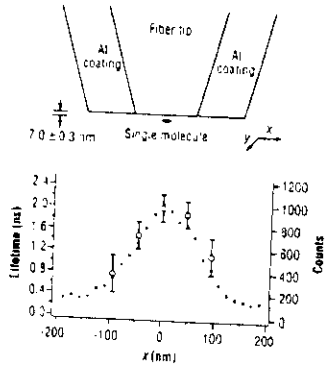
Fiber tip
Al coating
Al coating
Single molecule
Lifetime (ns)
Counts
x (nm)

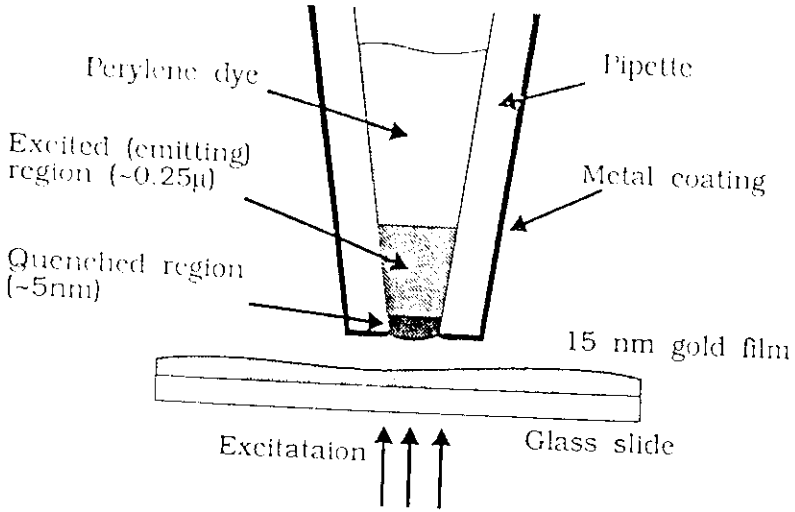
Perylene dye
Pipette
Excited (emitting)
region (~0.25μ)
Metal coating
Quenched region
(~5nm)
15 nm gold film
Excitataion
Glass slide

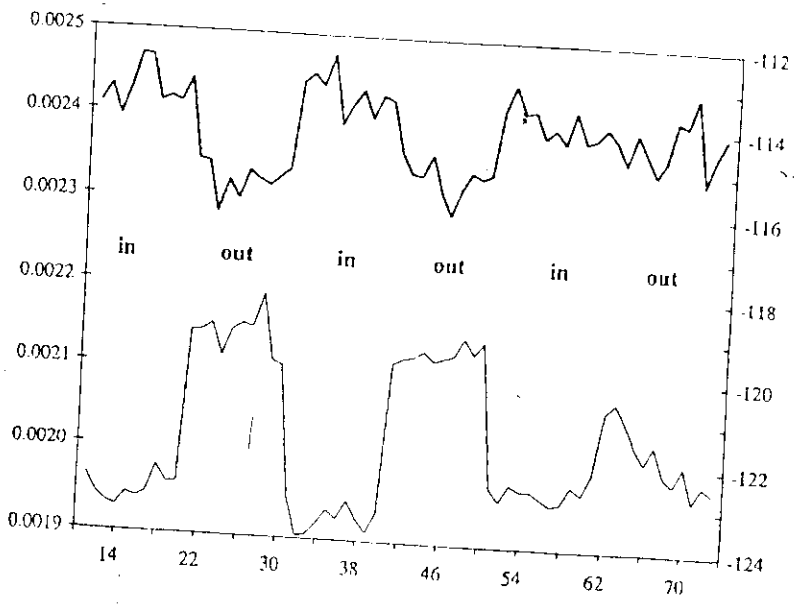
in
out
in
out
in
out

Fig 65

Fig 66

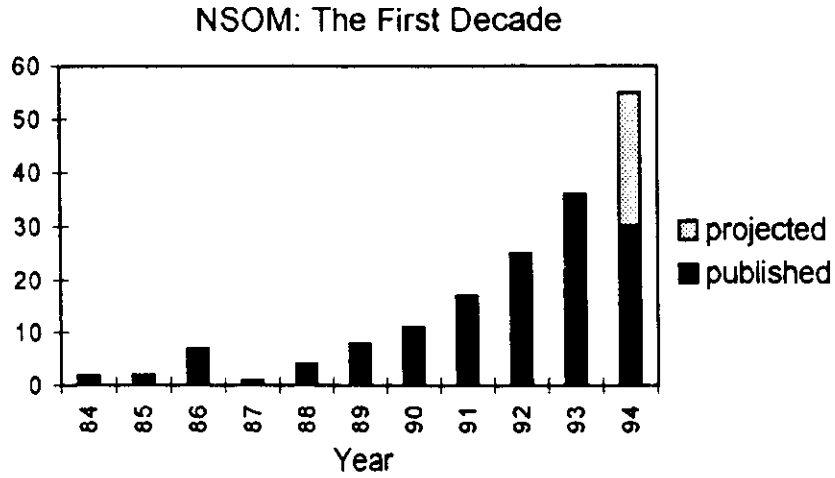
NSOM: The First Decade
60
50
40
30
20
10
0
84
85
86
87
88
89
90
91
92
93
94
Year
projected
published